Scientific report; WR 95-04

Ministerie van Verkeer en Waterstaat

Koninklijk Nederlands
Meteorologisch Instituut

Changes in tropospheric NO_x and O_3 due to subsonic aircraft emissions

W.M.F. Wauben
P.F.J. van Velthoven
H. Kelder

De Bilt, 1995

Scientific report; WR 95-04

Postbus 201
3730 AE De Bilt
Wilhelminalaan 10
Telefoon 030-206 911
Telefax 030-210 407

UDC: 551.510.42
551.510.534
629.7.016.54
621.43.06
ISSN: 0169-1651
ISBN: 90-369-2074-4

Changes in tropospheric NO_x and O_3 due to subsonic aircraft emissions

W.M.F. Wauben, P.F.J. van Velthoven and H. Kelder

KNMI, P.O.Box 201, 3730 AE De Bilt, The Netherlands

February 1995

Contents

Chapter 1

Introduction

Aircraft introduce combustion reaction products and unburned fuel components at high altitudes in the atmosphere. These aircraft emissions are relatively small on a global scale, e.g. less than 3 % of the anthropogenic NO_x emissions are due to aircraft. However, since the emissions occur at high altitudes, where except lightning no other sources are present and where NO_x has a relatively long residence time, they could have an important impact on the atmospheric composition. In addition, the sensitivity of radiative forcing to changes in e.g. ozone is largest directly below the tropopause, which is located near cruise altitudes at mid-latitudes. The aircraft emission of trace gases such as carbon dioxide (a greenhouse gas) and sulphur dioxide (which produces aerosol) contribute, together with water vapour and cloud condensation nuclei (which may lead to contrails), to changes in radiative forcing (cf. e.g. Schumann, 1994; Fortuin *et al.*, 1995). Nitrogen oxides ($NO_x = NO + NO_2$) emitted by aircraft contribute significantly to the background NO_x concentration in the upper troposphere at northern mid-latitudes (Ehhalt *et al.*, 1992). Its direct impact on climate is negligible (Fortuin *et al.*, 1995), but it plays an important role in the ozone chemistry of the atmosphere. The resulting increase of tropospheric and lower stratospheric O_3 is important. First, ozone is a greenhouse gas which produces local heating. Secondly, additional ozone reduces the amount of harmful UV radiation that reaches the surface. Hence, it may counteract the effect of ozone destruction in the stratosphere due to CFCs. Finally, ozone in the biosphere is bad for our health. Therefore a study into the effect of aircraft emissions on atmospheric ozone is justified.

Model studies using two-dimensional models have shown that near the tropopause aircraft NO_x emissions can lead to ozone production (Beck *et al.*, 1992), whereas they can lead to ozone depletion in the middle stratosphere (Hidalgo & Crutzen, 1977). The aircraft NO_x emissions exhibit strong spatial variations. NO_x has a typical lifetime in the upper troposphere and lower stratosphere of about 10 days, and therefore the resulting geographical distribution of the aircraft NO_x emissions is not zonally symmetric. Since the chemical processes of ozone production and destruction are non-linear, three-dimensional global models are needed in order to calculate the effect of the aircraft emissions correctly. In this study, such a three-dimensional chemical transport model is used to study the effect of aircraft emissions. Especially the effect

of aircraft on tropospheric NO_x and ozone are considered here.

Similar model calculations have been performed with the same chemical transport model as part of the AERONOX (1995) project. The results obtained with this model compared well with the results obtained by other models involved in the AERONOX project. Other emission data have been used in the AERONOX project, but the results are qualitatively similar to the ones that are reported here. Unlike the AERONOX project the simulations in this report include runs for future emission scenarios as well as a study of the sensitivity of the results to uncertainties in lightning sources.

Air traffic will increase in the near future. Although the resulting increase in aircraft emissions is expected to be less due to technical improvements of the engines, the relative importance of aircraft emissions relative to other sources will increase. Therefore, not only present day emission levels are used as input for the model calculations, but also predicted future emission levels are considered. The calculated effects of aircraft, now and in the future, can indicate whether action must be undertaken in order to reduce aircraft emissions. Although the duration of the effect of aircraft emissions in the atmosphere is relatively short, such actions must be taken well in advance. The reason hereof is that it takes a rather long time before changes in e.g. aircraft engines are made and before new aircraft can be equipped with them. Therefore, emission scenarios for 1990, 2003 and 2015 are used in the present study.

Despite all the efforts that have been made to construct reliable emission data sets, large uncertainties remain in them. In order to estimate the effect of these uncertainties model calculations can be performed using different annual global emission amounts for the sources. These calculations also give the sensitivity of the effect of aircraft to other sources. In this report the sensitivity to NO_x emissions by lightning is investigated, since its magnitude is still very uncertain. They may range from about 1 up to 100 times the NO_x emissions by aviation for the 1990 scenario. The aircraft emissions mainly occur at northern mid-latitudes whereas the lightning sources of NO_x are strongest over the continents near the tropics in the summer hemisphere.

Chapter 2

Model description

The three-dimensional chemical transport model of the KNMI (CTMK) has been adapted from the global tracer transport model TM2 (cf. Heimann, 1995). CTMK calculates the horizontal and vertical transport of tracer mass on the basis of 12 hourly output from the European Centre for Medium-range Weather Forecasts (ECMWF) model (cf. Velders *et al.*, 1994). The analysed meteorological fields of wind, surface pressure, geopotential height, temperature and humidity with a horizontal resolution of $2.5° \times 2.5°$ are used for this purpose. These meteorological data contribute to a rather realistic description of the actual meteorological situation since observations are included in the ECMWF analyses. The meteorological data are preprocessed for use in CTMK. This involves the evaluation of parameterizations of subgrid scale processes and the integration/interpolation of data to the model grid of CTMK.

2.1 Model resolution

For the present study CTMK was run with a horizontal resolution of 10° in longitude and about 8° in latitude. The longitudes (λ_i) and latitudes (β_j) of the centers of the grid boxes are located at

$$\lambda_i = -180° + \frac{360°(i-1)}{im} \tag{2.1}$$

and

$$\beta_j = -90° + \frac{180°(j-1)}{jm} \tag{2.2}$$

where $i = 1, 2, \ldots, im$ with $im = 36$ the number of boxes in the zonal and $j = 1, 2, \ldots, jm$ with $jm = 24$ the number of boxes in the meridional direction. Here, longitudes West of Greenwich and latitudes in the southern hemisphere are denoted by negative values of λ and β, respectively. The boundaries of the grid boxes are situated halfway between two neighbouring centers. There is only one grid box centered on each of the Poles (namely $i = 1$ for $j = 1$ and $j = jm$) and these polar grid boxes have a meridional extent of $90°/jm$, i.e. half the meridional extent of the grid boxes at other latitudes. The horizontal grid is illustrated in Fig. 2.1.

Vertically, the model has 15 σ-levels. The centers and boundaries of this vertical grid are given in Table 2.1. The lower boundary of this coordinate system coincides

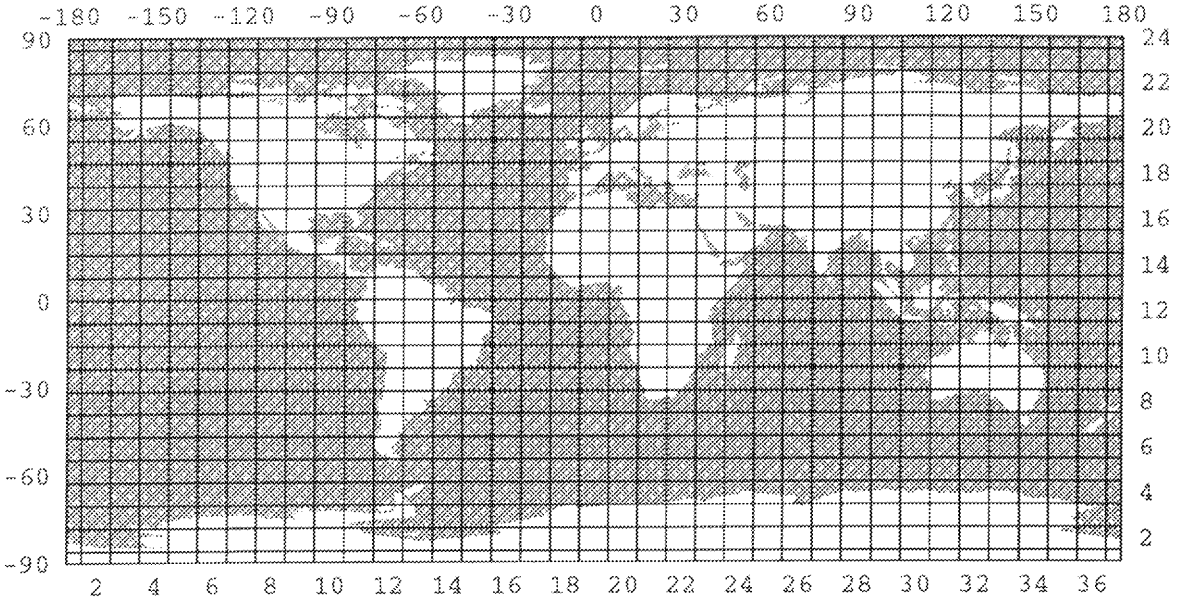

Figure 2.1 Illustration of the horizontal grid taken from Heimann (1995). The numbers on the top and left border denote longitude and latitude in degrees, whereas the numbers on the bottom and right border are the longitudinal (i) and latitudinal (j) indices of the grid boxes.

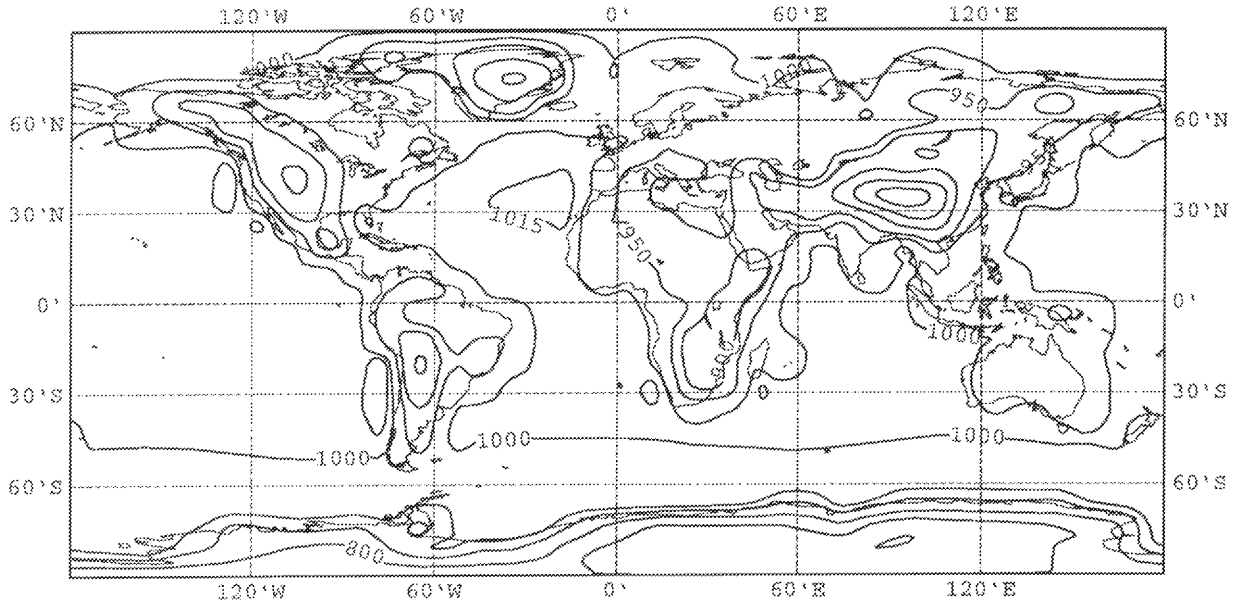

Figure 2.2 The annually averaged surface pressure obtained from the ECMWF analyses of 1990. Isolines are drawn at 600, 700, 800, 900, 950, 1000 and 1015 hPa.

Table 2.1 Centers and boundaries of the vertical grid of CTMK in σ-units. The corresponding pressure levels (in hPa) and altitudes (in km) pertaining to the US Standard Atmosphere (NASA, 1976) are also given.

	σ-coordinate		pressure		altitude	
level	boundary	center	boundary	center	boundary	center
	0.000000		5.0		36.00	
15		0.007661		12.7		29.62
	0.015322		20.4		26.48	
14		0.025536		30.7		23.80
	0.035751		41.0		21.93	
13		0.045965		51.3		20.49
	0.056180		61.6		19.32	
12		0.068948		74.5		18.11
	0.081716		87.4		17.09	
11		0.102145		108.0		15.74
	0.122574		128.6		14.63	
10		0.148110		154.3		13.46
	0.173647		180.1		12.48	
9		0.199183		205.8		11.63
	0.224719		231.6		10.88	
8		0.250255		257.3		10.20
	0.275792		283.1		9.57	
7		0.314096		321.7		8.71
	0.352400		360.3		7.93	
6		0.403473		411.8		6.99
	0.454545		463.3		6.14	
5		0.505618		514.8		5.37
	0.556691		566.3		4.65	
4		0.643514		653.8		3.55
	0.730337		741.4		2.56	
3		0.798774		810.4		1.85
	0.867211		879.4		1.18	
2		0.908069		920.6		0.80
	0.948927		961.8		0.44	
1		0.974464		987.3		0.22
	1.000000		1013.2		0.00	

with the surface whereas its upper boundary is situated at 5 hPa. The pressure p_k of the k-th σ-level can be obtained from

$$p_k = \sigma_k(p_s - p_t) + p_t \tag{2.3}$$

where p_s is the surface pressure and p_t is the pressure at the upper boundary of the model. The surface pressure depends on the location and varies in time. The main part of the spatial variation is due to differences in the elevation of the surface. Figure 2.2 clearly shows that the annually averaged surface pressure is closely related to the elevation. The high surface pressure values occur over the oceans, whereas the low values are located over elevated areas such as the Himalayas and the Antarctic.

2.2 Transport

The advection of tracers in CTMK is calculated with the slopes scheme of Russell & Lerner (1981). The amount of tracers in each grid box is specified by its mass and the slopes of the tracer mass in the zonal, meridional and vertical direction. The mass fluxes through each boundary of the grid box are computed from the ECMWF analyses in the preprocessing stage and stored for use in CTMK. The amount of tracer mass transported in a time step from one cell to another can then be calculated. This can be used to calculate the new tracer mass in a grid box and its slopes. If the gradients in the spatial distribution of tracer mass are strong, the slope might be such that a negative value of the tracer mass occurs at the boundary of a grid box. This may lead to advection of negative tracer mass and even to negative values for the total tracer mass in a grid box. Since this is not realistic and can lead to problems in the chemistry module, the slopes are limited such that no negative tracer masses occur at the boundaries of the grid boxes. The advection time step used for the computations on the $8° \times 10°$ horizontal grid of CTMK is 2 hours. One such model time step is a combination of 4 advection time steps in the East-West, 2 in North-South, and 1 in the vertical direction. Afterwards vertical adjustment is applied in order to conserve mass.

In addition to vertical advection, subgrid scale vertical transport occurs. This subscale transport is obtained from parameterizations for cumulus and shallow convection and vertical diffusion. The vertical transport associated with these processes is also determined from ECMWF analyses data in the preprocessing stage.

The subscale convection fluxes are evaluated according to the scheme of Tiedtke (1989). This scheme uses the water vapour convergence in combination with the evaporation from the surface in order to detect the presence of a cloud. In case a cloud is present a convection matrix is constructed which gives the fraction of tracer mass from one grid box that ends up in another due to the convection process. Here the altitude at which surface air condensates when lifted adiabatically gives the cloud base height and the altitude at which the cloud parcel is no longer buoyant defines its

top. The air mass flux remaining at the top of the cloud is detrained in the two layers above the cloud top to simulate overshooting.

The vertical diffusion is calculated based on the stability of air using the formulation of Louis (1979). This scheme, which utilizes a stability function involving the Richardson number, yields the largest diffusion coefficients in the boundary layer.

2.3 Chemistry

CTMK contains a chemistry module from the MOGUNTIA model (cf. Crutzen & Zimmermann, 1991). This scheme evaluates the time evolution of 13 trace gases according to the so-called quasi steady state assumption. This means that the chemical production and loss terms, denoted by P and L respectively, are assumed to be constant during the chemical time step Δt. The time evolution of the concentration of a trace gas C is then given by

$$\frac{dC}{dt} = P - LC. \tag{2.4}$$

The changes in the concentration of a trace gas due to advection and convection are not included in the above relation. These processes are considered in other modules of CTMK. The solution of the differential equation given above is

$$C_{t+\Delta t} = \left(C_t - \frac{P}{L}\right)\exp(-L\Delta t) + \frac{P}{L} \tag{2.5}$$

which is a relatively computer time demanding expression to evaluate. For trace gases with a relatively short lifetime ($L^{-1} << 1$) this expression can be approximated by the so-called steady state solution (i.e. $dC/dt = 0$)

$$C_{t+\Delta t} = \frac{P}{L}. \tag{2.6}$$

On the other hand, an expansion of the exponential factor in Taylor series yields

$$C_{t+\Delta t} = C_t + (P - LC_t)\Delta t, \tag{2.7}$$

which can be used for trace gases with a relatively long lifetime. This last solution is called explicit because the concentration on the right hand side of the differential equation is evaluated at time t. Sometimes, this technique leads to stability problems resulting in the occurrence of negative concentrations. The implicit technique, which uses the concentration at $t + \Delta t$, gives for trace gases with a relatively long lifetime

$$C_{t+\Delta t} = \frac{P\Delta t + C_t}{1 + L\Delta t}, \tag{2.8}$$

which is always stable. One of the above mentioned solutions for the differential equation describing the time evolution of a trace gasses is used for each trace gas, depending on its lifetime. The gases with relatively long lifetimes, i.e. O_3, NO_x, H_2O_2,

CH_4, CO, HNO_3 and CH_3OOH, are transported in CTMK, where after their change due to chemistry is computed. The concentrations of the trace gases with relatively short lifetimes, i.e. HCHO, NO, HO_2, CH_3O_2, $O(^1D)$ and OH, are calculated in the chemistry module by the assumption of steady state.

During daytime the chemical module contains 7 photodissociation reactions and 18 thermal reactions (cf. Table 2.2). Photodissociation is a chemical reaction in which a molecule absorbs a quantum of radiation $h\nu$ and dissociates. This can be written schematically as

$$A + h\nu \rightarrow B + C \tag{2.9}$$

with A, B and C concentrations of trace gases. The reaction rate of this photodissociation reaction is given by

$$\frac{dB}{dt} = Aj \tag{2.10}$$

with j the photolysis rate of the reaction. In the chemical module daytime averaged photolysis rates for O_3, NO_2, H_2O_2, HNO_3, CH_3OOH and HCHO are used, which have been computed off-line with the model described in Brühl & Crutzen (1989). Thermal reactions can schematically be written as

$$A + B \rightarrow C \tag{2.11}$$

and proceed at the rate

$$\frac{dC}{dt} = kAB \tag{2.12}$$

with k the rate coefficient of the reaction. Expressions for the rate coefficients are taken from De More *et al.* (1992) and Atkinson *et al.* (1992) and are listed in Table 2.2. These reaction rates are calculated by using the pressure, temperature and relative humidity fields from the ECMWF analyses. During nighttime the chemistry module evaluates an off-line parameterized heterogeneous reaction. This parameterization, which is based on the work of Dentener & Crutzen (1993), converts NO_2 and O_3 into HNO_3.

Additional sinks of trace gases are dry deposition of O_3, NO_2, H_2O_2, HNO_3, CH_3OOH and NO, and wet deposition of H_2O_2, HNO_3 and CH_3OOH. Constant deposition velocities are used for each of the tracers involved with distinctions between land and sea surfaces (cf. Hein, 1994). The precipitation data used for the parameterization of the wet deposition comes from the ECMWF forecast for 1987, whereas its vertical distribution is given by climatological data from Newell *et al.* (1974).

The chemistry scheme uses prescribed surface concentrations for CH_4 and CO according to Fung *et al.* (1991) and Dianov-Klokov & Yurganov (1981), respectively. In the stratosphere, destruction of CH_4 by chlorine atoms is taken into account by using destruction rates calculated with a 2-dimensional stratosphere model (Brühl & Crutzen, 1993). The ozone flux from the stratosphere into the troposphere is prescribed according to Holton (1990).

Table 2.2 The chemical reactions considered in CTMK during daytime and expressions for their reaction rates. Here n, T, p and H_2O denote the density, temperature, pressure and water vapour concentration of the air in a grid box.

code	reaction	rates
J1	$O_3+h\nu \rightarrow O(^1D)+O_2$	
J2	$H_2O_2+h\nu \rightarrow 2OH$	
J3	$NO_2+O_2+h\nu \rightarrow NO+O_3$	
J4	$HNO_3+h\nu \rightarrow NO_2+OH$	
J5	$HCHO+h\nu \rightarrow H_2+CO$	
J6	$HCHO+2O_2+h\nu \rightarrow 2HO_2+CO$	
J7	$CH_3OOH+O_2+h\nu \rightarrow HCHO+HO_2+OH$	
R1	$O(^1D)+O_2+M \rightarrow O_3+M$	kR1
R2	$O(^1D)+H_2O \rightarrow 2OH$	2.2×10^{-10}
R3	$HO_2+OH \rightarrow H_2O+O_2$	$4.8 \times 10^{-11} \exp(250/T)$
R4	$H_2O_2+OH \rightarrow HO_2+H_2O$	$2.9 \times 10^{-12} \exp(-160/T)$
R5	$O_3+OH \rightarrow HO_2+O_2$	$1.6 \times 10^{-12} \exp(-940/T)$
R6	$HO_2+HO_2 \rightarrow H_2O_2+O_2$	(kR6a+kR6b)kR6c
R7	$O_3+HO_2 \rightarrow OH+2O_2$	$1.1 \times 10^{-14} \exp(-500/T)$
R8	$HNO_3+OH+O_2 \rightarrow NO_2+O_3+H_2O$	kR8a+kR8c/(1+kR8c/kR8b)
R9	$NO_2+OH+M \rightarrow HNO_3+M$	kR9
R10	$NO+HO_2 \rightarrow NO_2+OH$	$3.7 \times 10^{-12} \exp(250/T)$
R11	$NO+O_3 \rightarrow NO_2+O_2$	$2.0 \times 10^{-12} \exp(-1400/T)$
R12	$CH_4+OH+O_2+M \rightarrow CH_3O_2+H_2O+M$	$2.9 \times 10^{-12} \exp(-1820/T)$
R13	$CO+OH+O_2 \rightarrow CO_2+HO_2$	$1.5 \times 10^{-13}(1 + 0.6p/1013.25)$
R14	$HCHO+OH+O_2 \rightarrow HO_2+H_2O+CO$	1.0×10^{-11}
R15	$CH_3O_2+HO_2 \rightarrow CH_3OOH+O_2$	$3.8 \times 10^{-13} \exp(800/T)$
R16	$CH_3OOH+OH \rightarrow CH_3O_2+H_2O$	$0.3 \times 3.8 \times 10^{-12} \exp(200/T)$
R17	$CH_3OOH+OH \rightarrow HCHO+OH+H_2O$	$0.7 \times 3.8 \times 10^{-12} \exp(200/T)$
R18	$CH_3O_2+NO+O_2 \rightarrow HCHO+HO_2+NO_2$	$4.2 \times 10^{-12} \exp(180/T)$

kR1 $= [1.4058 \times 10^{-11} \exp(110/T) + 6.704 \times 10^{-12} \exp(70/T)]$ n

kR9 = kR9l/(1+kR9l/kR9h) 0.6**(1/(1+(log(kR9l/kR9h))^2)) where

kR9l $= 2.6 \times 10^{-30}(T/300)^{-3.2}$ n and kR9h $= 2.4 \times 10^{-11}(T/300)^{-1.3}$

kR6a $= 2.3 \times 10^{-13} \exp(600/T)$

kR6b $= 1.7 \times 10^{-33} \exp(1000/T)$ n

kR6c $= 1.0 + 1.4 \times 10^{-21} \exp(2200/T)$ H_2O

kR8a $= 7.2 \times 10^{-15} \exp(785/T)$

kR8b $= 4.1 \times 10^{-16} \exp(1440/T)$

kR8c $= 1.9 \times 10^{-33} \exp(725/T)$ n

2.4 Main chemical reactions mechanisms

In this section the main chemical reaction mechanisms will be described. This description explains the oxidation of CH_4 via HCHO and CO into CO_2 by OH, the influence of NO_x on the various paths that can be followed in this oxidation chain, and the resulting effect for O_3. The chemical scheme continuously converts CH_4 and NO_x via several intermediary products, which contains all kinds of feedback reactions, into CO_2 and HNO_3, respectively. Emissions of CH_4 and NO_x therefore end up as CO_2, which is not chemically active, and HNO_3, which is removed from the atmosphere by deposition. These chemical mechanisms influence the concentration of O_3 and that of other trace gases. The O_3 production and destruction by chemical reactions in the troposphere is more than the stratospheric input of O_3 in the troposphere. A more detailed description, involving all the reactions listed in Table 2.2 and more, can be found in e.g. Dentener (1993), Crutzen (1995) and AERONOX (1995). Here, only a brief overview will be given.

OH plays an important role in the oxidation of most trace gases. The primary source of OH is photodissociation of O_3 (J1) followed by reaction with water vapour (R2), i.e.

$$O_3 + H_2O + h\nu \rightarrow 2OH + O_2. \tag{2.13}$$

The oxidation of CH_4 by OH gives CH_3O_2 (R12). In NO-rich air this CH_3O_2 oxidizes to HCHO (R18). In NO-poor regions it leads to CH_3OOH (R15), which oxidizes further to HCHO (R17, J7). HO_2 and CH_3O_2 are products of the oxidation of CH_4, which form NO_2 when being combined with NO (R10, R18). Photolysis of NO_2 leads to O_3 production in the troposphere and returns the NO again (J3). The net reaction in the NO_x catalyzed oxidation of CH_4 is, e.g. (R12+R18+R10+2J3)

$$CH_4 + 4O_2 + h\nu \rightarrow HCHO + H_2O + 2O_3. \tag{2.14}$$

Note that HO_2 and NO can also lead to the destruction of O_3 (R7, R11). The HCHO which is produced in the oxidation of methane is eventually transformed into CO (J6, J7, R14). The net oxidation of HCHO to CO is, e.g. (J6+2R10+2J3)

$$HCHO + 4O_2 \rightarrow CO + 2OH + 2O_3. \tag{2.15}$$

Oxidation of CO into CO_2 occurs via (R13). The net change due to oxidation of CO is either (R13+R10+J3)

$$CO + 2O_2 \rightarrow CO_2 + O_3 \tag{2.16}$$

or (R13+R7)

$$CO + O_3 \rightarrow CO_2 + O_2. \tag{2.17}$$

Hence, the oxidation of CO may lead to ozone production as well as destruction. In the presence of sufficient NO_x reaction (R10) will dominate reaction (R7), so that the

oxidation of CO leads to ozone production. In general, net chemical production of O_3 occurs in the NO_x-rich and destruction in the NO_x-poor regions of the troposphere.

The ratio between NO and NO_2 is mainly determined by the reaction of NO with O_3 that produces NO_2 (R11) and photolysis of NO_2 that converts it into NO again (J3). These reactions are so fast that a steady state is reached where

$$\frac{NO_2}{NO} = \frac{k_{11}}{j_3} O_3 \tag{2.18}$$

with k_{11} the rate coefficient of (R11) and j_3 the photolysis rate of (J3). NO_2 can be converted to HNO_3 (R9), which is efficiently removed by dry and wet deposition.

The above mechanisms are driven by photolysis and occur during day time. At night the main sources of $O(^1D)$, OH and NO are absent, so that these concentrations rapidly diminish. The only reaction that is considered in CTMK is then the parameterized heterogeneous reaction

$$2NO_2 + O_3 + H_2O \rightarrow 2HNO_3 + O_2. \tag{2.19}$$

Chapter 3

Emission sets

The emission data used for this study include emissions by aircraft, surface sources and lightning. Emission sets for aircraft and surface sources have been prepared in accordance with the so-called European Renaissance scenario for the years 1990, 2003 and 2015. The results have been provided to us by Olivier (1995). The lightning sources have been taken from the AERONOX (1995) project. In Table 3.1 the total annual emissions for all components contained in each of the emissions sets are listed. The NO_x emissions are given in units of NO_2.

Table 3.1 Total annual emissions for the 1990, 2013 and 2015 scenario in Tg.

type	component	source	1990	2003	2015
3-D sources	NO_x	aircraft	1.79	2.75	4.49
		lightning	16.4	16.4	16.4
	CO	aircraft	0.67	1.02	1.82
surface sources	NO_x	anthropogenic	72	94	116
		biomass burning	14	15	16
		soils	22	22	22
	CH_4	anthropogenic	132	157	181
		biogenic	101	108	114
		biomass burning	53	57	60
		oceans	10	10	10
		rice	91	104	118
		ruminants	80	100	119
	CO	anthropogenic	383	437	483
		biomass burning	716	766	809
		oceans	162	162	162
		soils	166	166	166

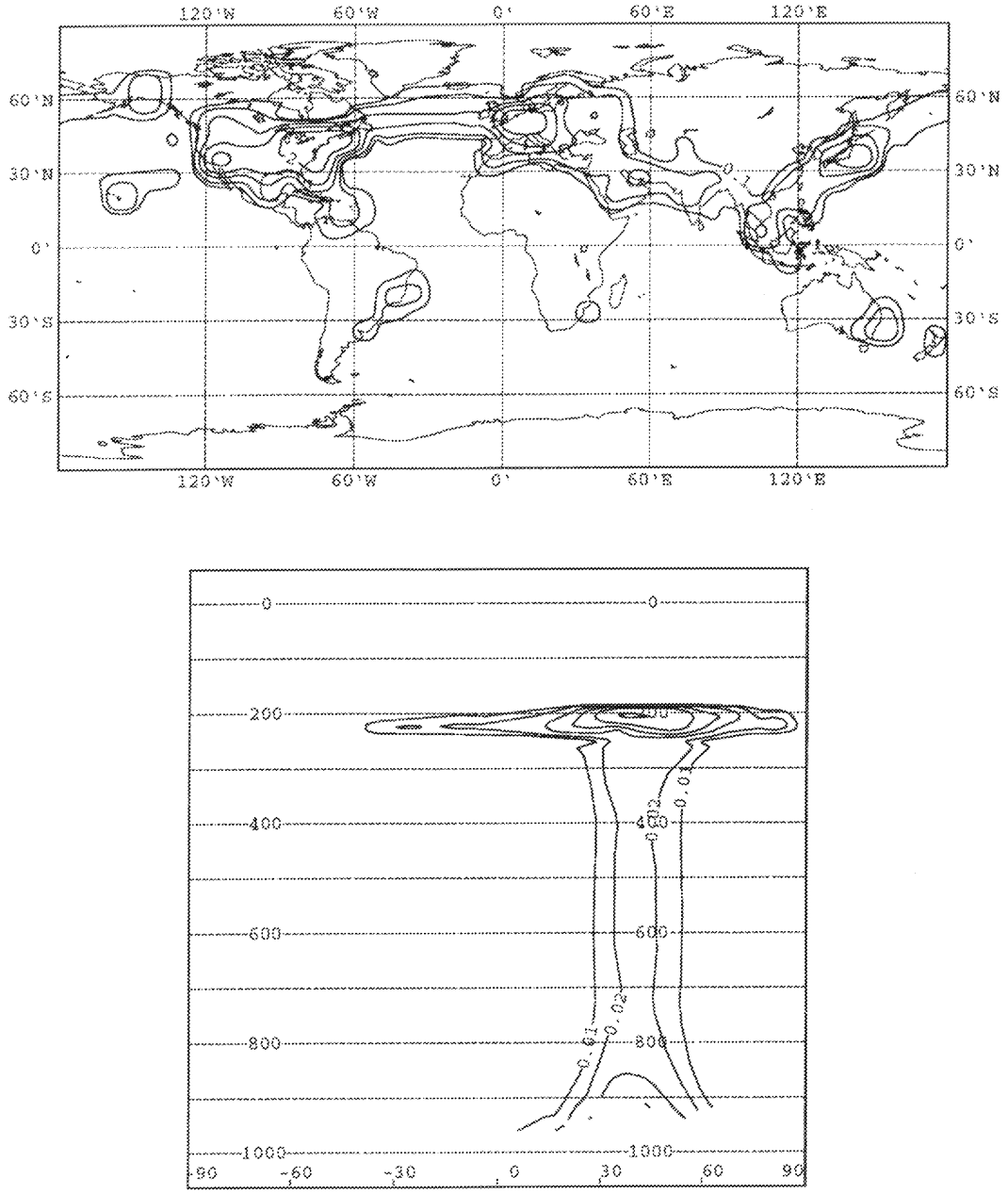

Figure 3.1 The geographical distribution of the vertically integrated (top) and latitude-altitude distribution of the zonal mean (bottom) NO_x emissions from aircraft for the 1990 scenario. Isolines for the annual mean emissions are drawn at 0.1, 0.2, 0.5, 1 and 2×10^{-9}g (NO_2) m^{-2} s^{-1} for the geographical and 0.01, 0.02, 0.05, 0.1, 0.2 and 0.5×10^{-12}g (NO_2) m^{-3} s^{-1} for the zonal mean distribution.

Below, a brief description of the emission sets will be given. This will be restricted to the NO_x emissions since the effect of CO and CH_4 on ozone is much smaller than that of NO_x. The emission data were provided to us on various grids. They have been converted to the grid of CTMK by filling each cell with the overlapping fractions of the original grid cells.

3.1 Aircraft emissions

The aircraft emissions of NO_x and CO have been derived from the Warren Spring Laboratory (WSL) database (McInnes & Walker, 1992). Regions/links and aircraft types/ranges extracted from this database have been used to estimate the spatial distribution of future emissions. The results are split in three regions with different seasonal time profiles. The transatlantic flights between northern America and western Europe and the flights within western Europe have a seasonal variation, whereas the remaining flights have constant emissions. The seasonal variation is the same for the aircraft emission scenarios for 1990, 2003 and 2015. The total annual emissions of NO_x and CO are listed in Table 3.1.

The annual mean of the geographical distribution of the vertically integrated, and the latitude-altitude distribution of the zonal mean emissions of NO_x by aircraft for 1990, 2003 and 2015 are presented in Figs. 3.1, 3.2 and 3.3, respectively. The main emissions occur over the US, Europe and Japan. The North Atlantic Flight Corridor (NAFC), and the routes from Europe to eastern Asia and from there to the US are clearly visible. The emissions over western Europe and in the NAFC are approximately 60 and 45 % larger for July compared to January. The geographical distributions are different for the 2003 and 2015 scenarios. The maximal emissions over the US, western Europe and Japan increase about 25, 50 and 140 %, respectively, from 1990 to 2003 and about 80, 120 and 380 %, respectively, from 1990 to 2015. The zonal mean distributions show that the main emissions areas are near the surface and near cruise altitudes at northern mid-latitudes. The seasonal variation for the zonal mean aircraft emissions is small. This is a result of the relatively large fraction (about 75 % for 1990) of the aircraft NO_x emissions that takes place outside the transatlantic route between northern America and western Europe and outside western Europe, and where no seasonal variation has been imposed. The zonal mean emissions near cruise altitudes at northern mid-latitudes increase by about 60 % from 1990 to 2003 and by about 160 % from 1990 to 2015.

The total annual emission of NO_x from aircraft used in this report is 1.79 Tg NO_2 for the 1990 scenario. Other aircraft emission databases are (i) WSL (McInnes & Walker, 1992) with 1.91 Tg for the reference year 1989; (ii) NASA (Wuebbles *et al.*, 1993) with 1.92 Tg for 1990, and (iii) ANCAT (1995) with 2.78 Tg for 1991/1992. All the numbers reported above have been scaled to a 100 % fuel match. The large difference between the ANCAT database and the other databases is mainly the result

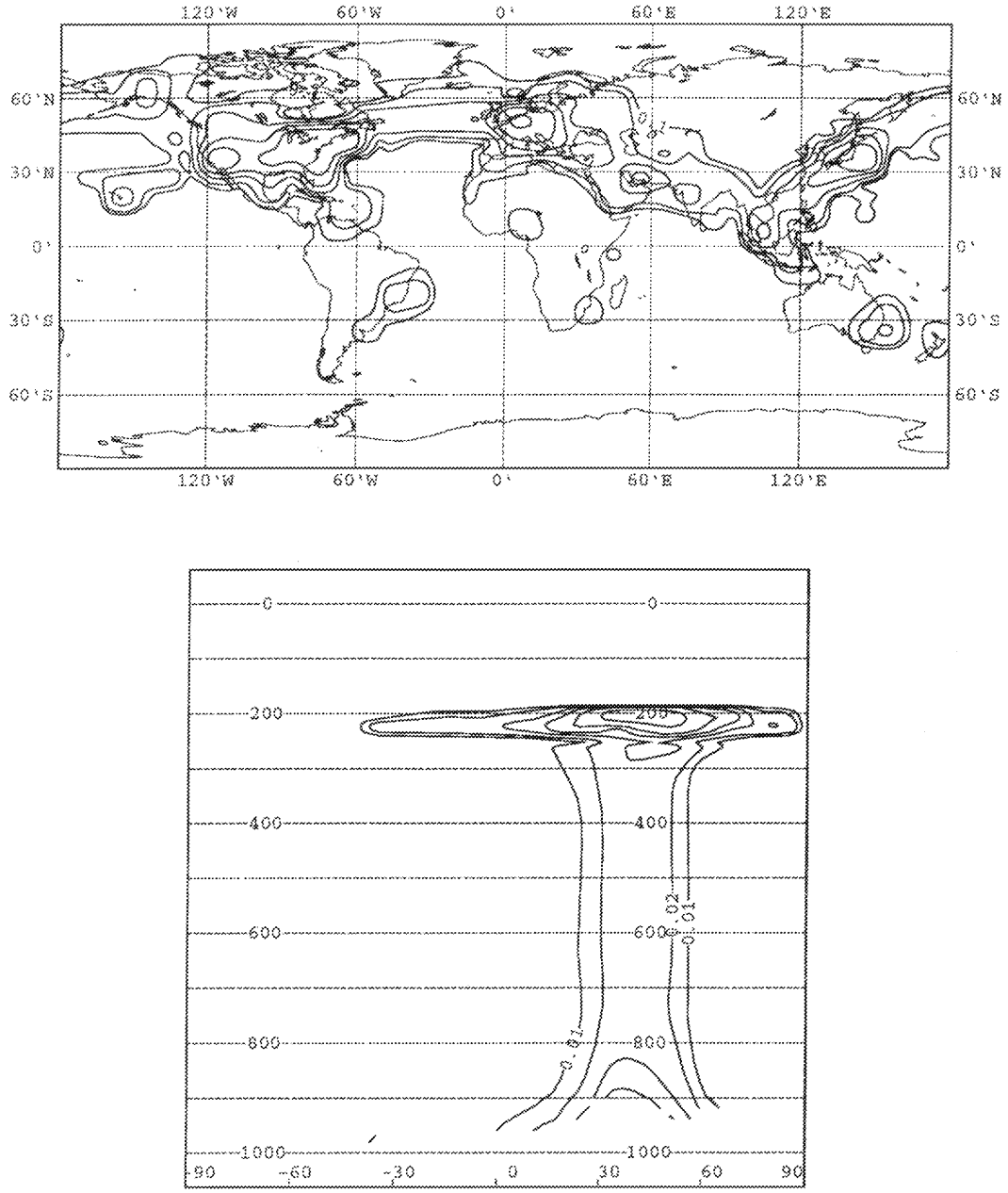

Figure 3.2 As Fig. 3.1, but for the 2003 aircraft emission scenario. Isolines are drawn at 0.1, 0.2, 0.5, 1, 2 and 5×10^{-9}g (NO_2) m^{-2} s^{-1} for the geographical and 0.01, 0.02, 0.05, 0.1, 0.2 and 0.5×10^{-12}g (NO_2) m^{-3} s^{-1} for the zonal mean distribution.

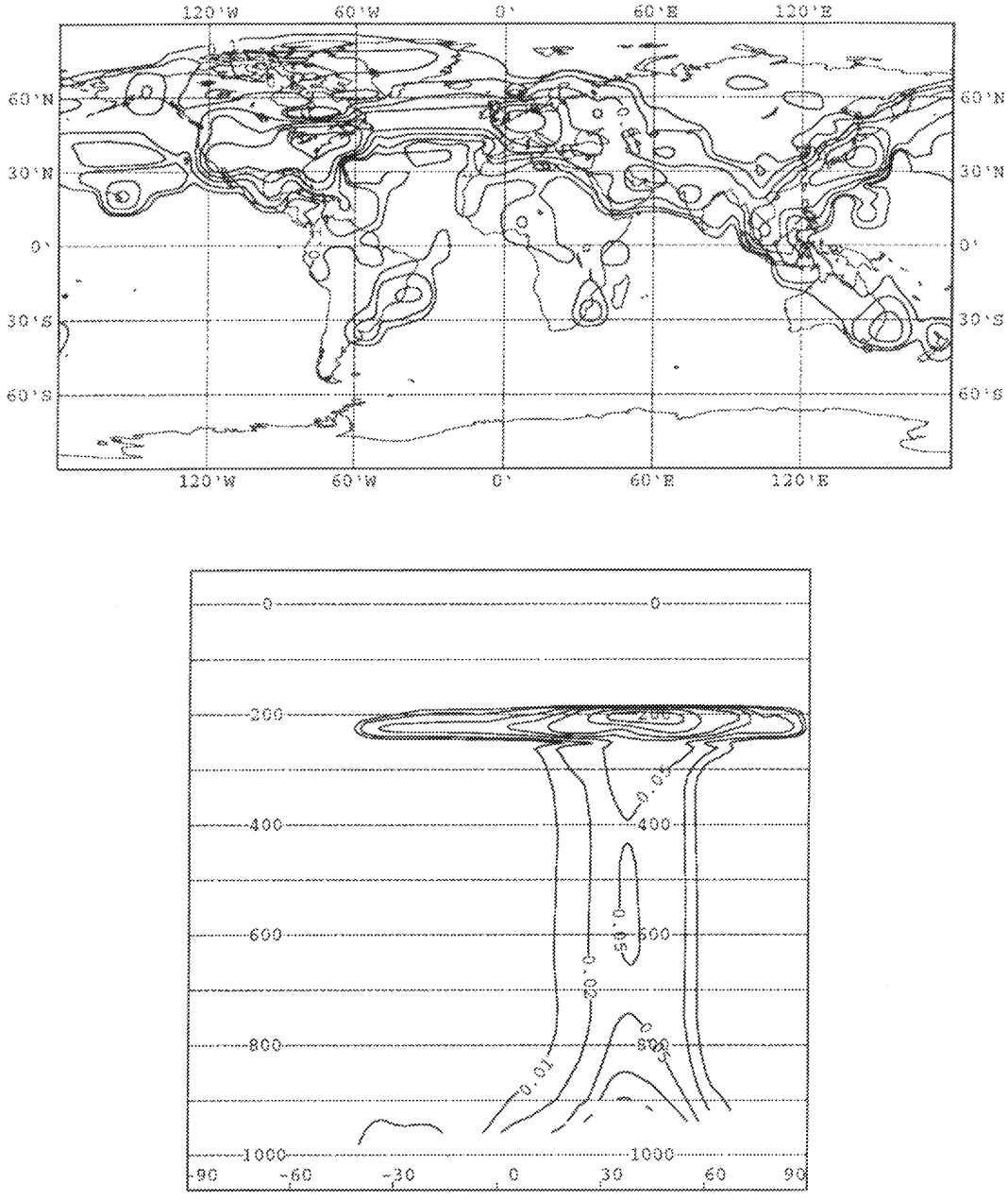

Figure 3.3 As Fig. 3.1, but for the 2015 aircraft emission scenario. Isolines are drawn at 0.1, 0.2, 0.5, 1, 2 and 5×10^{-9}g (NO_2) m^{-2} s^{-1} for the geographical and 0.01, 0.02, 0.05, 0.1, 0.2, 0.5 and 1×10^{-12}g (NO_2) m^{-3} s^{-1} for the zonal mean distribution.

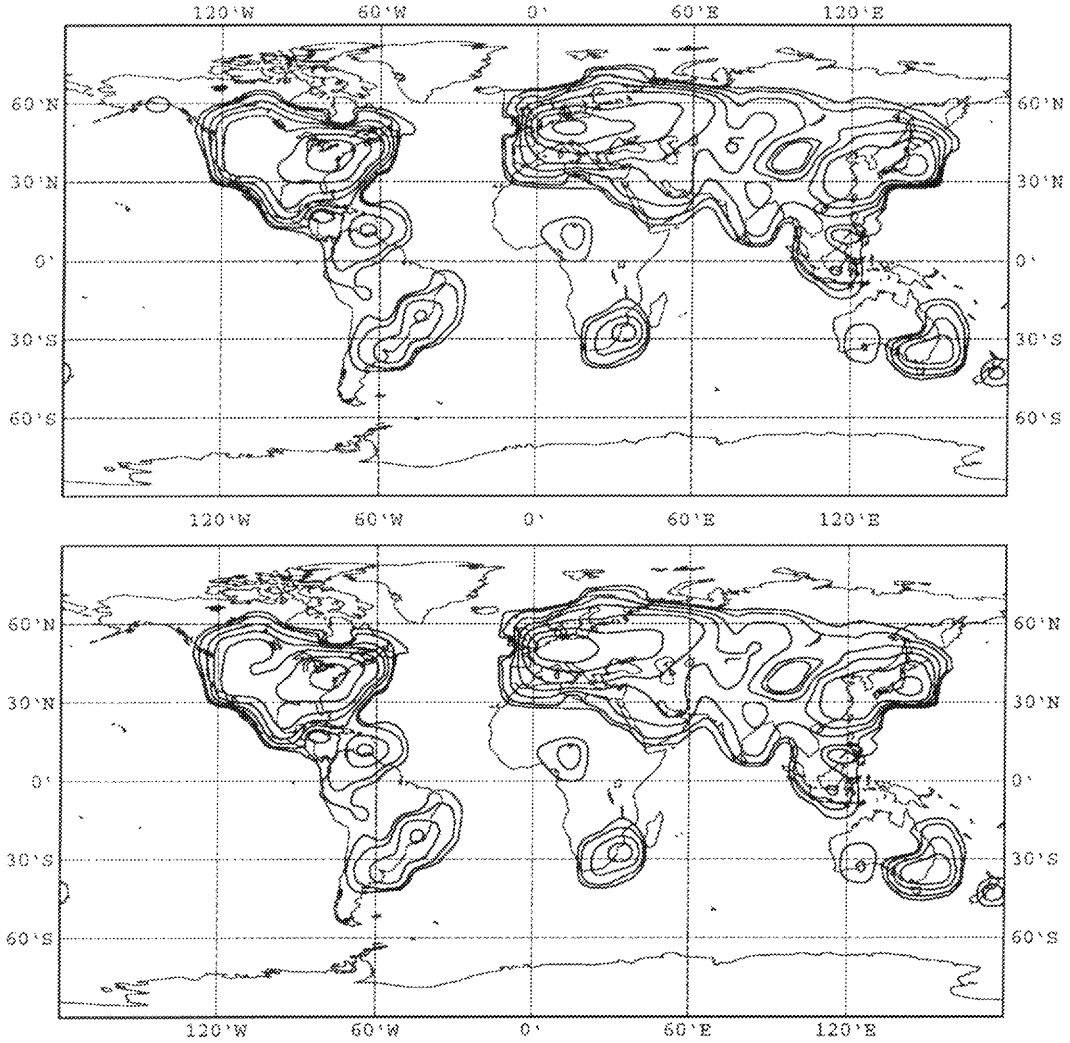

Figure 3.4 The geographical distribution of the anthropogenic NO_x emissions for January (top) and July (bottom) 1990. Isolines are drawn at 1, 2, 5, 10, 20, 50, 100 and only for July also at 200×10^{-9}g (NO_2) m^{-2} s^{-1}.

of a larger value for the emission index of NO_x, which indicates the amount of NO_x produced per kg of fuel. Geographical and zonal mean plots of the NO_x emissions from the other three aircraft emission databases mentioned above are given in the AERONOX (1995) report.

3.2 Surface emissions

The surface emissions have been derived from the databases of Muller (1992), but with updates and extensions (cf. Olivier, 1995). These emissions will be part of the Emission Database for Global Atmospheric Research (EDGAR). The emissions include various sources for NO_x, CO and CH_4. A full list is given in Table 3.1.

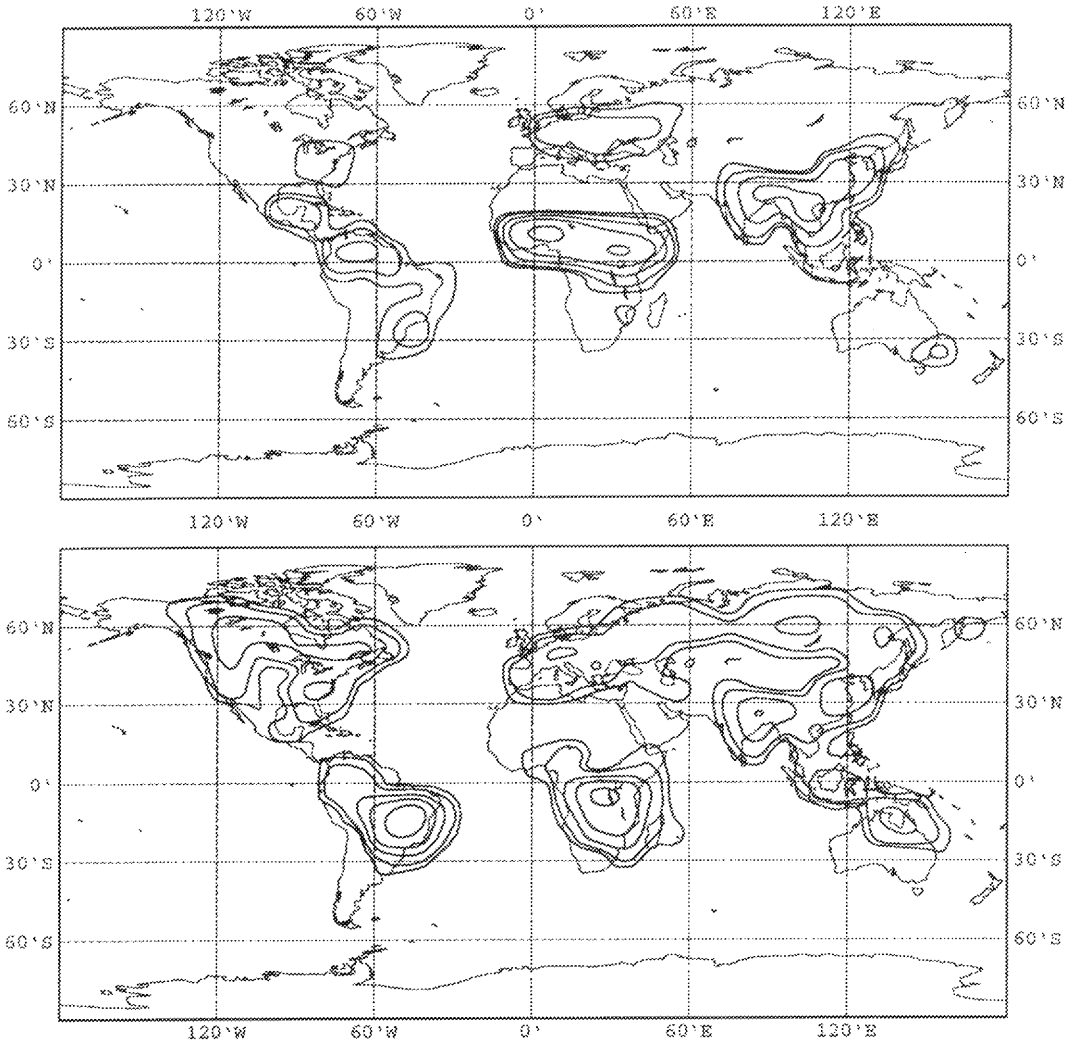

Figure 3.5 As Fig. 3.4, but for biomass burning and with isolines at 1, 2, 5, 10 and 20×10^{-9}g (NO_2) m^{-2} s^{-1}.

The geographical distributions of the NO_x surface sources due to anthropogenic sources, biomass burning and soils are given in Figs. 3.4, 3.5 and 3.6, respectively. The largest NO_x emissions come from anthropogenic sources in the industrialized areas of northern America, Europe and eastern Asia. The global anthropogenic NO_x emissions are about 15 % larger in January than for July. The geographical distributions for January and July are, however, similar. The distribution of the emissions from biomass burning for January and July clearly differ. In January these emissions occur mainly in the tropical regions north of the equator. In July the maximal emissions are located in the tropical regions south of the equator, but there are also emissions over the continents at northern mid-latitudes. The global NO_x emissions from biomass burning are about 40 % larger in July than in January. The global NO_x emissions from soils are about 65 % larger in July than in January. Again NO_x emissions over the continents

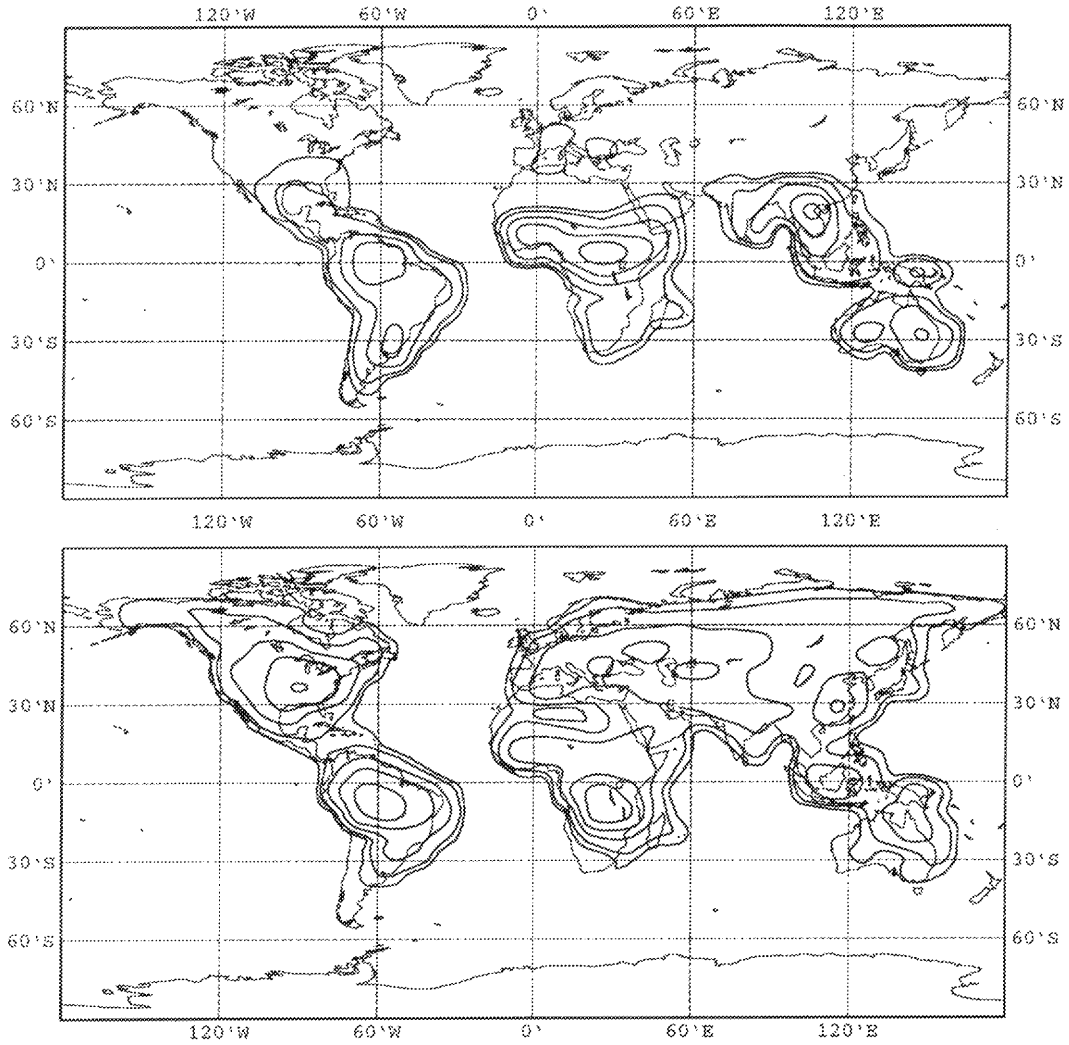

Figure 3.6 As Fig. 3.4, but for soils and with isolines at 1, 2, 5, 10 and 20×10^{-9}g (NO_2) m^{-2} s^{-1}.

at northern mid-latitudes occur in July and not in January and the maxima of the emissions near the tropics are located north of the equator in January and south of the equator in July. The total annual surface emissions of NO_x for the 1990 scenario (cf. Table 3.1) fall within the range given by IPCC (1992).

The NO_x surface emissions for 2003 and 2015 have the same distribution and seasonal dependence as for 1990, but the global emissions of the three surface sources have been scaled up to obtain the values indicated in Table 3.1. Thus, the NO_x emissions from soils do not change, whereas the emissions from biomass burning increase by 7 and 17 % from 1990 to 2003 and 2015, respectively, and the anthropogenic sources increase by 31 and 60 % over the same period.

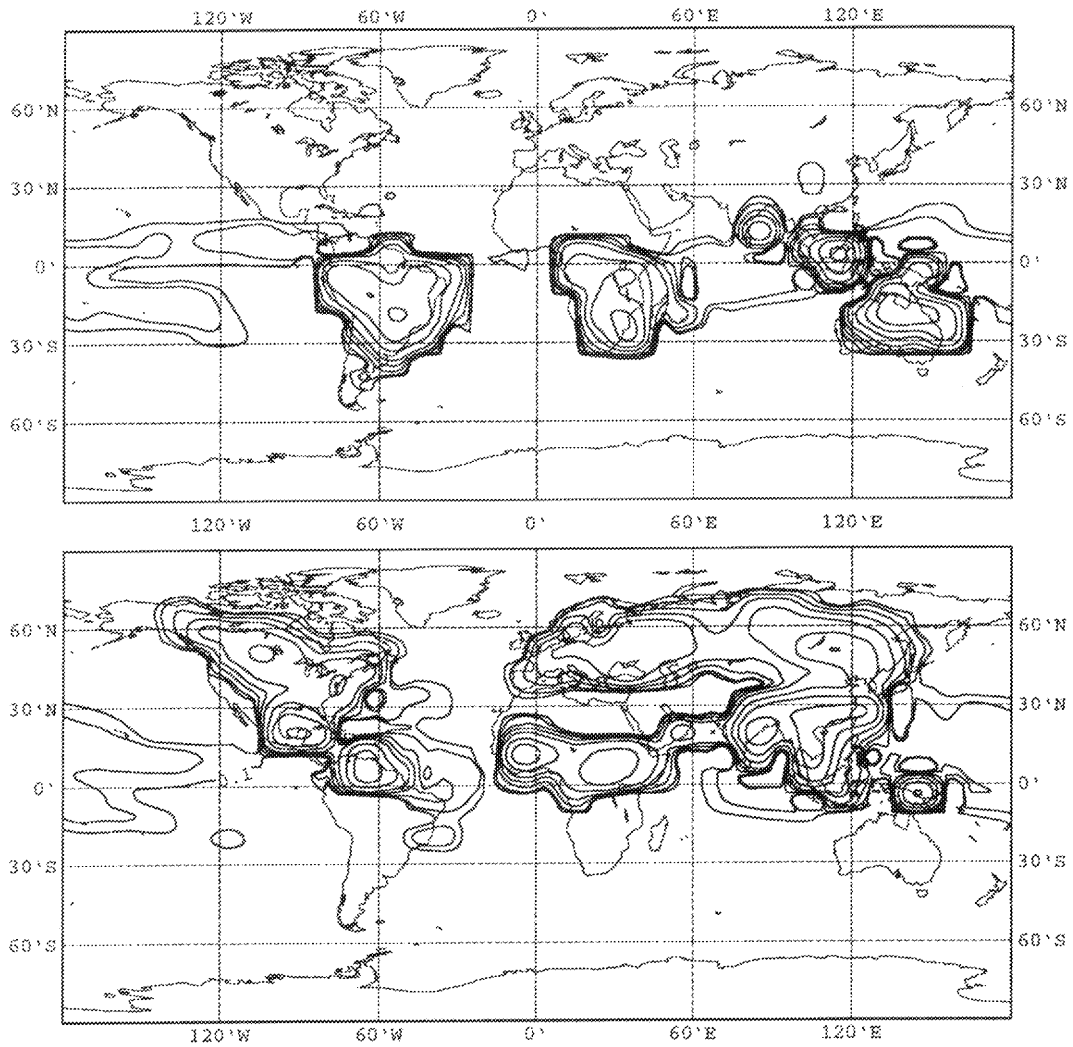

Figure 3.7 The geographical distribution of the vertically integrated NO_x production by lightning for January (top) and July (bottom). Isolines are drawn at 0.1, 0.2, 0.5, 1, 2, 5, 10 and 20×10^{-9}g (NO_2) m^{-2} s^{-1}.

3.3 Lightning emissions

The lightning sources of NO_x have been derived from the convective activity in the general circulation model ECHAM as part of the AERONOX (1995) project. The flash rates during convection events have been obtained by using the parameterization of Price & Rind (1990). The NO_x emissions from cloud-to-cloud and cloud-to-ground lightning have been computed by using the method described in Kowalczyk & Bauer (1982). This methods yields different results over oceans and continents and gives a latitudinal dependence. Vertically, the emissions have been distributed homogeneously between the surface and the cloud top height. The total annual NO_x production from lightning has been scaled to 16.4 Tg NO_2. This value has been proposed by Kowalczyk

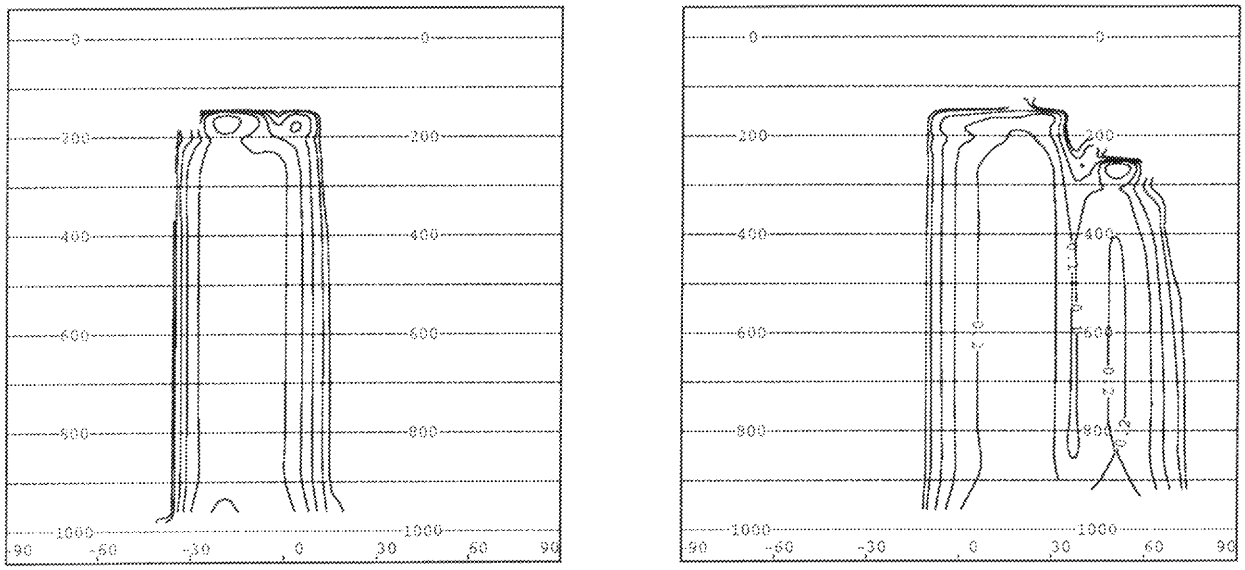

Figure 3.8 The latitude-altitude distribution of the zonal mean NO_x production by lightning for January (left) and July (right). Isolines are drawn at 0.01, 0.02, 0.05, 0.1, 0.2 $\times 10^{-12}$g (NO_2) m^{-3} s^{-1}.

& Bauer (1982) and lies within the broad range of estimates which can be found in the literature.

Figure 3.7 shows the geographical distribution of the lightning sources, while its latitude-altitude distribution is given in Fig. 3.8. The main production areas are located over the landmasses of the tropics in the summer hemisphere. The NO_x production by lightning is small over the oceans due to the low updraft velocities. The vertical extent of the sources is highest in the tropics (up to about 100 hPa) and decreases toward the poles. In January, the NO_x emissions from lightning are mainly between 10°N and 40°S, whereas for July they are between 10°S and 60°N. The global emissions for July are about 10 % higher than for January. This is a result of the larger land cover in the northern hemisphere.

Chapter 4

Background concentrations

CTMK has been run by using all the emissions given in Chapter 3 for a period of 2 years. The first year was used to initialize the model. The monthly mean results for NO_x and O_3 from the second year are discussed below. Zonal mean cross sections (latitude versus altitude) and geographical distributions at 200 hPa (longitude versus latitude) of NO_x and O_3 are considered for January and July. The zonal mean plots give an impression of the global distribution of the trace gases. These plots can also directly be compared with results obtained with 2-D models. The geographical distribution at 200 hPa is of particular interest because it is in the range of cruise altitudes of aircraft, where a large fraction of their emissions occurs. Both January and July are considered because the photochemistry in these months gives different results. Since the chemistry module contains only tropospheric chemistry, the results above 100 hPa are not considered.

In the following Sections 4.1, 4.2 and 4.3 the NO_x and O_3 concentrations obtained with the emission scenarios for 1990, 2003 and 2015, respectively, are presented. In all three scenarios the meteorological data of 1990 have been used. In Section 4.4 the results are discussed. [1]

4.1 1990 scenario

The zonal mean volume mixing ratios of NO_x and O_3 for January and July are presented in Fig. 4.1 for the 1990 emission scenario.

The distribution of NO_x reflects the presence of NO_x sources. The anthropogenic NO_x emissions dominate in the northern hemisphere. The NO_x concentrations in the lower troposphere are lower in summer due to the shorter lifetime of NO_x, which is a result of the higher solar insolation. The emissions from biomass burning and soils in the extra-tropics occur in the northern hemisphere in January, but in the southern hemisphere in July. Hence, the NO_x concentrations in the extra-tropics are higher during winter. This is further promoted by the lower OH concentrations during winter (cf. Kasibhatla *et al.*, 1991). Above the major surface source regions, the NO_x volume

[1] In this report the background concentrations have been obtained by using all emission data, i.e. including the aircraft emissions

mixing ratio first decreases with altitude, reaches a minimum, and increases again with altitude in the upper troposphere and lower stratosphere. In areas remote from industrialized regions, such as the southern polar region, the NO_x volume mixing ratio generally increases with altitude. In the upper troposphere near 200 hPa, the NO_x concentrations for July are larger (smaller) in the northern (southern) hemisphere than the corresponding concentrations for January, since the lightning sources are largest during summer. There is no clear evidence of the NO_x lightning sources in the lower troposphere near the tropics. This is probably the result of the short lifetime of NO_x due to the high photochemical activity and the effective wet deposition in the tropics.

Some general features of the ozone distribution, such as the higher values in the northern than in the southern hemisphere, the excursion of low values near the equator towards high altitudes, the generally increasing values towards the poles at high altitudes, and the characteristic dip near 30° north, are also obtained with other model computations (cf. e.g. Crutzen & Zimmermann, 1991) and can be seen in observations as well (cf. e.g. Crutzen, 1995). The zonal mean ozone distribution for January and July generally show the same features, but the ozone values in the lower troposphere of the southern hemisphere is lower in January compared to July due to the lower NO_x values. The ozone volume mixing ratio increases with altitude from the surface to the lower stratosphere. The characteristic sine curve of the 100 ppbv isoline results from the ozone flux from the stratosphere into the troposphere at mid-latitudes and the upward transport of low ozone values in the tropics due to convection. The stratosphere-troposphere flux is higher in the northern than in the southern hemisphere, and higher in winter than in summer.

The geographical distributions of NO_x and O_3 for January and July at 200 hPa are shown in Fig. 4.2. In January, the NO_x emissions from lightning dominate at 200 hPa over the continents south of the equator. There are local minima over the equatorial regions of the Pacific and the Indian ocean due to the absence of NO_x sources. The NO_x emissions from aircraft are visible east of the US and western Europe. In July, the aircraft and lightning sources are closer together and the effect of aircraft cannot easily be separated. The NO_x volume mixing ratio generally increases from the poles to the equator. The maximal values are reached south (north) of the equator in January (July). In the northern polar region the NO_x concentrations are higher in July, whereas they are higher in January in the southern polar region.

The isocontours at 200 hPa for O_3 are more zonally symmetric due to the larger lifetime of O_3 compared to NO_x. The low ozone values over the equatorial regions of the Pacific and the Indian ocean coincide with the local minima for NO_x. At 200 hPa the ozone volume mixing ratio generally increases towards the poles, and the values for July are smaller than for January.

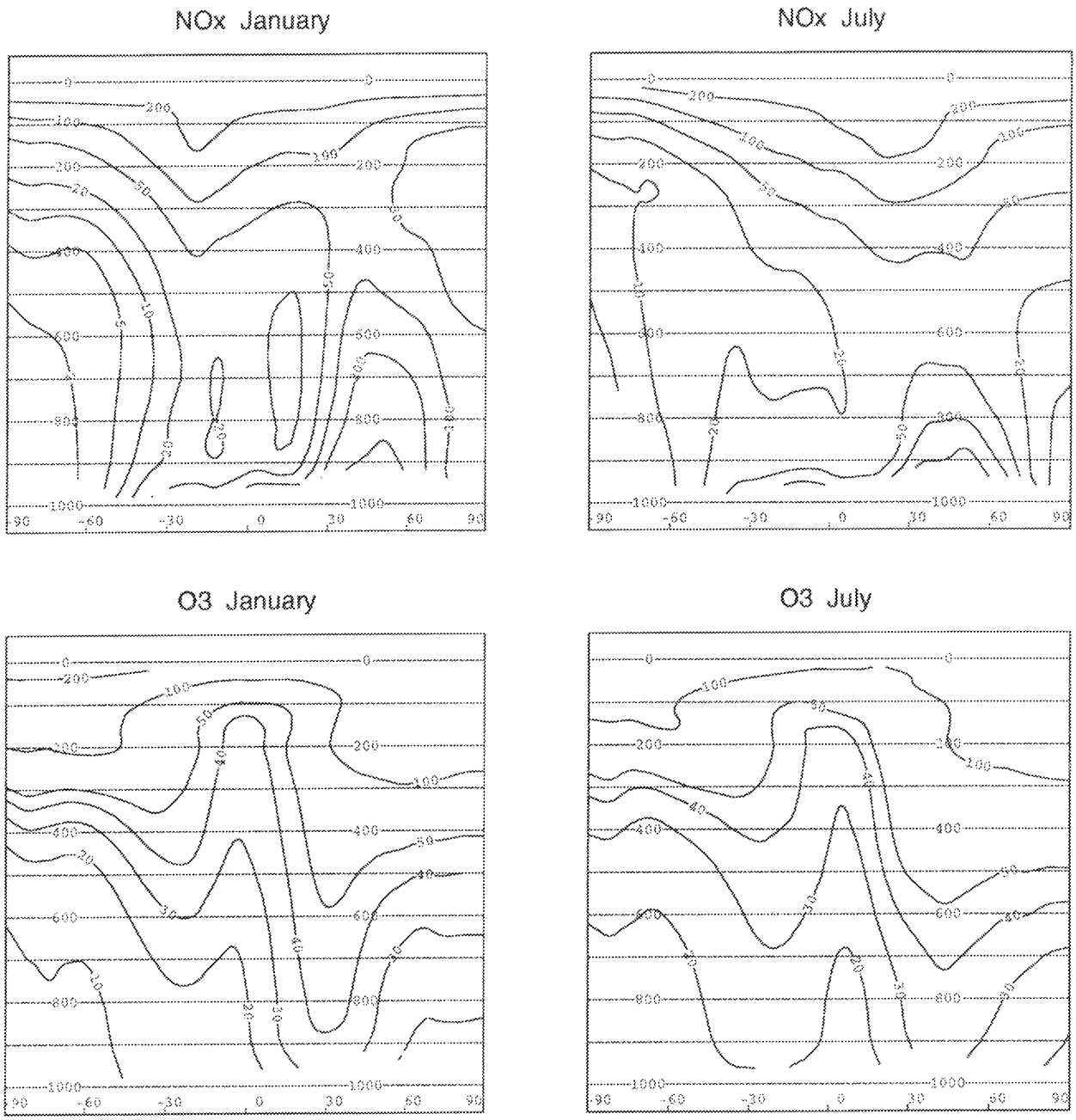

Figure 4.1 Zonal and monthly mean volume mixing ratios of NO_x (top) and O_3 (bottom) in ppbv and pptv, respectively, for January (left) and July (right). The dashed horizontal lines indicate pressure levels at 100 hPa intervals. Isolines are drawn at 2, 5, 10, 20, 50, 100 and 200 pptv for NO_x and 10, 20, 30, 40, 50, 100 and 200 ppbv for O_3.

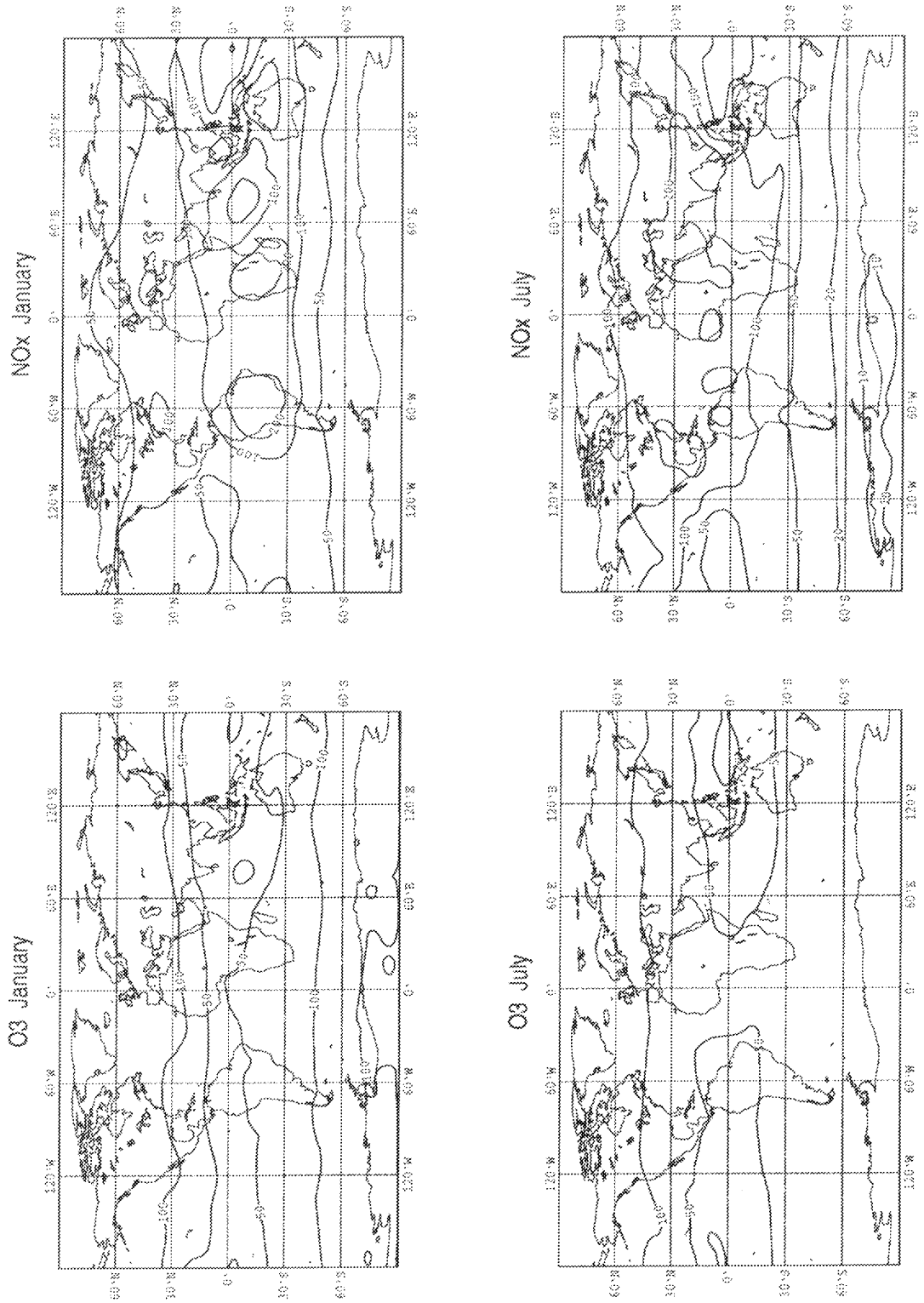

Figure 4.2 As Fig. 4.1, but for 200 hPa. Isolines are drawn at 10, 20, 50, 100 and 200 pptv for NO_x and 20, 50 and 100 ppbv for O_3.

4.2 2003 scenario

The volume mixing ratios of NO_x and O_3 obtained with the emission scenario for 2003 are described here. The relative increase in these species compared to the 1990 scenario is given in Figs. 4.3 and 4.4 for the zonal mean and 200 hPa results, respectively.

The largest increase in the zonal mean volume mixing ratio of NO_x comes from the increasing aircraft emissions. The zonal mean NO_x near cruise altitudes at northern mid-latitudes increases maximally more than 40 % from 1990 to 2003 in January and more than 25 % in July. The difference between January and July is a result of the longer lifetime of NO_x in January and the lower NO_x background for 1990 near cruise altitudes at northern mid-latitudes in January. NO_x also increases in the lower troposphere at northern mid-latitudes due to the 30 % increase of the anthropogenic sources. This increase in zonal mean NO_x is more than 20 % in January and 10 % in July, although the background concentrations for 1990 are also higher in January. In January, the NO_x increases in the entire troposphere poleward of 30°N more than 20 %. NO_x in the lower troposphere at southern mid-latitudes increases about 5 % in January and 10 % in July, since the increasing emissions from biomass burning occur in the southern hemisphere in July. While the maximal increases due to aircraft and anthropogenic emissions occur close to the location of the sources, the maximal increase in the southern hemisphere occurs south of the biomass burning sources. There is only a small increase of NO_x in the equatorial region since the NO_x lightning source, which dominate there, is identical to the one used in the 1990 scenario.

The zonal mean O_3 increases maximally 5 % in January and 7 % in July from 1990 to 2003. These maxima do not occur near cruise altitudes at northern mid-latitudes, but near the surface, where the background O_3 for 1990 is lower. The location of the maxima are south and north of the surface maxima for NO_x in January and July, respectively. The ozone in the lower and middle troposphere of the southern hemisphere poleward of 30°S increases typically 3 %.

In January, the NO_x distribution at 200 hPa increases more than 20 % poleward of 30°N with maxima of up to 50 % north-east of the main aircraft emission areas over the US, Europe and Japan. In the southern hemisphere the increase is typically 3 % with local minima in the region containing the main lightning sources. In July, the increase in the northern hemisphere is smaller (up to 30 % in the NAFC and south of Japan), but it is larger in the southern hemisphere (more than about 6 %). This is a result of the larger (smaller) NO_x background for 1990 in the northern (southern) polar region in July compared to January.

The O_3 distribution at 200 hPa in January increases typically 2 % at northern mid-latitudes and 1 % in the southern hemisphere. The maximal increase of 3 % occurs over the equatorial region of the west Pacific. Due to the large lifetime of O_3 the produced increase of O_3 can be transported to this O_3 poor area. This is not the case for NO_x since its lifetime is shorter. In July, the increase is typically 5 % at northern

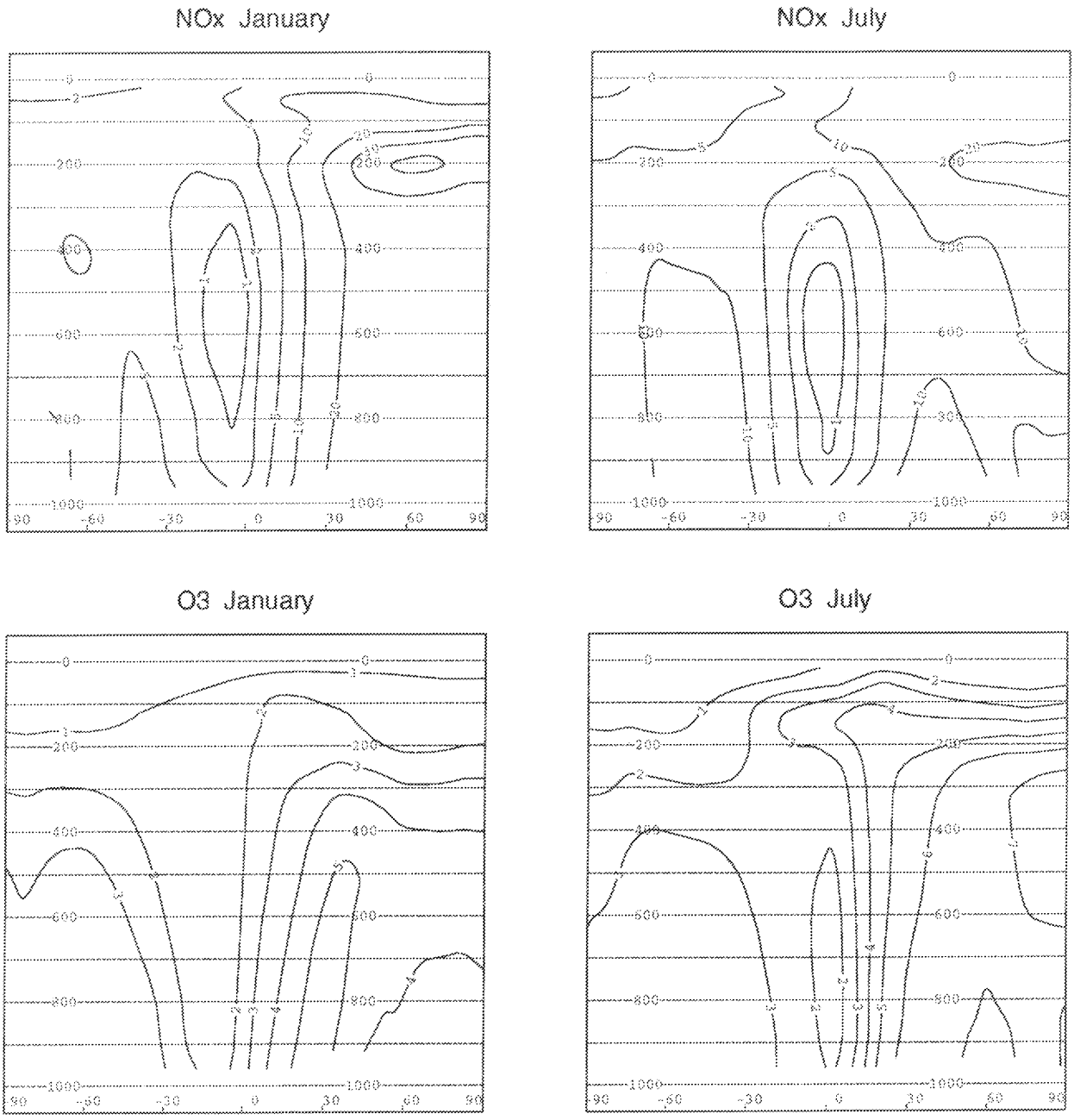

Figure 4.3 Relative increase of zonal and monthly mean volume mixing ratios for 2003 compared to 1990 of NO_x (top) and O_3 (bottom) for January (left) and July (right). Isolines are drawn at 1, 2, 5, 10, 20, 30 and 40 % for NO_x and 1, 2, 3, 4, 5, 6 and 7 % for O_3.

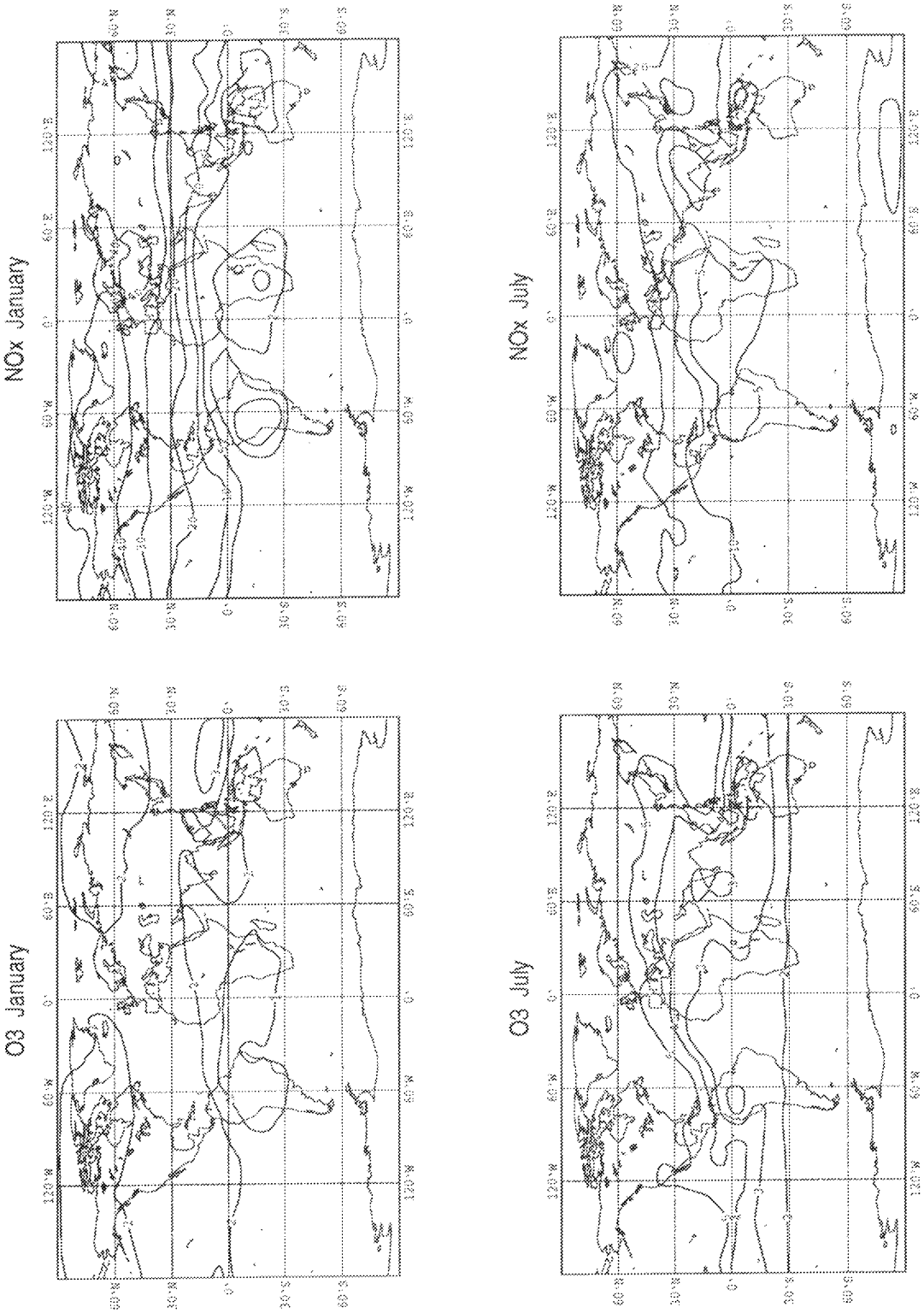

Figure 4.4 As Fig. 4.3, but for 200 hPa. Isolines are drawn at 1, 2, 5, 10, 20, 30 and 40 % for NO_x and 1, 2, 3, 4 and 5 % for O_3.

mid-latitudes and 1-3 % in the southern hemisphere. The higher contribution in July than for January is in agreement with the lower O_3 concentrations in July compared to January.

4.3 2015 scenario

Finally, the relative increase of NO_x and O_3 for the 2015 scenario is presented in Figs. 4.5 and 4.6. These results generally show the same features as the results for the 2003 scenario. Of course, the increase in NO_x and O_3 concentrations for the 2015 scenario is larger than for the 2003 scenario.

The changes in zonal mean NO_x for January and July amount to, respectively, up to 100 % and more than 50 % near cruise altitudes at northern mid-latitudes, and more than 50 % and about 20 % in the lower troposphere at northern mid-latitudes and maximally 10 % and about 20 % in the southern hemisphere. The zonal mean O_3 in the northern hemisphere increases by 5-10 % in January and by 10 % in July. A minimal ozone increase of 2 % occurs at about 20°S in January and is about 4 % over the equator in July. In the southern hemisphere the changes are 5-7 %.

In January the NO_x distribution at 200 hPa increases more than 50 % poleward of 30°N with a maximum of almost 130 % north-east of Japan and 7-9 % in the southern hemisphere. Increases of less than 5 % occur over the continents in the tropics south of the equator. For July, the changes are smaller in the northern hemisphere, with maxima of 70 % over the NAFC and 60 % south of Japan. The increase in the southern hemisphere is 10-20 % in July. The ozone change at 200 hPa in the northern hemisphere is 4-5 % in January and about 10 % for July. The maxima of 6-7 % occur over the equatorial region of the Pacific in January while the maxima of 12 % occur over Greenland and the western part of the equatorial Pacific in July. In the southern hemisphere the increase is 3 % for January and ranges between 2 % in the polar region and 10 % near the equator for July.

4.4 Discussion

The NO_x and O_3 fields obtained with CTMK for the 1990 scenario seem realistic. The results are similar to those obtained with CTMK, but by using other emission data (cf. Wauben *et al.*, 1994; AERONOX, 1995). They also compare well with the NO_x and O_3 fields obtained by other 2-D and 3-D models (cf. AERONOX, 1995) as well as with observations (cf. e.g. Crutzen, 1995 and Ehhalt & Drummond, 1988). In accordance with scarcely available observations, the volume mixing ratios of NO_x exceed 500 pptv over the main emission areas at northern mid-latitudes and are in the order of 100 pptv near cruise altitudes. Compared to other models and with observations the O_3 concentrations in CTMK seem to small. Some preliminary calculations indicate that prescribing the O_3 concentrations at 50 hPa according to climatological data (cf.

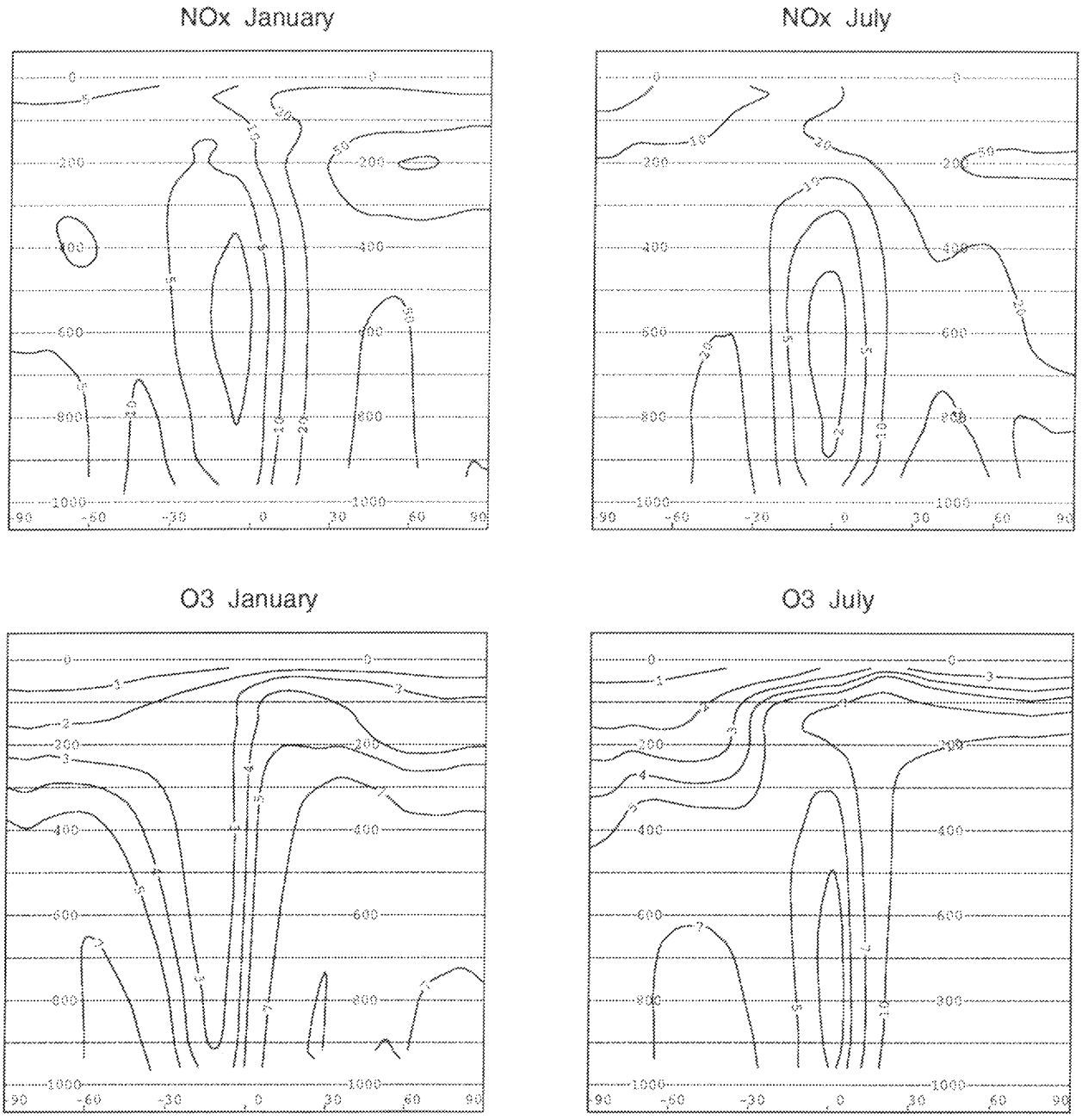

Figure 4.5 As Fig. 4.3, but for the 2015 scenario. Isolines are drawn at 2, 5, 10, 20, 50 and 100 % for NO_x and 1, 2, 3, 4, 5, 7 and 10 % for O_3.

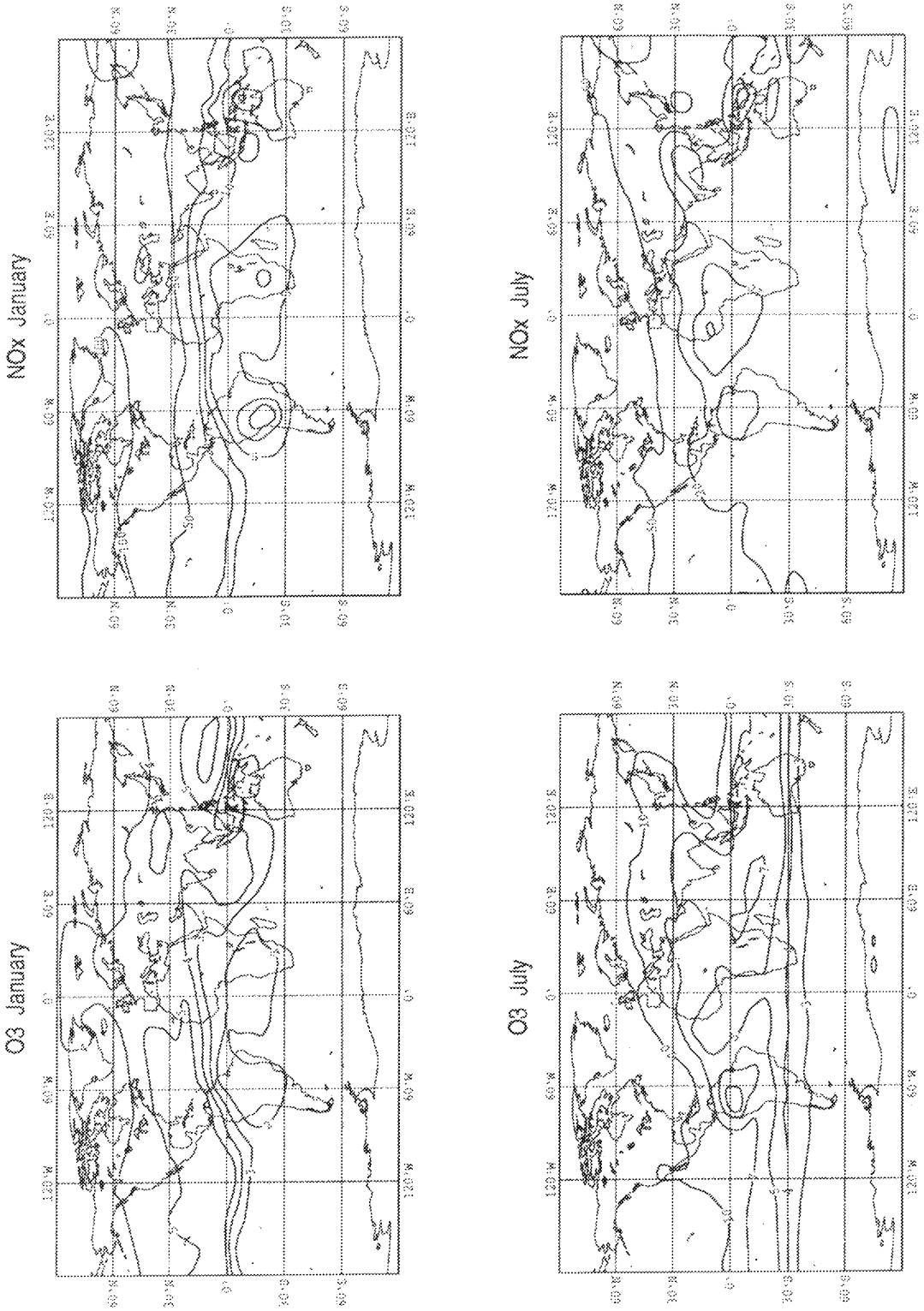

Figure 4.6 Relative increase of monthly mean volume mixing ratios at 200 hPa for 2015 compared to 1990 of NO_x (top) and O_3 (bottom) for January (left) and July (right). Isolines are drawn at 1, 2, 5, 10, 50 and 100 % for NO_x and 2, 3, 4, 5, 7 and 10 % for O_3.

Table 4.1 Relative increase (in %) of the NO_x and O_3 concentrations for the 2003 and 2015 scenarios compared to the 1990 scenario. Typical values are reported for both the southern (SH) and northern hemisphere (NH) as well as for cruise altitudes at northern mid-latitudes (CR).

2003	SH		NH		CR	
	January	July	January	July	January	July
NO_x	4	10	20	10	40	25
O_3	2	3	4	6	2	5
2015	SH		NH		CR	
	January	July	January	July	January	July
NO_x	8	20	50	20	100	60
O_3	5	6	8	10	4	10

Fortuin & Langematz, 1995) gives a larger cross tropopause flux of ozone than the prescribed O_3 flux (cf. Sect. 2.3) which has been used in CTMK for the calculations that have been used for this report. Prescribing the O_3 concentrations also given better agreement when comparing ozone profiles with observed profiles, especially in the upper troposphere.

In Table 4.1 typical values are given for the relative increase of NO_x and O_3 concentrations for the 2003 and 2015 scenarios compared to the 1990 scenario for three regions. The concentrations of the species increase from 1990 to 2003 and further from 2003 to 2015. This increase is largest in the northern hemisphere and especially near cruise altitudes at northern mid-latitudes for NO_x. A region of low NO_x increase due to the constant NO_x emissions from lightning can be found in the tropics.

Chapter 5

Effects of aviation

Computations similar to the ones reported in Chapter 4, but without taking the aircraft emissions into account have been performed. Differences between the results obtained with and without aircraft emissions show the effect of aircraft on the atmospheric composition. The absolute and relative contribution of aircraft emissions to the zonal mean and geographical distribution of tropospheric NO_x and O_3 is presented in this Section. The geographical distribution at 200 hPa is considered because it is in the range of cruise altitudes used by aviation. Again monthly mean fields of NO_x and O_3 for January and July are shown in the following sections for the 1990, 2003 and 2015 scenario.

5.1 1990 scenario

The differences between the zonal and monthly mean NO_x obtained with and without aircraft emissions are shown in Fig. 5.1 for January and July. The absolute contribution of aircraft to the zonal mean NO_x is typically 20 pptv near 200 hPa at northern mid-latitudes, with maxima of 37 and 30 pptv in January and July, respectively. The contribution of aircraft NO_x extends to lower altitudes at northern mid-latitudes and to a lesser degree at southern mid-latitudes. In the lower and middle troposphere the contribution is generally less than 1 pptv, except at northern mid-latitudes. The relative contribution of aircraft to zonal mean NO_x near 200 hPa at northern mid-latitudes reaches values of about 50 and 30 % for January and July, respectively, with secondary maxima of about 2 and 6 % at southern mid-latitudes. The higher relative contribution at northern mid-latitudes in January is a result of the lower NO_x background concentrations in January compared to July. At 200 hPa in southern mid-latitudes the reverse is true, i.e. the background concentrations are higher in January than in July. The relative contribution in the lower and middle troposphere is less than 1 % except between 10 and 30°N where the relative contribution is about 2 %. These maxima are located at the southern edge of the high NO_x regions near the major sources in northern mid-latitudes.

The differences between the monthly mean NO_x at 200 hPa obtained with and without aircraft emissions is presented in Fig. 5.2. The absolute contribution of aircraft

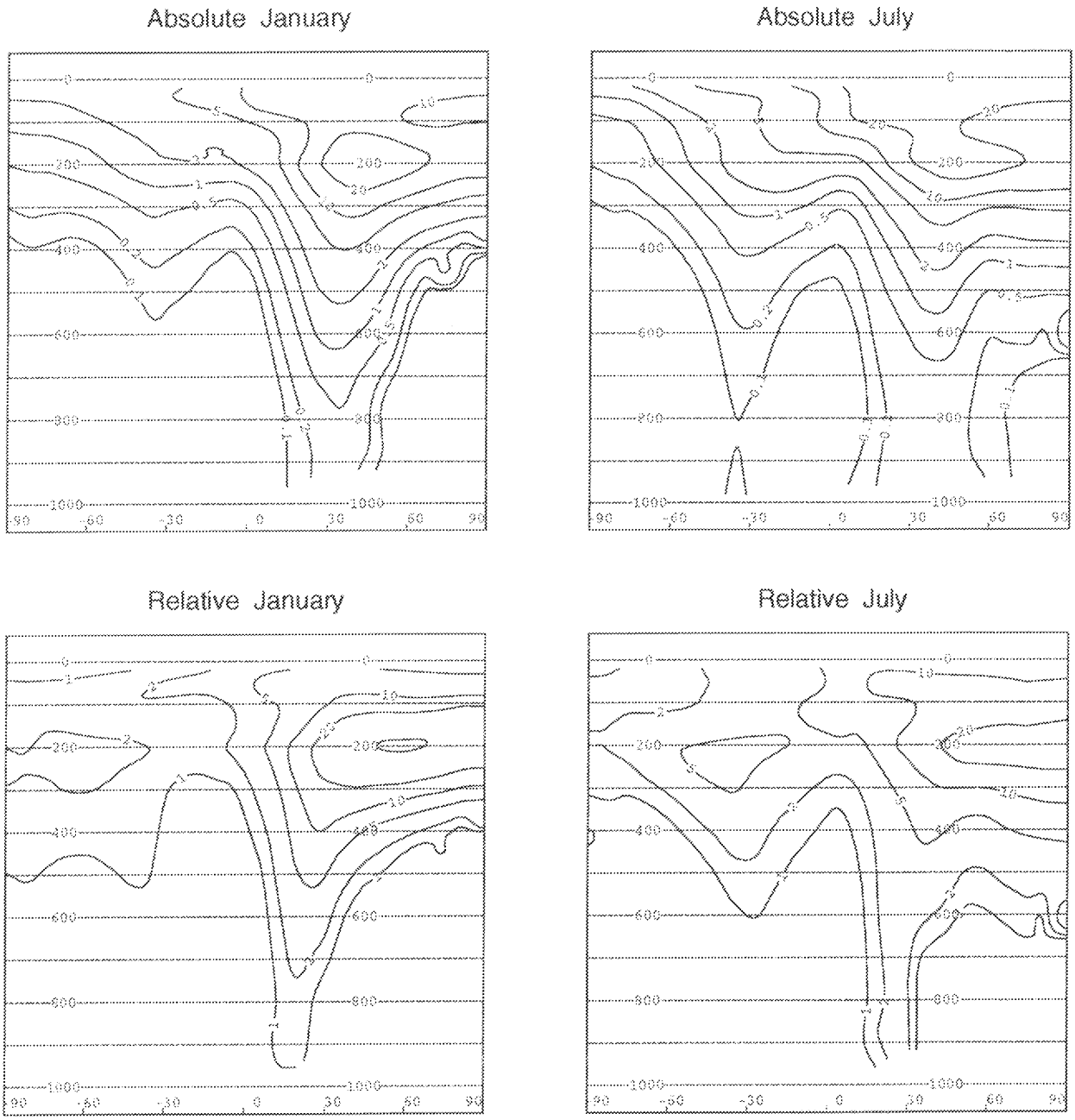

Figure 5.1 Differences between zonal and monthly mean volume mixing ratios for NO_x obtained with and without aircraft emissions for the 1990 scenario. The contribution of aircraft is given in absolute values (top: in pptv) and in relative values (bottom: in percent) for January (left) and July (right). Isolines are drawn at 0.1, 0.2, 0.5, 1, 2, 5, 10 and 20 pptv (top) and 1, 2, 5, 10, 20 and 50 % (bottom).

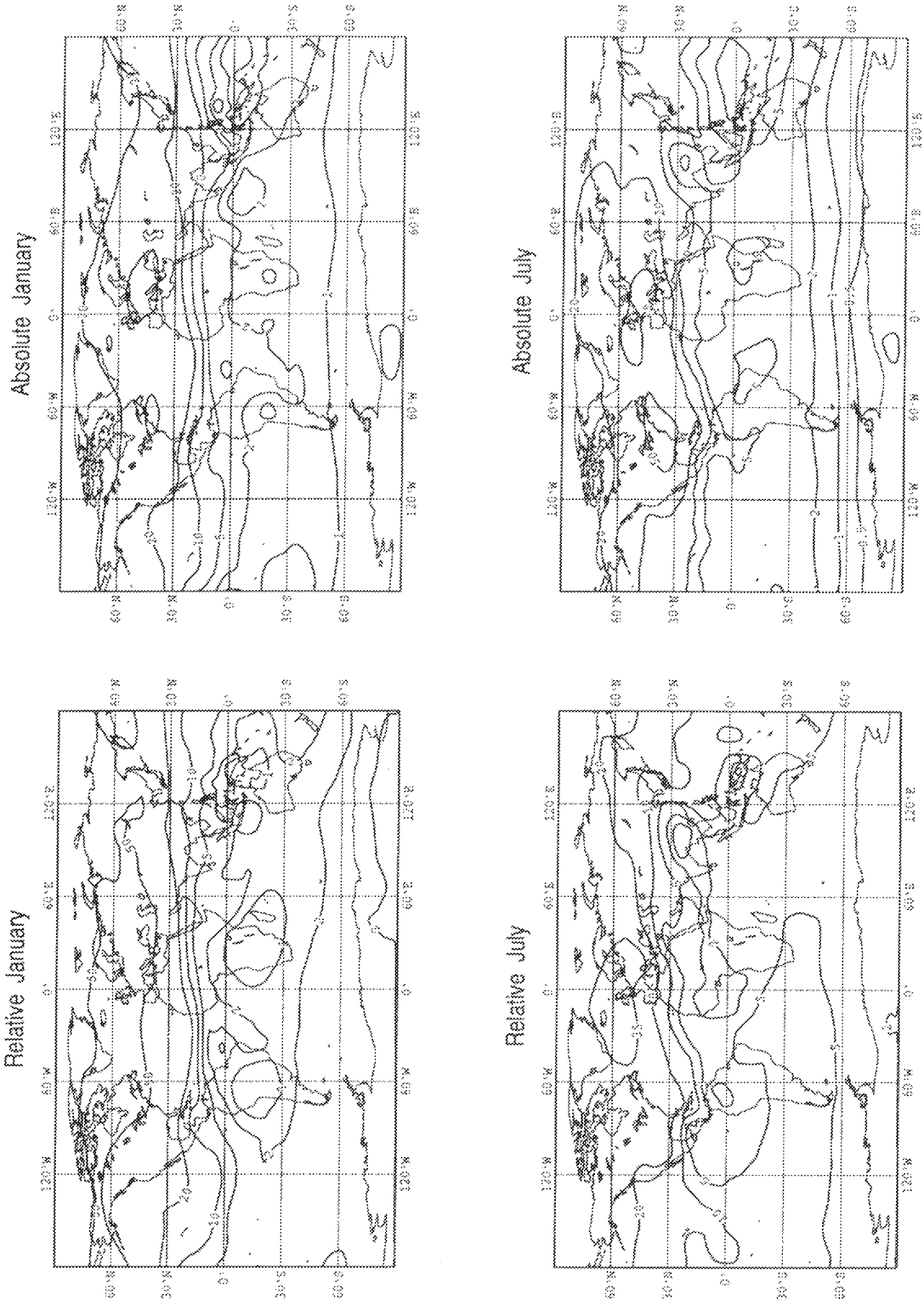

Figure 5.2 As Fig. 5.1, but for 200 hPa. Isolines are drawn at 0.5, 1, 2, 5, 10, 20 and 50 pptv (top) and 1, 2, 5, 10, 20 % and 35 or 50 % (bottom).

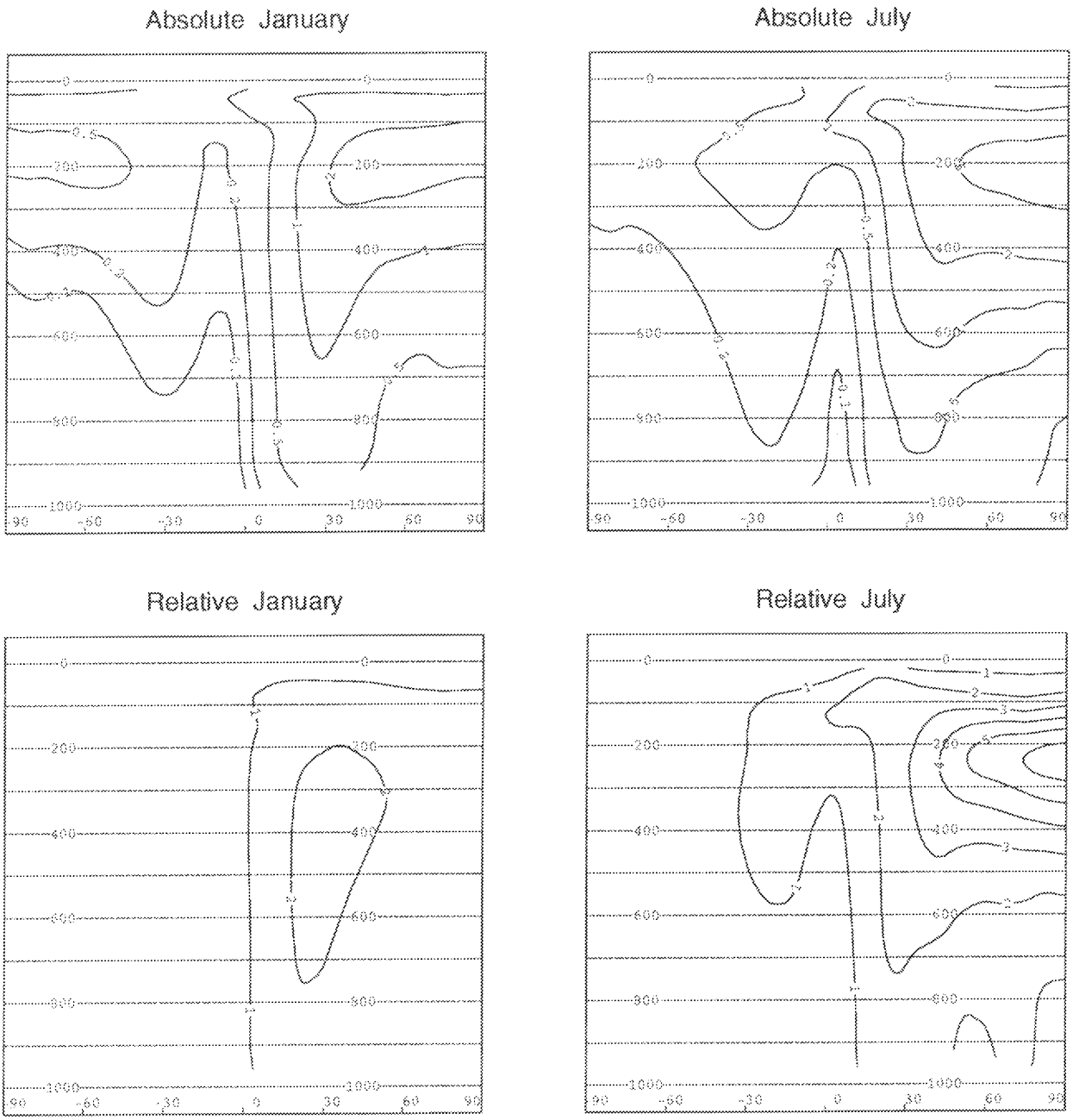

Figure 5.3 As Fig. 5.1, but for ozone. Isolines are drawn at 0.1, 0.2, 0.5, 1, 2 and 5 ppbv (top) and 1, 2, 3, 4, 5 and 6 % (bottom).

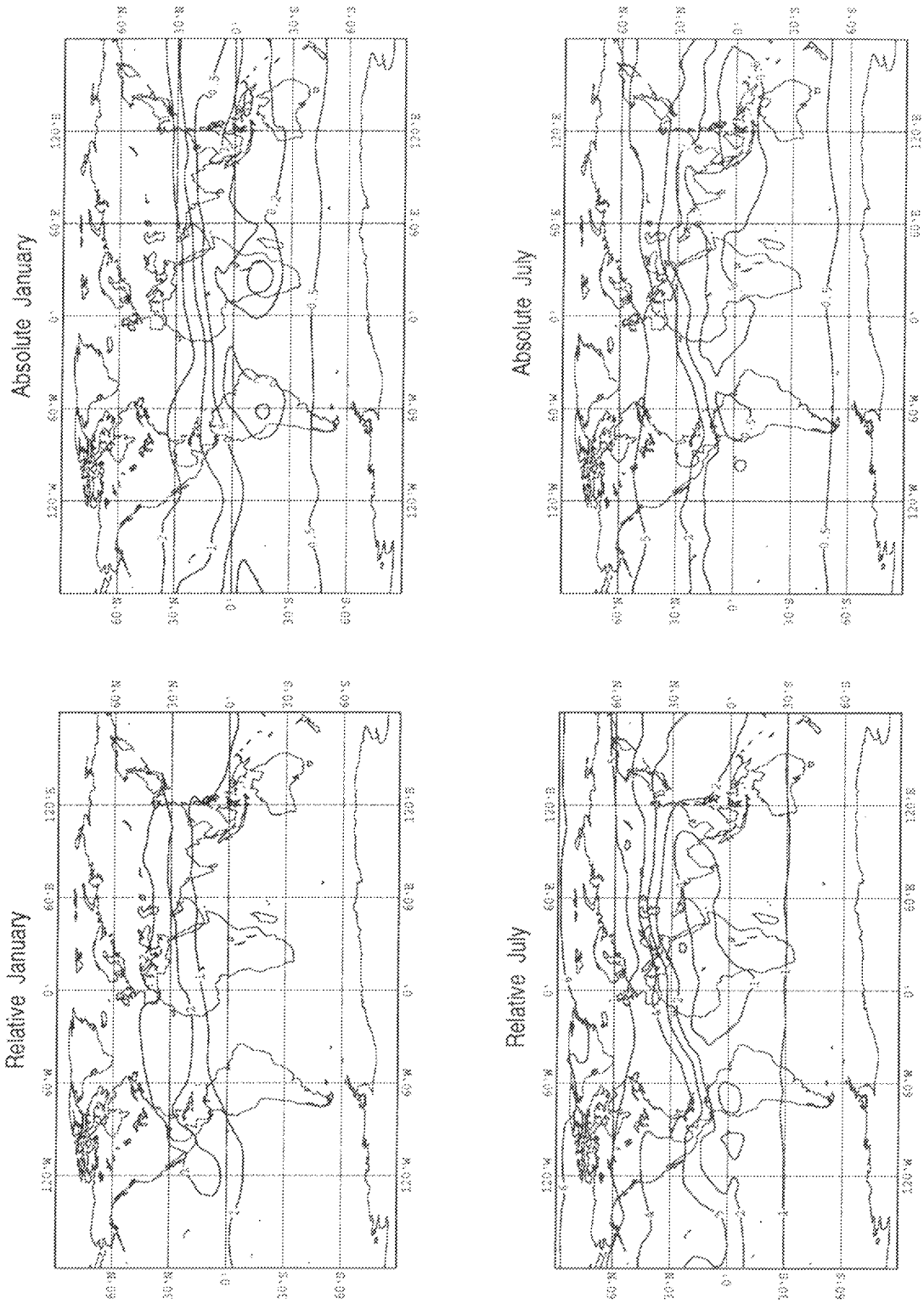

Figure 5.4 As Fig. 5.1, but for ozone and at 200 hPa. Isolines are drawn at 0.1, 0.2, 0.5, 1, 2 and 5 ppbv (top) and 1, 2, 3, 4, 5 and 6 % (bottom).

to the NO_x at 200 hPa for January and July is typically 20 pptv at northern mid-latitudes with contributions of more than 50 pptv over the eastern part of the US and western Europe. In January this contribution is about 1 to 2 pptv in the southern hemisphere, but in July the contribution in the southern hemisphere is slightly higher over the equatorial region (up to 5 pptv) and lower over the polar region (less than 0.5 pptv). This is a result of the realistic transport in CTMK. Many other models do not show clear differences between mid-latitudes and polar regions (AERONOX, 1995). In January the relative contribution of aircraft to the NO_x at 200 hPa is more than 50 % over large areas at northern mid-latitudes with maxima of 65 % in the NAFC and 60 % north-east of Japan. In the southern hemisphere the contribution of aircraft is 1 % over the main regions of NO_x lightning emissions and 2 % elsewhere. In July, the contribution is typically 20 % at northern mid-latitudes with a maximum of 45 % in the NAFC. In the southern hemisphere the contribution generally decreases from equator to pole and ranges between 3 and 6 %.

The differences between the monthly mean O_3 fields obtained with and without aircraft emissions are given in Figs. 5.3 and 5.4 for zonal mean and 200 hPa results, respectively. The aircraft emissions contribute maximally 3 and 5 ppbv to the zonal mean O_3 near cruise altitudes at northern mid-latitudes for January and July, respectively. Below 200 hPa the contribution of aircraft to O_3 decreases with decreasing altitude and is less than 0.5 ppbv near the surface in the northern hemisphere. In the southern hemisphere the contribution is about 0.5 ppbv at 200 hPa and decreases to about 0.05 ppbv in January and less than 0.2 ppbv in July. The relative contribution of aircraft to the zonal mean O_3 is maximally 3 % in January and 6 % in July. While the maximum for January is located at 350 hPa near 30°N (below and south of the region with the maximum aircraft emissions), the maximum for July is at 200 hPa over the pole (north of the aircraft emissions). In the northern hemisphere the contribution is 1 to 2 % near the surface and in the southern hemisphere it is less than 1 % for all altitudes.

The absolute contribution of the aircraft emissions to O_3 at 200 hPa is almost zonally symmetric, except for the low contributions of less than 0.2 ppbv in January and 0.5 ppbv in July near the source regions of NO_x due to lightning. The contribution generally decreases from the polar region in the northern hemisphere to that of the southern hemisphere. It varies from about 3 to 0.5 ppbv in January and about 9 to 0.5 ppbv in July. The relative contribution of aircraft to the ozone at 200 hPa in January is about 2 % in a narrow zonal band south of the main emission regions between 120°W and 120°E, slightly more than 1 % elsewhere in the northern hemisphere and just below 1 % in the southern hemisphere. In July, the relative contribution varies from 6 % in the north polar region to about 2 % near the equator and less than 1 % southward of 30°S.

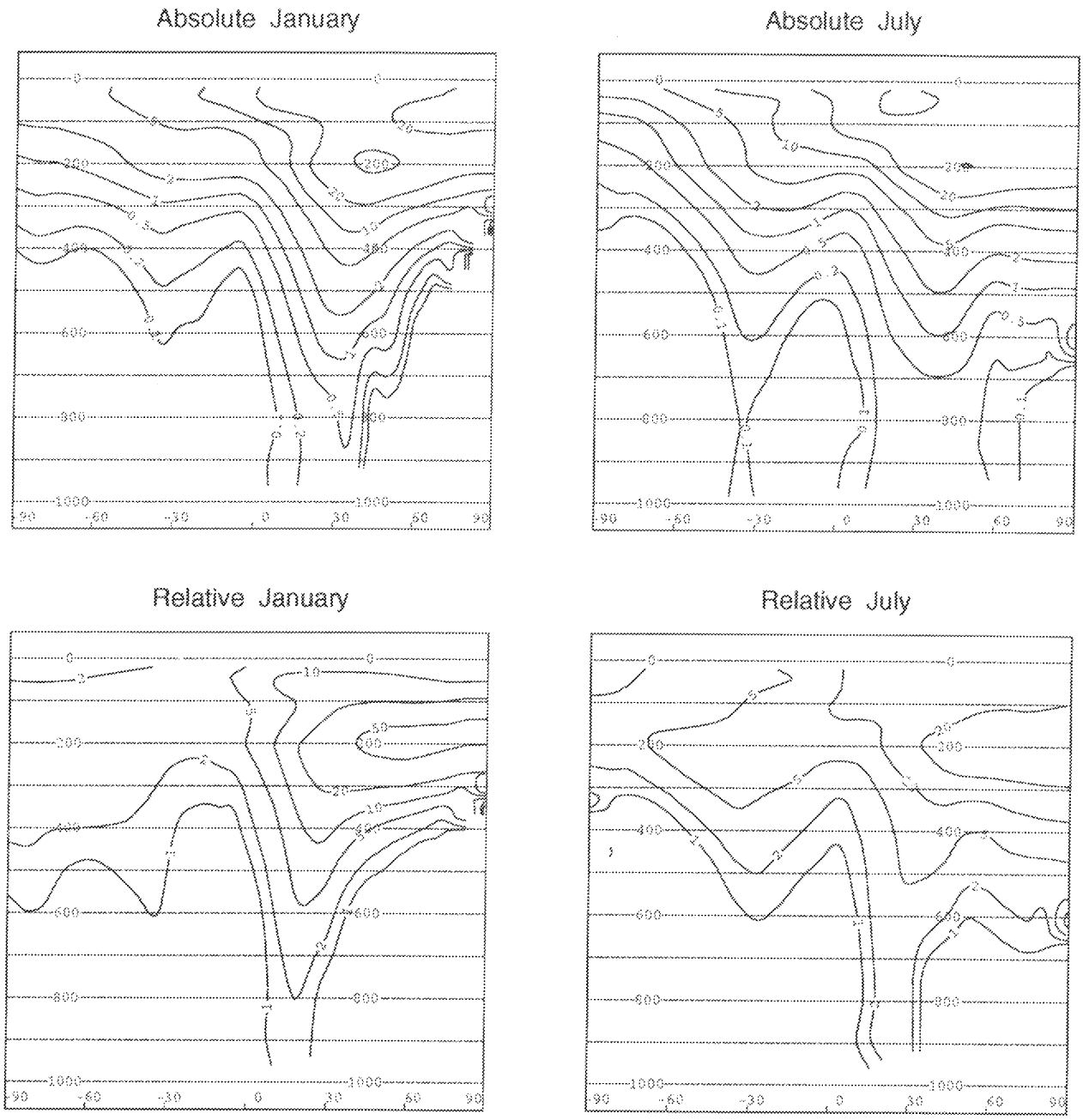

Figure 5.5 Differences between zonal and monthly mean volume mixing ratios for NO_y obtained with and without aircraft emissions for the 2003 scenario. The contribution of aircraft is given in absolute values (top: in pptv) and in relative values (bottom: in percent) for January (left) and July (right). Isolines are drawn at 0.1, 0.2, 0.5, 1, 2, 5, 10, 20 and 50 pptv (top) and 1, 2, 5, 10, 20 and 50 % (bottom).

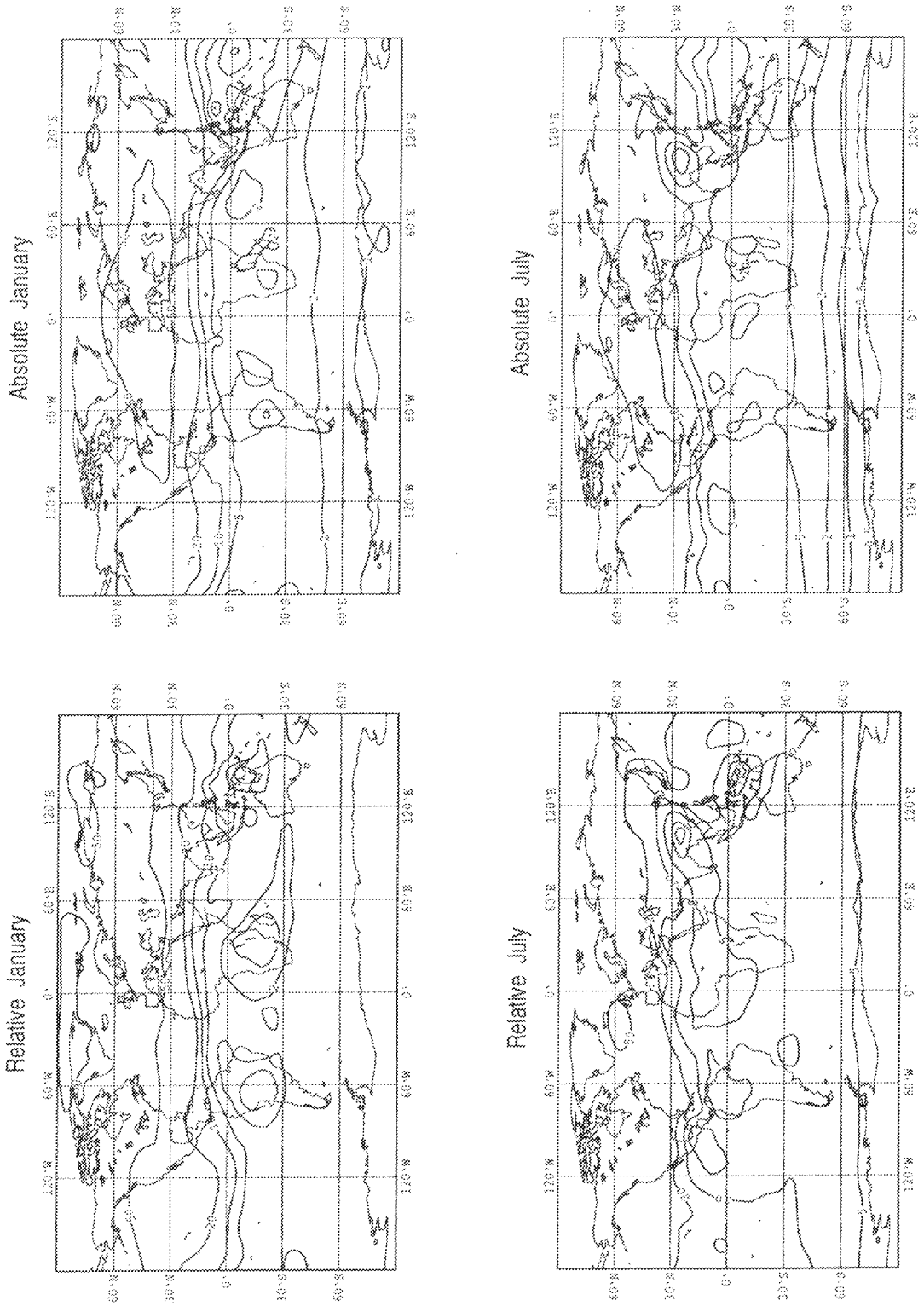

Figure 5.6 As Fig. 5.5, but for 200 hPa. Isolines are drawn at 0.5, 1, 2, 5, 10, 20 and 50 pptv (top) and 1, 2, 5, 10, 20 and 50 % (bottom).

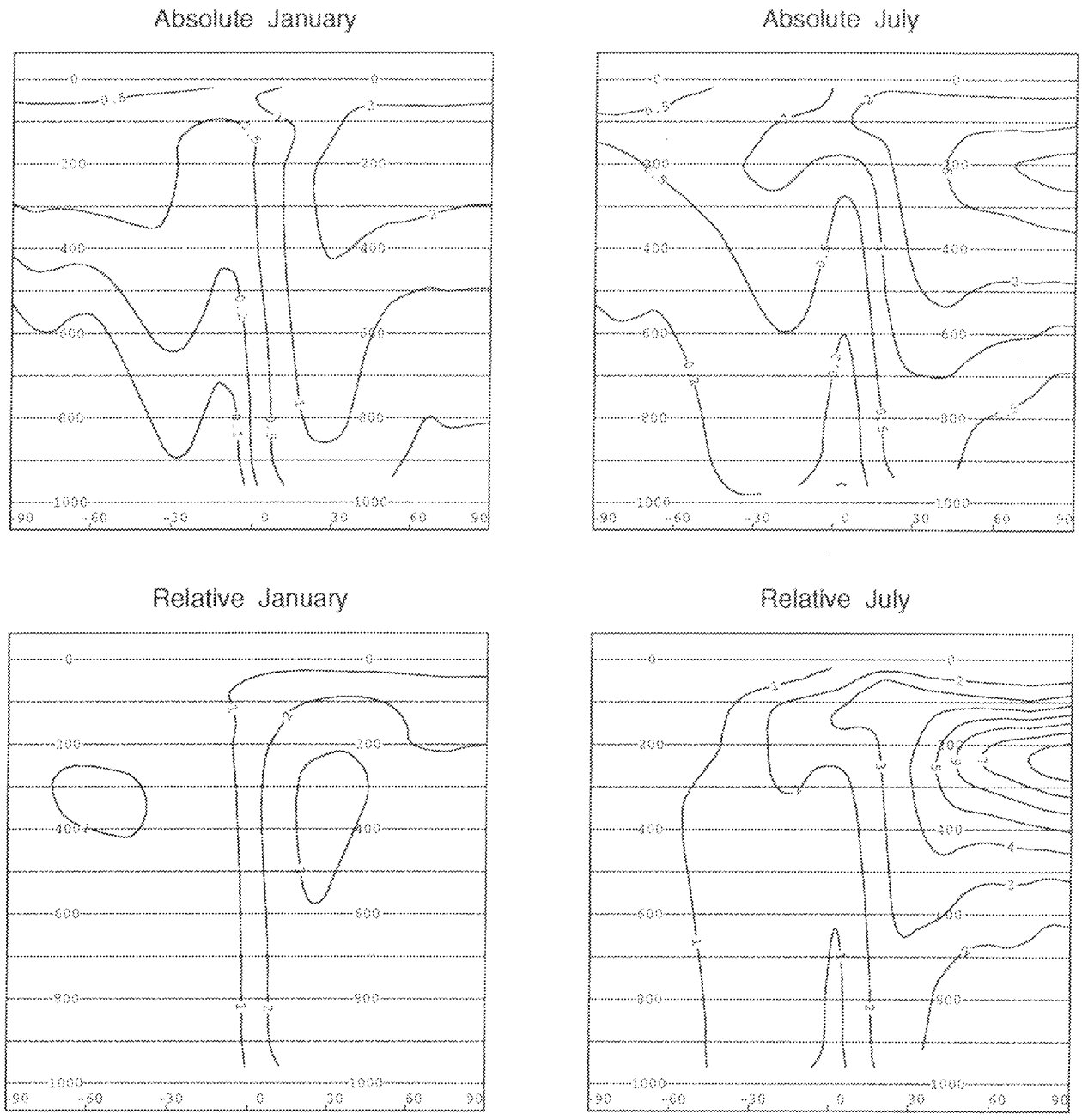

Figure 5.7 As Fig. 5.5, but for ozone. Isolines are drawn at 0.1, 0.2, 0.5, 1, 2, 5 and 10 ppbv (top) and 1, 2, 3, 4, 5, 6, 7 and 8 % (bottom).

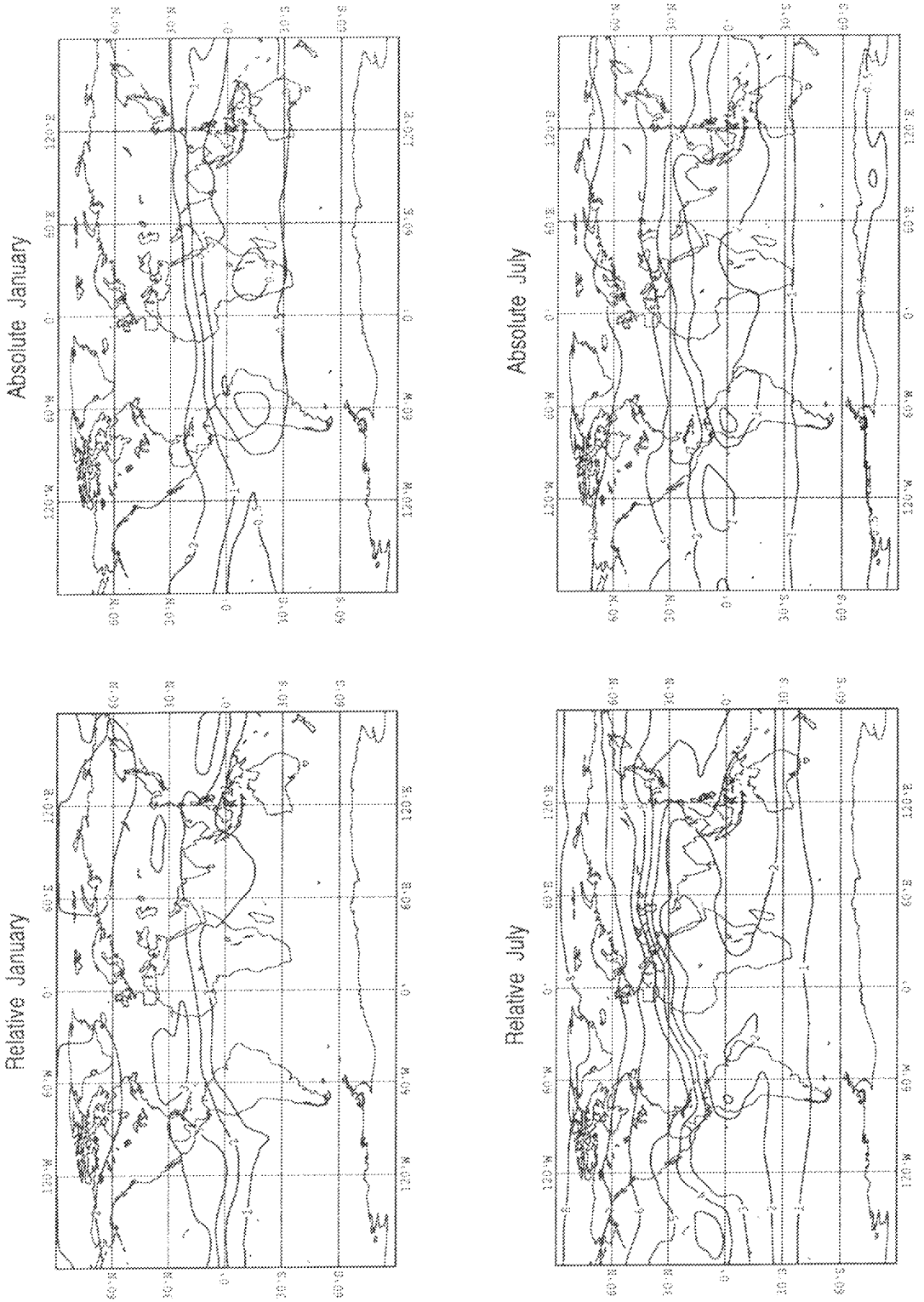

Figure 5.8 As Fig. 5.5, but for ozone and at 200 hPa. Isolines are drawn at 0.2, 0.5, 1, 2, 5 and 10 ppbv (top) and 1, 2, 3, 4, 5, 6, 7 and 8 % (bottom).

5.2 2003 scenario

The absolute and relative contribution of aircraft emissions to the zonal mean NO_x and the NO_x at 200 hPa are given in Figs. 5.5 and 5.6, respectively, for the 2003 scenario. The contributions are similar to those of the 1990 scenario, but the absolute as well as the relative contribution of aircraft are larger for the 2003 scenario. This could be expected since the aircraft emissions are larger for the 2003 scenario than the 1990 scenario, and this increase between the 1990 and 2003 scenario is larger for the aircraft emissions than for the other emissions (cf. Table 3.1). The absolute contribution of aircraft to the zonal mean NO_x is maximally 58 and 50 pptv near 200 hPa at northern mid-latitudes for January and July, respectively, while its relative contribution is maximally 61 and 36 %. The relative contribution is still less than 1 % in the lower and middle troposphere of the southern hemisphere. The absolute contribution of aircraft to the NO_x near 200 hPa (cf. Fig. 5.6) is now more than 20 pptv poleward of 30°N, and more than 50 pptv over the eastern US, the Atlantic and Europe with maxima of nearly 100 pptv. The maximum relative contribution near 200 hPa is about 70 % in January and 55 % in July. Both maxima occur in the NAFC. In the southern hemisphere 4 % of the NO_x near 200 hPa comes from aircraft in January and 3-10 % in July.

The contribution of aircraft to O_3 for the 2003 scenario shows also the same features as the 1990 scenario, but again the contribution for the 2003 scenario is larger. The aircraft now contribute maximally 4 ppbv in absolute numbers to the zonal mean O_3 in January and 10 ppbv in July, while their relative contribution is 4 and 8 %, respectively (cf. Fig. 5.7). In January maximally 4 ppbv of the O_3 near 200 hPa at northern mid-latitudes comes from aircraft emissions (cf. Fig. 5.8). The maximum is about 12 ppbv over the polar region in July. The contribution of aircraft in the southern hemisphere and also near the major source regions of lightning are higher than for the 1990 scenario. The relative contribution to O_3 near 200 hPa is maximally 3 % in January and 8 % in July.

5.3 2015 scenario

For the 2015 scenario the contribution of aircraft emissions is even higher than for the 2003 scenario. The contribution of aircraft to the zonal mean NO_x is maximally 93 pptv in January and about 60 pptv in July, and the maximal relative contribution is 70 % and 45 %, respectively (cf. Fig. 5.9). The aircraft emissions account for more than 100 pptv of the NO_x at 200 hPa over eastern US, the NAFC and Europe (Fig. 5.10). The relative contribution is maximally 78 % in January and 62 % in July. Up to 5 ppbv of the zonal mean O_3 in January and more than 10 ppbv in July comes from aircraft (cf. Fig. 5.11). Its relative contribution is 5 % in January and more than 10 % in July. At 200 hPa (Fig. 5.12) maximally 6 ppbv ozone results from aircraft in

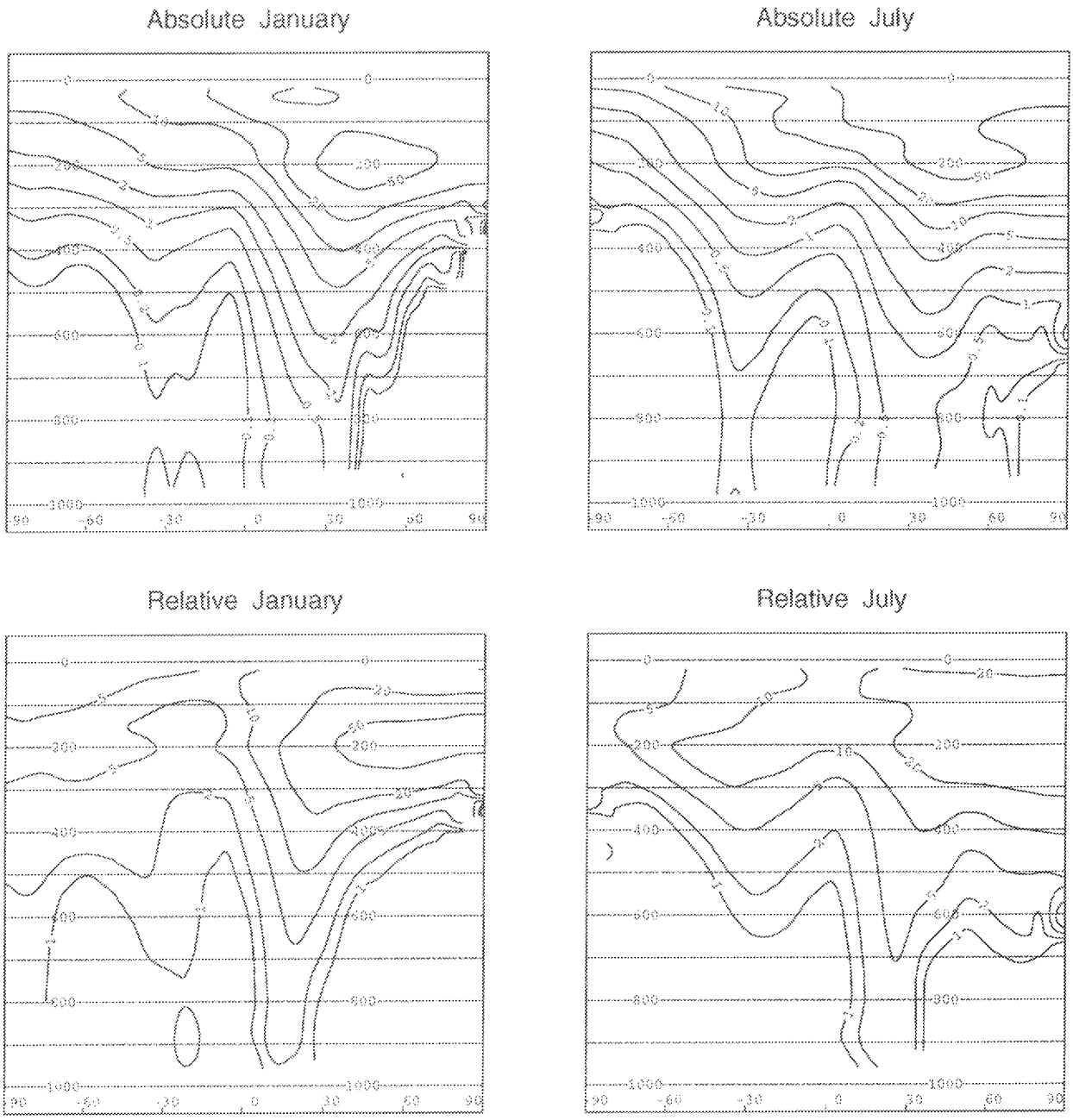

Figure 5.9 Differences between zonal and monthly mean volume mixing ratios for NO_x obtained with and without aircraft emissions for the 2015 scenario. The contribution of aircraft is given in absolute values (top: in pptv) and in relative values (bottom: in percent) for January (left) and July (right). Isolines are drawn at 0.1, 0.2, 0.5, 1, 2, 5, 10, 20 and 50 pptv (top) and 1, 2, 5, 10, 20 and 50 % (bottom).

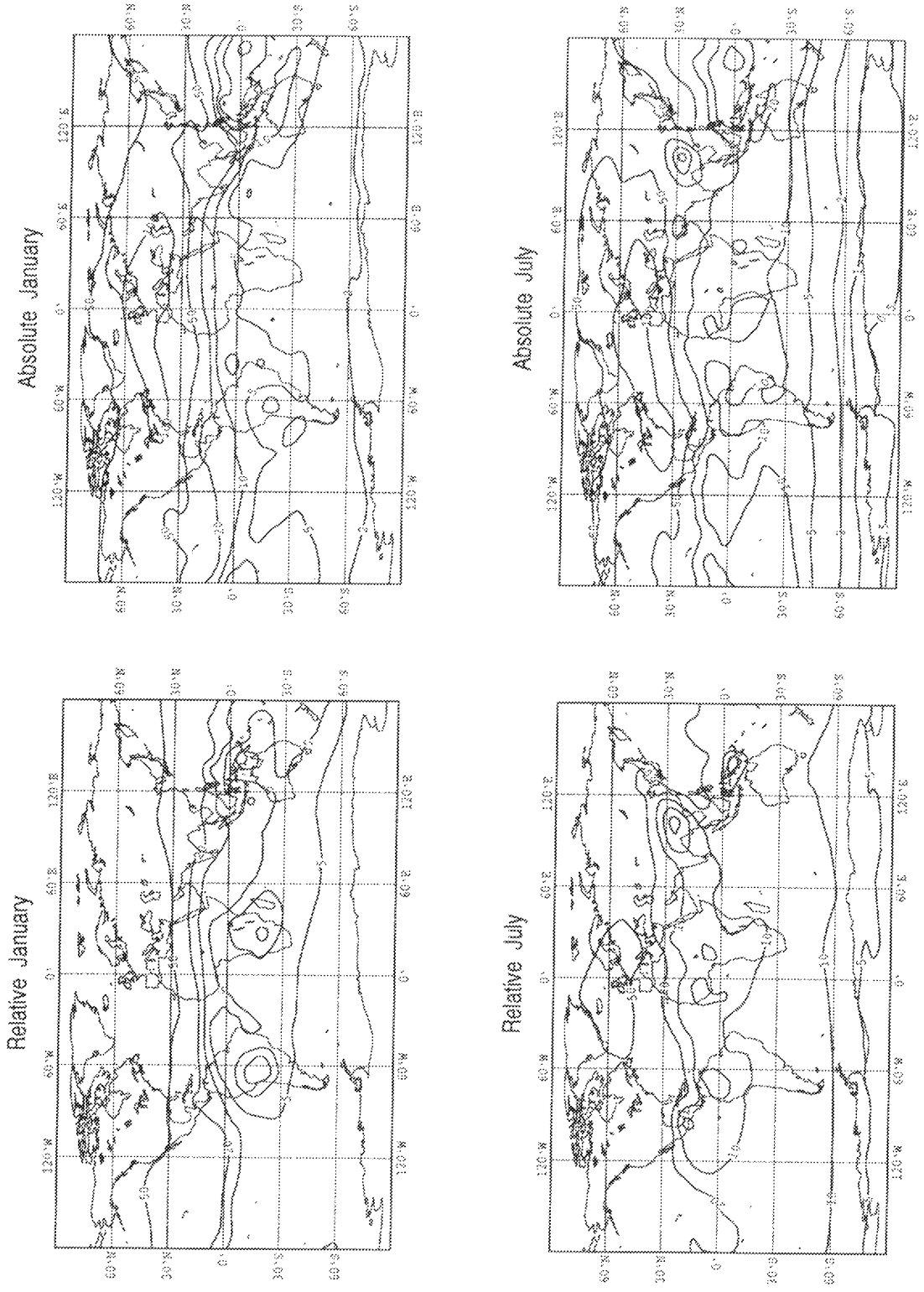

Figure 5.10 As Fig. 5.9, but for 200 hPa. Isolines are drawn at 0.5, 1, 2, 5, 10, 20, 50 and 100 pptv (top) and 1, 2, 5, 10, 20 and 50 % (bottom).

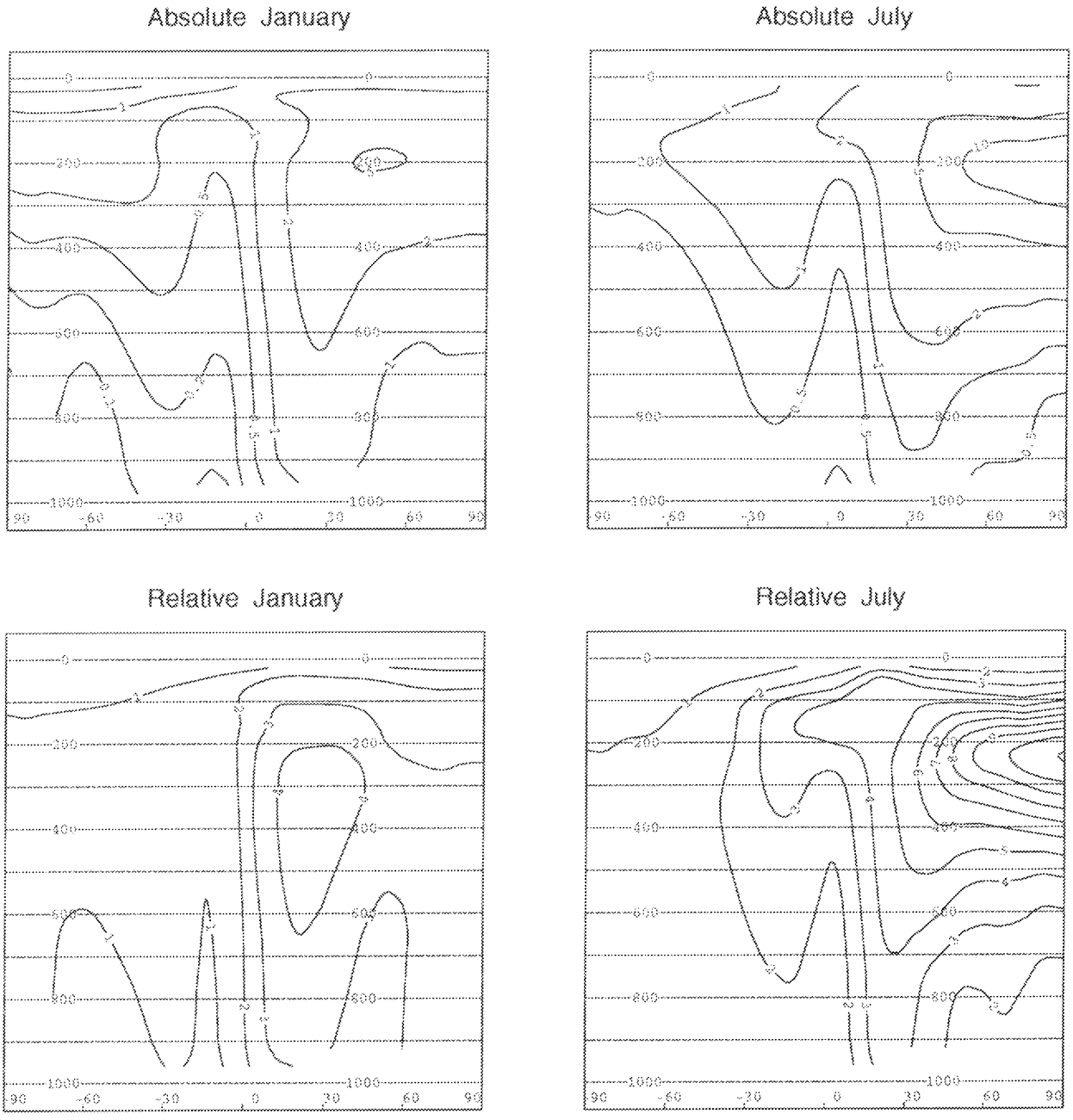

Figure 5.11 As Fig. 5.9, but for ozone. Isolines are drawn at 0.1, 0.2, 0.5, 1, 2, 5 and 10 ppbv (top) and 1, 2, 3, 4, 5, 6, 7, 8, 9, 10 and 11 % (bottom).

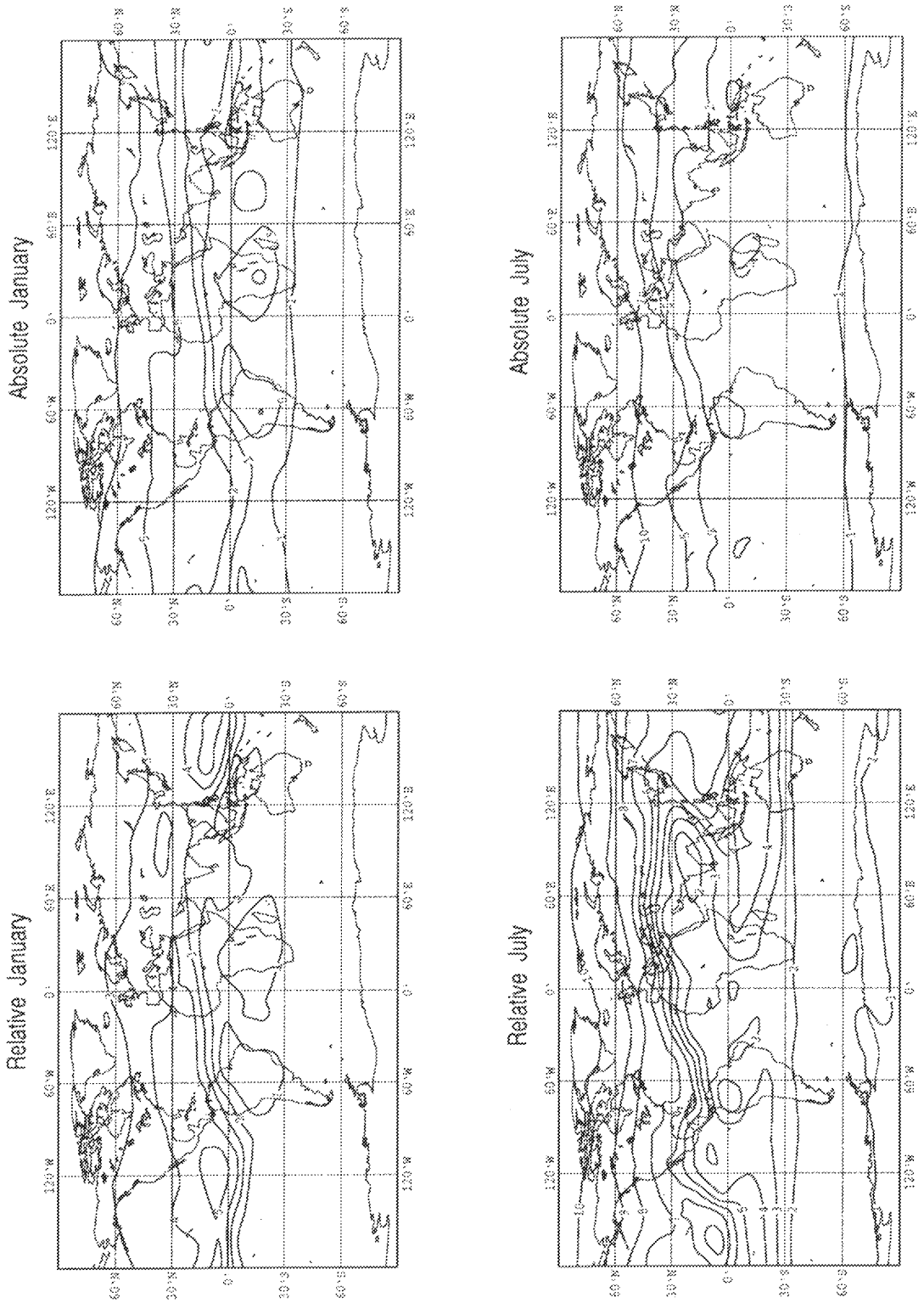

Figure 5.12 As Fig. 5.9, but for ozone and at 200 hPa. Isolines are drawn at 0.2, 0.5, 1, 2, 5 and 10 ppbv (top) and 1, 2, 3, 4, 5, 6, 7, 8, 9 and 10 % (bottom).

January and 17 ppbv in July. The relative contribution is maximally 5 % and 11 % in January and July, respectively. The aircraft contribution to ozone at 200 hPa in the southern hemisphere is now typically 1 % in January and slightly larger in July.

5.4 Discussion

Table 5.1 gives an overview of both the absolute and relative contribution of aircraft emissions to the NO_x and O_3 for January and July. Reported are the contributions to the total tracer amount up to 125 hPa, the maximal contribution to the zonal mean tracer amount, and the maximal local contribution. These results are given for the 1990, 2003 and 2015 scenario. The absolute contribution of aircraft to NO_x listed in Table 5.1 is almost the same for January and July. Its relative contribution is larger in January due to the smaller background concentrations for NO_x. Both the absolute and relative contribution of aircraft to O_3 is larger in July. The relative contribution of aircraft to NO_x locally reaches values of up to 60 % in January, whereas for O_3 the relative contribution of aircraft is locally maximally 6 % in July. The relative contribution of aircraft to the total tropospheric tracer amount is 4 % for NO_x and 2 % for O_3. This relative contribution to NO_x is larger in January than in July. The results for the contribution of aircraft emissions for 1990 to NO_x and O_3 are similar to the corresponding results obtained within the AERONOX (1995) project.

The emission scenarios for 2003 and 2015 give an increasing contribution of aircraft with local maxima of 75 % for NO_x in January and 11 % for O_3 in July for the 2015 emission scenario. The relative contribution of aircraft to the total tropospheric tracer amount for 2015 is 8 % for NO_x and 4 % for O_3. The absolute contribution of aircraft to NO_x doubles from the 1990 to the 2015 emission scenario. The relative contribution of aircraft to NO_x doubles for the total tropospheric tracer amount, but the increase of the maximal relative aircraft contribution to the zonal mean NO_x over the same period is about 1.5, and it is even less for the maximal local aircraft contribution. Both the absolute and relative contribution of aircraft to O_3 almost doubles from the 1990 to the 2015 emission scenario for all three regions considered in Table 5.1.

Table 5.1 Contributions of aircraft emissions to NO_x and O_3 for January and July. Reported are absolute (in pptv for NO_x and ppbv for O_3) and relative (in %) contributions to the *total* tracer amount up to 125 hPa, the maximal contribution to the *zonal* mean tracer amount, and the maximal *local* contribution for the 1990, 2003 and 2015 scenario.

1990	January			July		
component	total	zonal	local	total	zonal	local
absolute NO_x	2	37	60	2	31	71
relative NO_x	2	53	63	4	28	46
absolute O_3	1	3	3	1	8	9
relative O_3	1	3	3	2	6	6
2003	January			July		
component	total	zonal	local	total	zonal	local
absolute NO_x	3	59	95	3	50	95
relative NO_x	3	62	71	5	37	56
absolute O_3	1	4	4	1	12	12
relative O_3	2	4	4	3	8	9
2015	January			July		
component	total	zonal	local	total	zonal	local
absolute NO_x	4	93	148	5	80	144
relative NO_x	4	70	77	8	46	66
absolute O_3	1	5	6	2	16	17
relative O_3	3	5	6	4	11	11

Chapter 6

Sensitivity to lightning sources

Various runs have been performed with CTMK by using different multiplication factors for the emission data (cf. Table 6.1). The first run with the full surface, lightning and aircraft sources has been used to obtain the background concentrations given in Chapter 4. A combination of the first run with all emissions and the second run without the aircraft emissions gave the contribution of aircraft emissions to the background concentrations (cf. Chapter 5). Additional runs have been performed to obtain the sensitivity of the results to uncertainties in total annual emissions amounts. The chemical module that is used in CTMK (cf. Section 2.3) is non-linear, i.e. the sum of the concentrations obtained by using the surface, lightning and aircraft sources individually (runs 5, 6 and 7 in Table 6.1) is not equal to the concentrations obtained by using all sources (run 1). Also note that even without emissions (run 8), photochemical reactions lead to non-zero NO_x and O_3 concentrations. The effect of aircraft may be different when using e.g. the distribution of lightning sources given in Section 3.3, but scaled up or down to another global production.

Table 6.1 Multiplication factors for the emission data used in the various runs that have been performed with CTMK.

run	surface	lightning	aircraft
1	1	1	1
2	1	1	0
3	1	1/2	1
4	1	1/2	0
5	1	0	0
6	0	1	0
7	0	0	1
8	0	0	0

The global production of NO_x by lightning is assumed to be 16.4 $Tg(NO_2)/yr$ (cf. Sect. 3.3). However, estimates in the literature vary from about 3 to more than

100 Tg(NO_2)/yr. This uncertainty in the lightning sources of NO_x is probably the most important factor in studies of the effects of aircraft emissions. This is not only the result of the large uncertainty in the lightning sources, but also because these lightning sources lead to emissions high in the atmosphere. In order to investigate the effect of the lightning sources on the atmospheric composition and on the contribution of aircraft emissions, runs for the 1990 scenario have also been performed with the lightning sources reduced by a factor of 2, i.e. using runs 3 and 4. Comparison of the results obtained with the full and the reduced lightning sources gives an indication of the sensitivity of the results to the lightning sources.

6.1 Background

Here the monthly mean distribution of NO_x and O_3 obtained by using all sources of the 1990 scenario are described. In Fig. 6.1 the absolute and relative difference in the zonal mean NO_x between the runs using the full lightning source given in Sec. 3.3 and the same source, but reduced by a factor of 2 are presented. The reduction of the lightning source leads to a decrease of NO_x. This reduction is maximally 72 pptv (35 %) in January and 55 pptv (26 %) in July for the zonal mean NO_x at about 150 hPa in the equatorial region. The maxima are located south and north of the equator in January and July, respectively, since the major NO_x lightning source regions are then south and north of the equator. The reduction of NO_x is largest high in the troposphere because its lifetime is longest there. At 200 hPa on northern mid-latitudes the reduction of NO_x is less than 5 pptv (10 %) in January and 5-20 pptv (5-10 %) in July. The change of NO_x in the lower and middle troposphere in January is 2-15 pptv (10-25 %) between 30°S and the equator and less than 1 pptv (1 %) elsewhere. In July this change is less than 1 pptv (1 %) in the southern hemisphere and 1-50 pptv (1-20 %) in the northern hemisphere. The decrease of NO_x at 200 hPa is shown in Fig. 6.2. The maximum changes of more than 100 pptv occur above the major source regions of lightning. At northern mid-latitudes the reduction is typically less than 5 pptv in January and 5-10 pptv in July. In relative numbers the change in January typically increases from 10-30 % from the polar region to the equator in the southern hemisphere, is less than 10 % at northern mid-latitudes and is about 1 % above the northern polar region. In July typical values are less than 10 % poleward of 60°S, 20-30 % near the equator and 5-10 % poleward of 45°N.

The reduction of the lightning source also leads to a decrease of ozone. The decrease of zonal mean O_3 is given in Fig. 6.3. The maximal change of 7 ppbv occurs at 250 hPa near 30°S in January and is 5 ppbv near 15°N in July. Near 200 hPa at northern mid-latitudes the change is typically 2 ppbv in January and 4 ppbv in July. The maximal relative change is located near 350 hPa and is about 15 %. Near 200 hPa at northern mid-latitudes the decrease is 1-2 % in January and 2-4 % in July. In the southern hemisphere the change is typically 4 %. At 200 hPa the reduction of the lightning

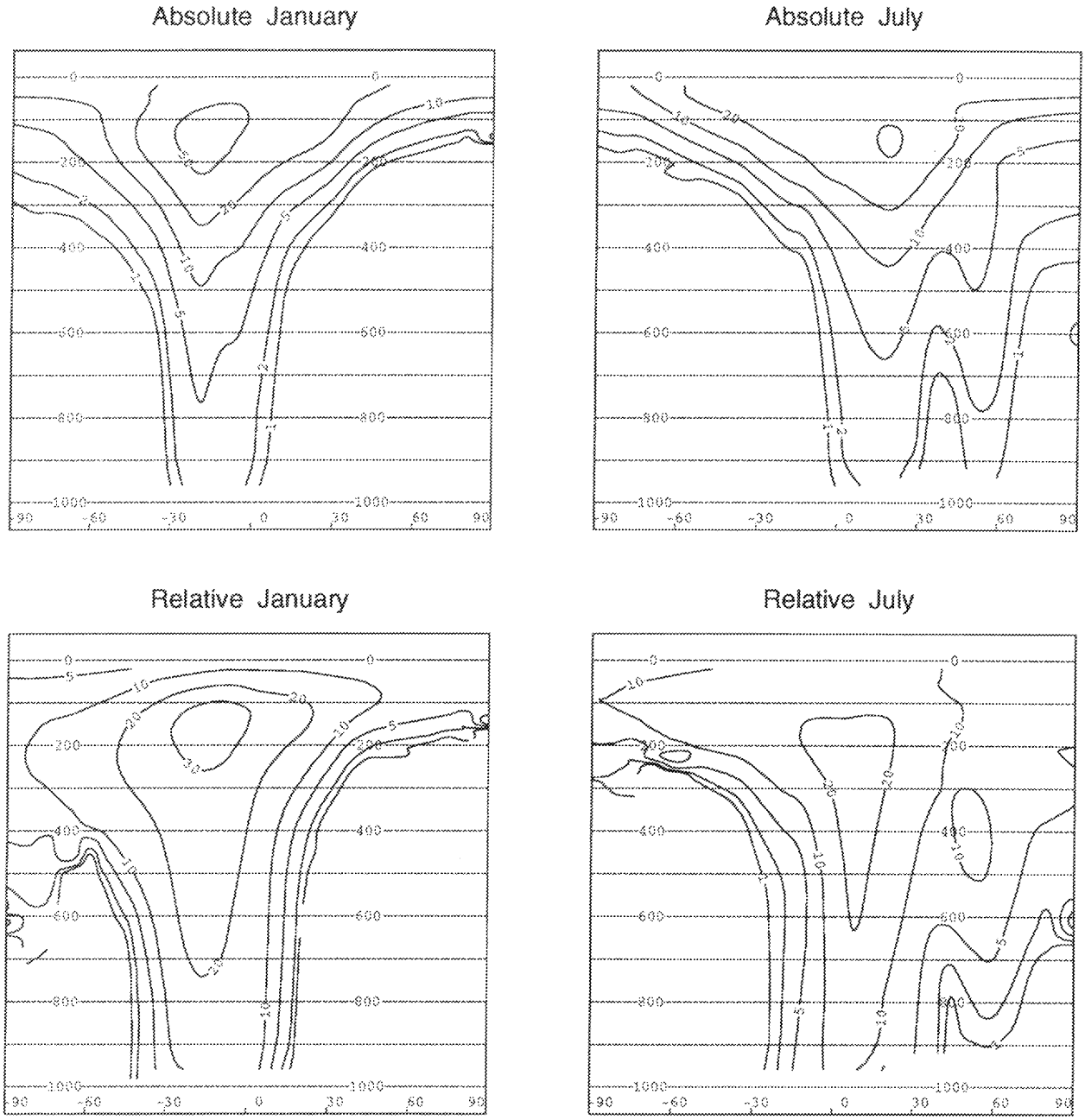

Figure 6.1 Differences between zonal and monthly mean volume mixing ratios for NO_x obtained with full and reduced lightning sources for the 1990 scenario. The decrease is given in absolute values (top: in pptv) and in relative values (bottom: in percent) for January (left) and July (right). Isolines are drawn at 1, 2, 5, 10, 20 and 50 pptv (top) and 1, 2, 5, 10, 20 and 30 % (bottom).

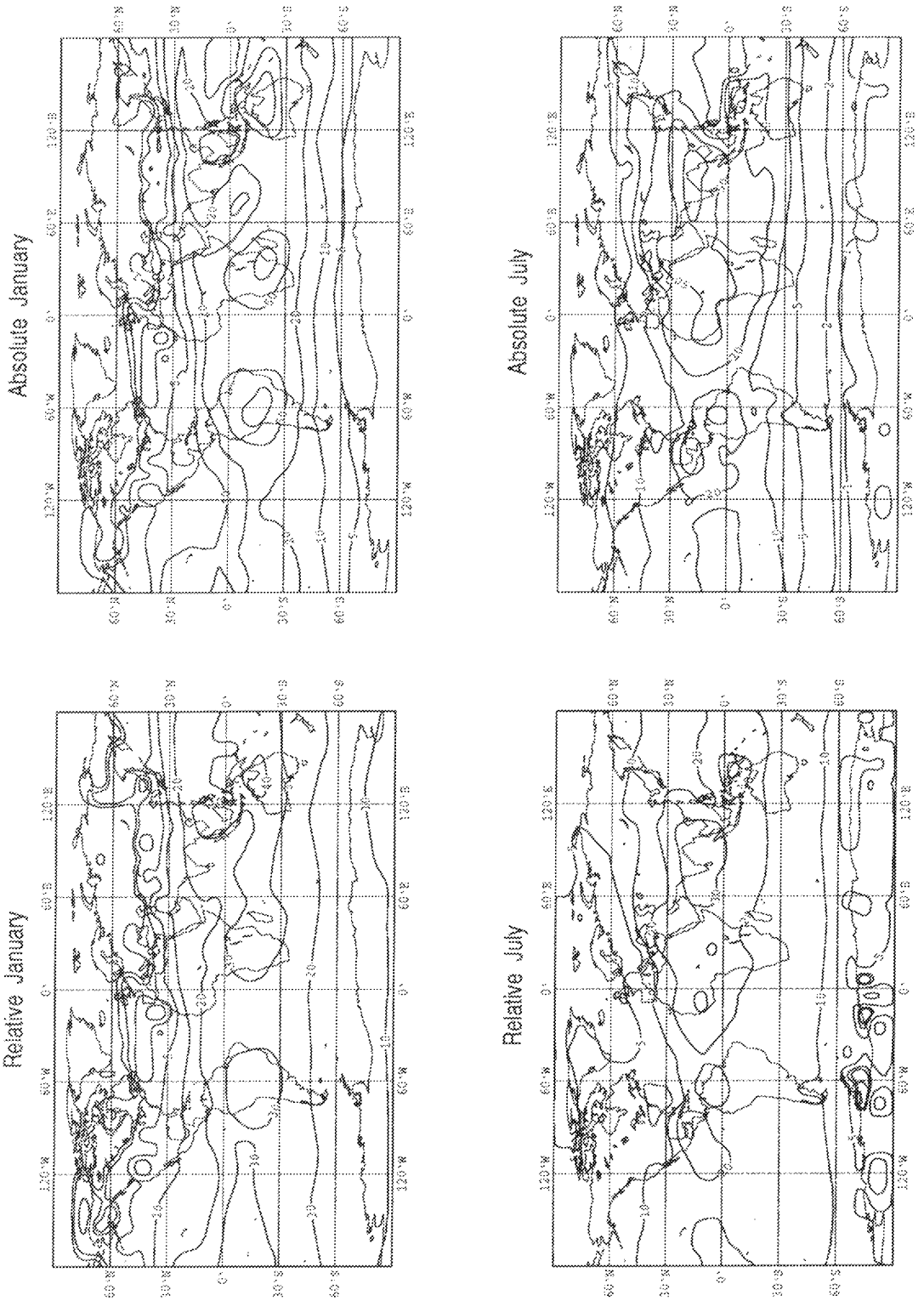

Figure 6.2 As Fig. 6.1, but for 200 hPa. Isolines are drawn at 1, 2, 5, 10, 20, 50 and 100 pptv (top) and 1, 2, 5, 10, 20, 30 and 40 % (bottom).

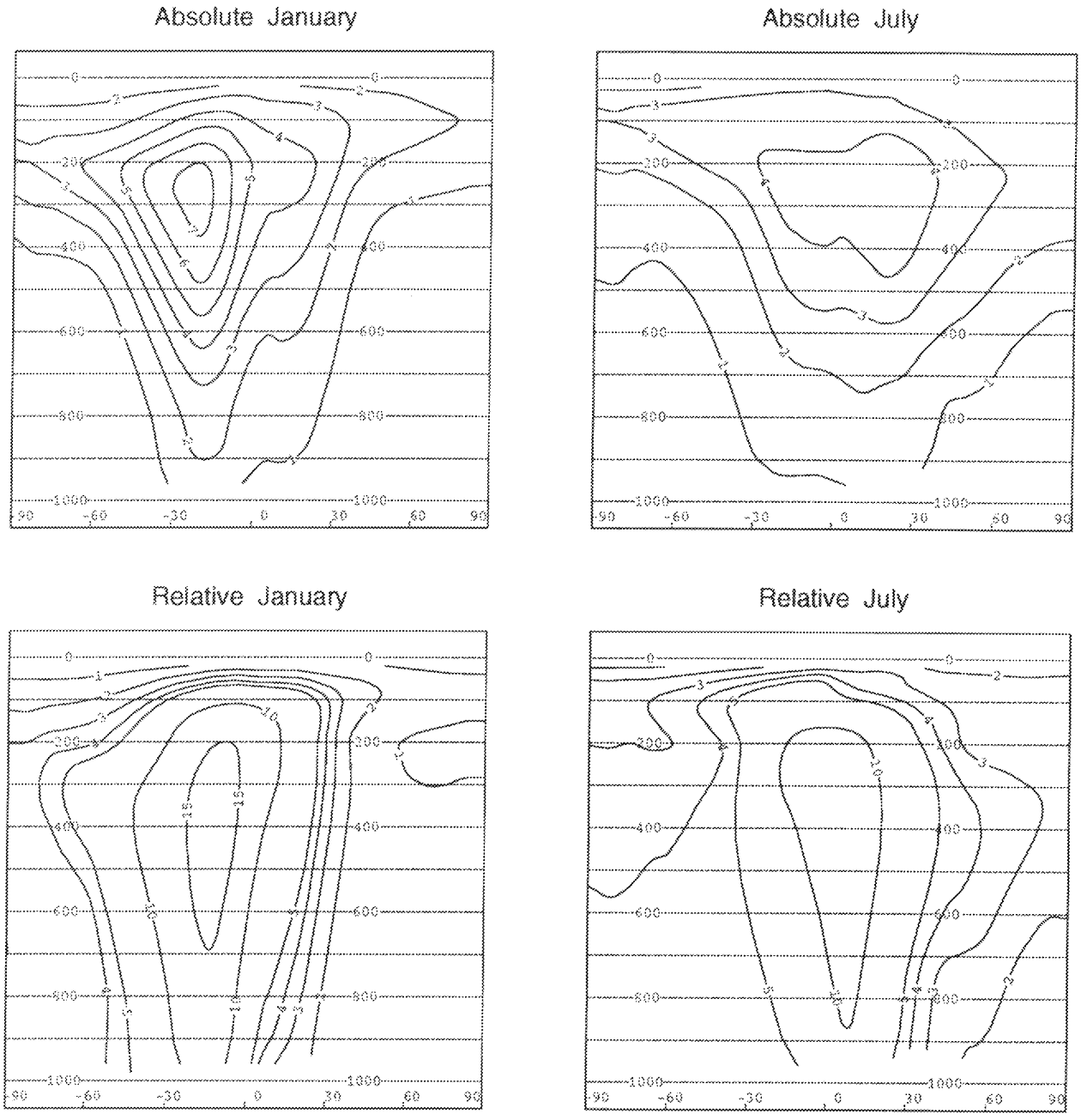

Figure 6.3 As Fig. 6.1, but for ozone. Isolines are drawn at 1, 2, 3, 4, 5, 6 and 7 ppbv (top) and 1, 2, 3, 4, 5, 10 and 15 % (bottom).

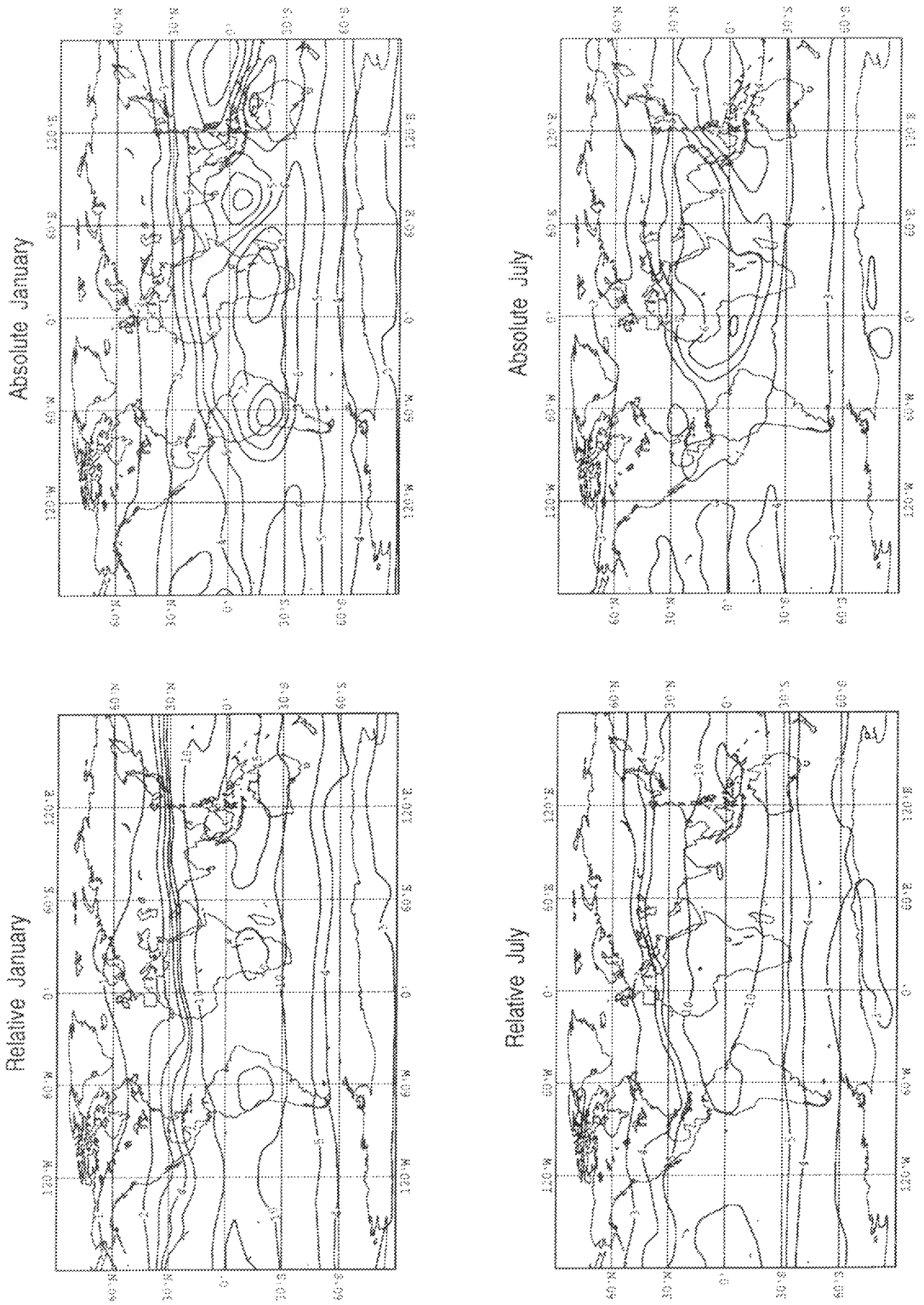

Figure 6.4 As Fig. 6.1, but for ozone and at 200 hPa. Isolines are drawn at 2, 3, 4, 5, 6, 7, 8 and 9 ppbv (top) and 1, 2, 3, 4, 5, 10 and 15 % (bottom).

source leads to a decrease of maximally 10 ppbv over the major lightning source regions in January (cf. Fig. 6.4). The ozone reduction is 3-5 ppbv at southern mid-latitudes and about 2 ppbv at northern mid-latitudes. In July the ozone decreases 5 ppbv over the major source regions of lightning and typically 3-4 ppbv at mid-latitudes. In relative values the ozone is reduced by about 3 % over the southern polar region, 15 % near the equator and 1-2 % at northern mid-latitudes in January and 3-4 % in July. These changes in O_3 at northern mid-latitudes are of the same order as the effects of aircraft (cf. Section 5.1).

6.2 Aircraft

Next the effect of aircraft emissions on NO_x and O_3 is given for the 1990 scenario with the lightning NO_x sources reduced by a factor of 2. The contribution of aircraft to the zonal mean NO_x is given in Fig. 6.5. These results are almost identical to those obtained with the full lightning sources (cf. Fig. 5.1). Due to the reduced lightning sources the effect of aircraft is slightly larger here. The relative contribution of aircraft emissions to the zonal mean NO_x are only slightly higher in the northern hemisphere (maximally 53 % and 30 % in January and July, respectively, compared to 52 % and 28 % with the full lightning sources). In the southern hemisphere the aircraft contribution is maximally slightly more than 2 % in January and 7 % in July, whereas it was 2 % and 6 % with the full lightning sources. The absolute and relative contribution of aircraft to the NO_x at 200 hPa presented in Fig. 6.6 is again slightly larger than before, even over the major regions of the NO_x lightning emissions.

The contribution of aircraft emissions to the zonal mean ozone with the reduced lightning sources (Fig. 6.7) is also only slightly higher than for the corresponding contribution, but with the full lightning sources (Fig. 5.3). The same is true for the ozone at 200 hPa which comes from aircraft emissions (compare Figs. 6.8 with 5.4). The area with small aircraft contributions over the major source regions of lightning are smaller with the reduced lightning sources and the contribution of aircraft at northern mid-latitudes is slightly higher, i.e. maximally 3 % in January and 7 % in July.

6.3 Discussion

Reduction of the lightning sources of NO_x by a factor of 2 leads to a reduction of the NO_x concentrations in the tropics of up to about 30 %. At northern mid-latitudes the reduction of NO_x is less than 1 % in January and 1 to 10 % in July. The resulting reduction of O_3 in the tropics is about 15 %. At northern mid-latitudes the reduction is 1 to 2 % in January and 2 to 5 % in July. The changes in NO_x at northern mid-latitudes due to the factor of two difference in the lightning source is less than the change in NO_x which results from aircraft emissions. However, the change in O_3 at northern mid-latitudes due to the difference in the lightning source is typically

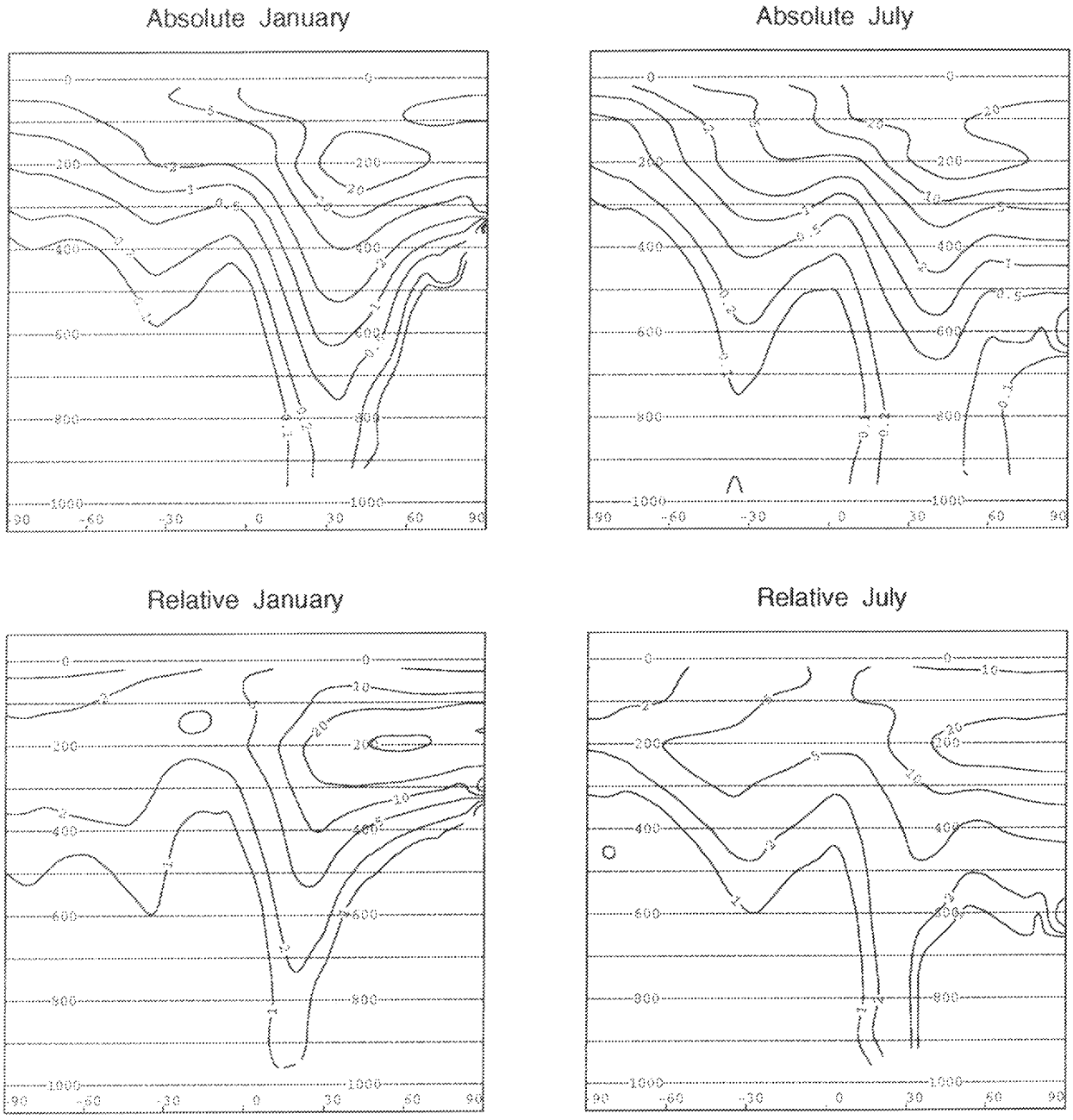

Figure 6.5 Differences between zonal and monthly mean volume mixing ratios for NO_x obtained with and without aircraft emissions for the 1990 scenario with reduced lightning sources. The contribution of aircraft is given in absolute values (top: in pptv) and in relative values (bottom: in percent) for January (left) and July (right). Isolines are drawn at 0.1, 0.2, 0.5, 1, 2, 5, 10 and 20 pptv (top) and 1, 2, 5, 10, 20 and 50 % (bottom).

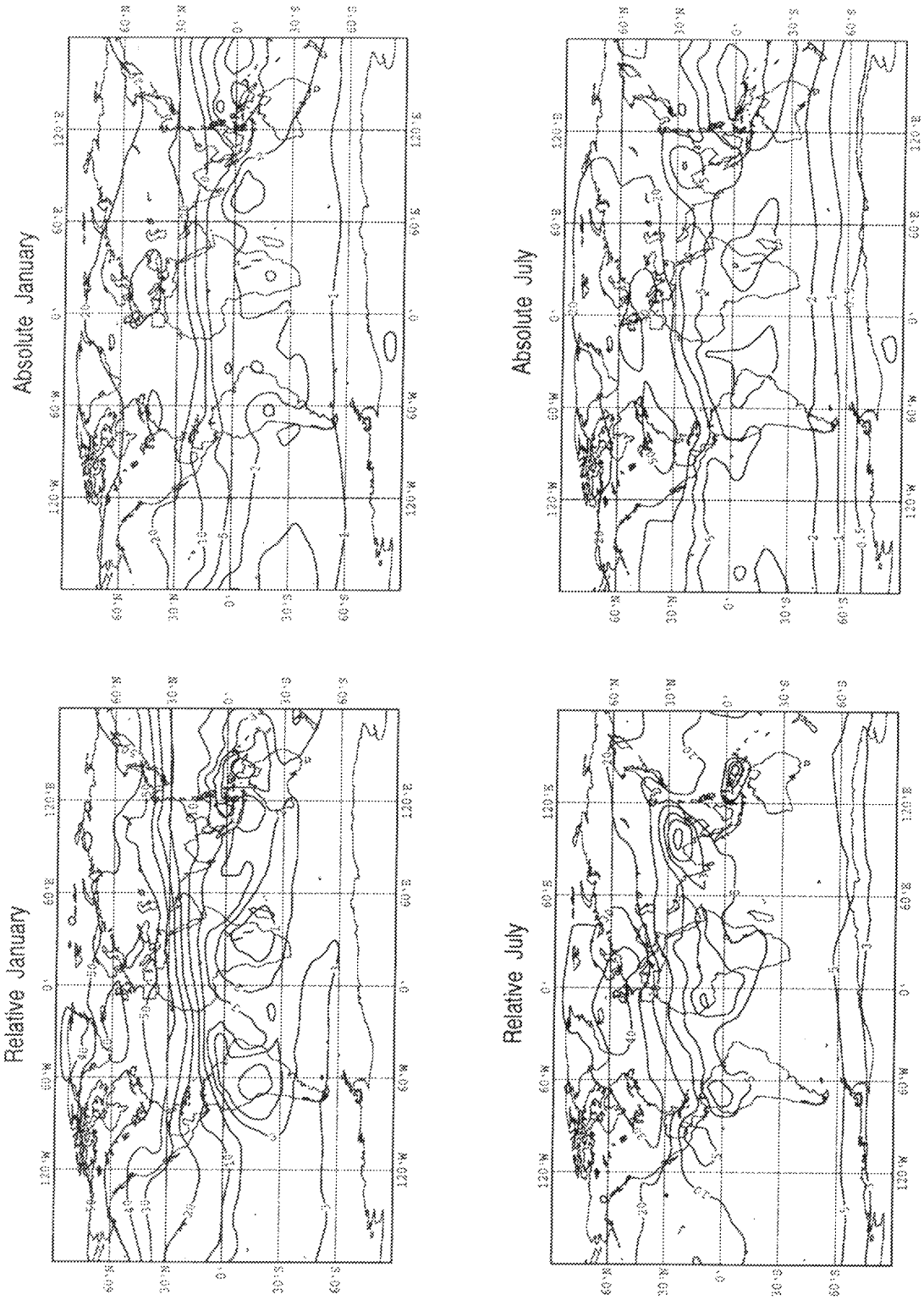

Figure 6.6 As Fig. 6.5, but for 200 hPa. Isolines are drawn at 0.5, 1, 2, 5, 10, 20 and 50 pptv (top) and 1, 2, 3, 5, 10, 20, 30, 40, 50 and 60 % (bottom).

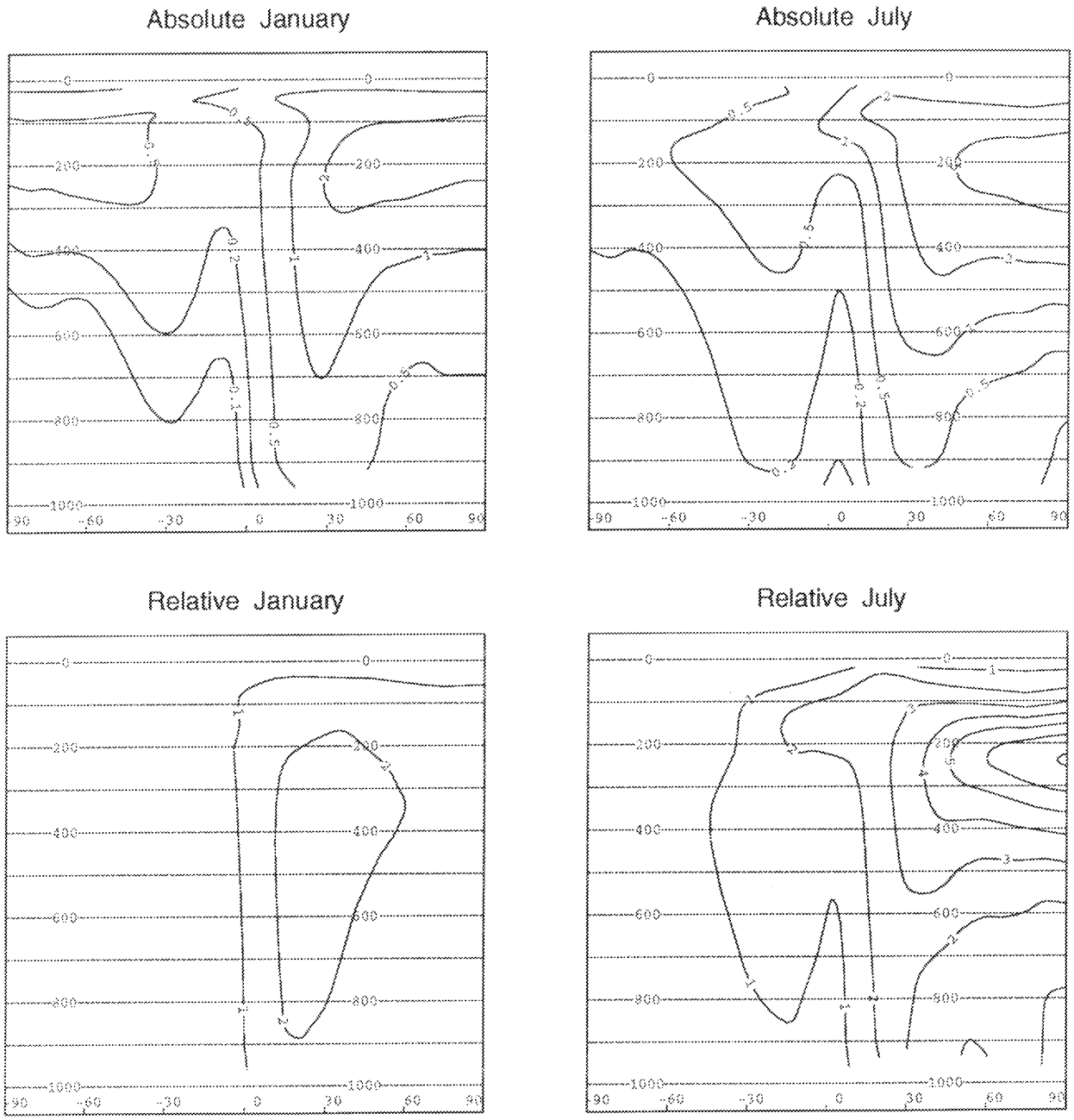

Figure 6.7 As Fig. 6.5, but for ozone. Isolines are drawn at 0.1, 0.2, 0.5, 1, 2 and 5 ppbv (top) and 1, 2, 3, 4, 5, 6 and 7 % (bottom).

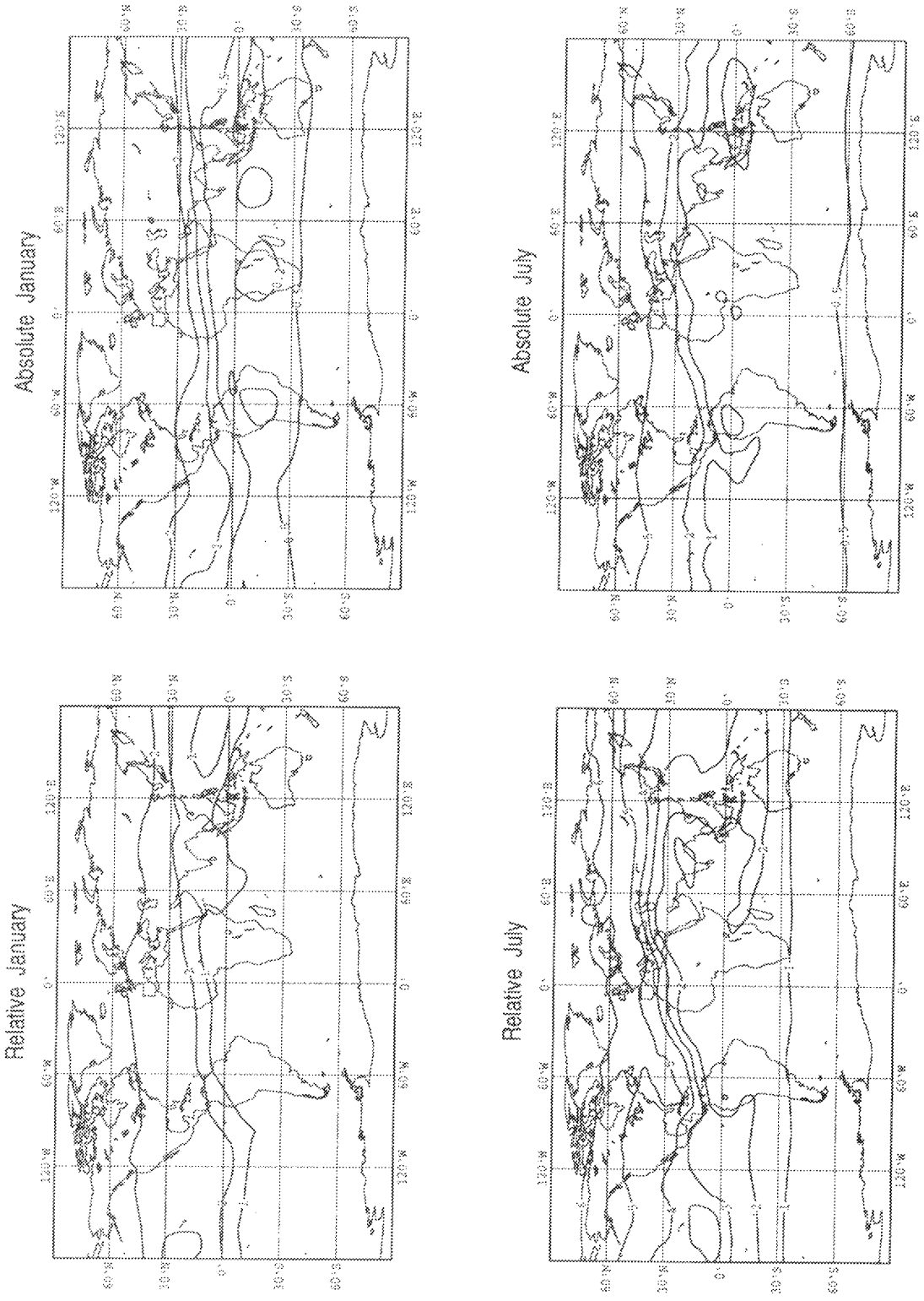

Figure 6.8 As Fig. 6.5, but for ozone and at 200 hPa. Isolines are drawn at 0.2, 0.5, 1, 2 and 5 ppbv (top) and 1, 2, 3, 4, 5 and 6 % (bottom).

of the same order of magnitude as that of the aircraft emissions. The effects of the aircraft emissions on tropospheric NO_x and O_3 obtained from the runs with the reduced lightning source are only slightly larger than those obtained from the runs with the full lightning source. This because the lightning sources and aircraft emissions of NO_x are separated geographically.

The effect of aircraft emissions on the NO_x concentrations at northern mid-latitudes seem larger than the corresponding effect of uncertainties in lightning NO_x emissions. Therefore observations of NO_x concentrations at northern mid-latitudes should indicate the presence of aircraft emissions. The effect of aircraft emissions on O_3 concentrations at northern mid-latitudes are of the same order of magnitude as the changes which resulted from the reduced lightning source of NO_x. This uncertainty needs to be reduced in order to be able to ascribe a fraction of the observed O_3 undoubtfully to aircraft emissions. Measurements closely behind aircraft may, however, reveal effects due to aircraft that are not perceptible with the present resolution of CTMK. As part of the POLINAT (1994) project such measurements are performed and analysed. These measurements also give a first indication of the background NO_x concentrations in the NAFC.

Also note that the sensitivity study presented here takes only two values for the total annual emissions due to lightning into account, which are both on the low side of the uncertainty range that is presently considered in the literature.

In the AERONOX (1995) project a simplified linear chemical scheme has been used in order to get the contribution of the individual sources to the NO_x concentration as well as the contribution of any linear combination of these sources. This reduced chemical scheme gave results for NO_x that were comparable to those obtained with the chemical module that has been used in this work. Therefore such a reduced chemical scheme is useful for sensitivity studies. It has, however, the disadvantage that O_3 fields are prescribed. Hence, the effect of aircraft emissions on O_3 can not be investigated. The effect of different geographical distributions for the sources has, just as for CTMK, to be studied with additional model runs. For policy purposes all these effects can be taken into account by using an approach that uses model output to construct empirical repro-functions that describe the effects that emissions at certain locations have on the concentrations of all relevant species elsewhere under different situations (Kouwenhoven, 1995).

Chapter 7

Conclusions and outlook

The effect of aircraft emissions on the atmospheric composition has been studied with the three-dimensional chemical transport model CTMK. CTMK has already been used to investigate the effect of aircraft on the chemical composition of the atmosphere (Wauben *et al.*, 1994; AERONOX, 1995). The results obtained with CTMK in the AERONOX project compared well with the results obtained by other models. Other emission data have been used in the previous studies with CTMK, but the results are qualitatively similar to the ones that are reported here.

CTMK gives realistic values for the tropospheric concentrations of the tracers involved. However, validation of the model with observations is needed. In the near future, the 3-D ozone distribution obtained with CTMK will be compared with a compilation of ozone observations made by Fortuin & Langematz (1995). Model calculations of the contribution of aircraft emissions to the background concentrations of trace gases can also be validated with measurements obtained during e.g. the POLINAT (1994) project.

Unlike the previous studies with CTMK, the simulations in this report include results for future emission scenarios as well as a study of the sensitivity of the results to uncertainties in lightning sources.

The main conclusions regarding the effects of present day aircraft emissions on the atmospheric composition, their changes for future emission scenarios, and its sensitivity to lightning sources of NO_x are:

- Model calculations with CTMK show that aircraft emissions in 1990 account for 30 to 70 % of the NO_x near cruise altitudes at northern mid-latitudes, where the effect of aircraft emissions is most pronounced, while on a global scale the contribution of aircraft to tropospheric NO_x is about 2 to 4 %. The resulting contribution to O_3 is globally 1 to 2 % and in the North Atlantic Flight Corridor about 3 to 6 %. These relative contributions to the trace gases depend on the background concentrations which vary strongly with season. Also note that local effects are restricted by the resolution of the global model, which is $8° \times 10°$ in this work.

- The scenario runs for 1990, 2003 and 2015 show that the chemical composition of the atmosphere will become more perturbed in the future. Table 4.1 gives some typical values for the relative increase of NO_x and O_3 concentrations for the 2003 and 2015 scenarios compared to the 1990 scenario. The contribution of aircraft will increase since their emissions grow more rapidly than that of other sources. Table 5.1 gives an overview of the contribution of aircraft emissions to the NO_x and O_3 concentrations for the 1990, 2003 and 2015 scenario. Model calculations with CTMK show that the contribution of aircraft emissions to tropospheric ozone will approximately double from 1990 to 2015.

- The lightning sources of NO_x mainly affect the chemical composition over the tropics. Since the aircraft emissions occur at other locations their effect is small in the tropics and the effect of aircraft is not strongly influenced by the lightning sources. The contribution of aircraft emissions to NO_x at northern mid-latitudes is significant and will probably be larger than the contribution from lightning emissions of NO_x. For O_3 concentrations at northern mid-latitudes the contributions from aircraft and lightning emissions are of the same order of magnitude.

Many improvements/extensions could be made to the present study. However, this field of research is relatively new and basic input such as the emission data still have large uncertainties. Also the chemical and physical processes in the atmosphere are not completely understood. Things that could be improved are:

- Other aircraft emissions such as SO_2, H_2O and soot should also be considered in studies of the effect of aircraft emissions on the atmospheric composition and on climate.

- Inclusion of the diurnal variation of emissions. Diurnal variations in emissions have an impact on global model results (AERONOX, 1995). Air traffic in e.g. the NAFC shows such a strong diurnal variation. Future emission data sets should include these variations.

- Use of lightning sources derived from ECMWF analyses. The lightning sources used in the global model should be consistent with the convection parameterization that has been obtained from meteorological data. This ensures that the emissions occur in regions with high convective activity, and hence with large vertical motions and clouds, which influence chemistry and photolysis rates.

- On-line computations of photolysis rates. This produces the diurnal cycle in chemistry module and gives photolytic rates that are consistent with clouds, aerosol and ozone columns that are also used in the chemistry module. This leads to a feedback of photolysis on chemistry.

- More detailed chemical modules should be used. The chemical module that has been used for the present work includes basic tropospheric chemistry. However, trace gases such as NO_3, N_2O_5, PAN, HONO and HNO_4 also affect the distribution of NO_x. In addition, other chemical species that are emitted by aircraft such as SO_x need to be taken into account in the chemical module. Heterogeneous chemistry on aerosols and in or on cloud droplets should eventually be included as well.

- Study of the direct and indirect effects of aircraft on radiative forcing. A first investigation has been made by using literature estimates for the changes in the relevant atmospheric constituents due to aircraft emissions (Fortuin *et al.*, 1995). As a next step to the climate effects due to aircraft, which should eventually be made with a general circulation model, the 3-dimensional fields containing changes in atmospheric composition due to aircraft that have been obtained with CTMK will be used as input for the radiative forcing calculations. This will not only be done for O_3, but also other constituents such as NO_x, CH_4, water vapour and aerosols should be taken into account. The sensitivity of the radiative forcing to the altitude of the tropopause needs also to be considered.

- Stratospheric chemistry is needed for a realistic assessment of the effects of aircraft in the stratosphere, especially for super-sonic aircraft. In the stratosphere NO_x emissions by aircraft lead to a destruction of ozone. The stratosphere-troposphere exchange must be improved and validated to give the correct fluxes at the top of the troposphere. In view of the large difference in the lifetime of NO_x in the troposphere and stratosphere the results are quite sensitive to stratosphere-troposphere exchange.

Acknowledgements

We are indebted to several people who contributed to the work presented in the report.

- Dr. M. Heimann from the Max-Planck-Institut für Meteorologie in Hamburg made the TM2 model available to us.
- The chemistry module was kindly provided within Eurotrac's GLOMAC project by Prof.dr. P.J. Crutzen, Dr. P.H. Zimmermann and Dr. R. Hein from the Max-Planck-Institut für Chemie in Mainz.
- The NO_x emissions from lightning were produced within the AERONOX project.
- Drs. J. Olivier from RIVM/LAE supplied the other emission data.
- RLD supported this work financially in the framework of the policy analysis project for air pollution and air traffic AERO (Aviation Emissions and evaluation of Reduction Options).
- We thank Ir. J.W. Pulles from RLD and Dr. J.P.M. Kouwenhoven from Resource Analysis for constructive discussions.

References

AERONOX: "The Impact of NO_x Emissions from Aircraft upon the Atmosphere at Flight Altitudes 8–15 km" Report of Sub-Project 3 on Global Atmosphere Model Simulations, EU Project, in preparation (1995).

ANCAT: "A Global Inventory of Aircraft NO_x Emissions for the EC AERONOX Research Project", in preparation (1995).

Atkinson, R., D.L. Baulch, R.A. Cox, R.F. Hampson, J.A. Kerr and J. Troe: "Evaluated Kinetic and Photochemical Data for Atmospheric Chemistry Supplement IV" *J. Phys. Chem. Ref. Data* **21**, 1125-1568 (1992).

Beck, J.P., C.E. Reeves, F.A.A.M. de Leeuw and S.A. Penkett: "The Effect of Aircraft Emissions on Tropospheric Ozone in the Northern Hemisphere" *Atmos. Env.* **26A**, 17-29 (1992).

Brühl, C. and P.J. Crutzen: "On the Disproportionate Role of Tropospheric Ozone as a Filter against Solar UV-B Radiation" *Geophys. Res. Lett.* **16**, 703-706 (1989).

Brühl, C. and P.J. Crutzen: "MPIC Two-Dimensional Model" in *The Atmospheric Effects of Stratospheric Aircraft: Report of the 1992 Models and Measurements Workshop* M.J. Prather and E.E. Remsberg (Eds.), NASA Reference Publication 1292, Vol. I, Washington, DC, p.103-104 (1993).

Crutzen, P.J.: "Ozone in the Troposphere" in *Composition, Chemistry, and Climate of the Atmosphere* H.B. Singh (Ed.) , Von Nostrand Reinhold Publ., in preparation (1995).

Crutzen, P.J. and P.H. Zimmermann: "The Changing Photochemistry of the Troposphere" *Tellus* **43AB**, 136-151 (1991).

De More, W.B., S.P. Sander, D.M. Golden, R.F. Hampson, M.J. Kurylo, C.J. Howard, A.R. Ravishankara, C.E. Kolb and M.J. Molina: "Chemical Kinetics and Photochemical Data for use in Stratospheric Modelling" J.P.L. Publ. 92-20, Pasadena, CA (1992).

Dentener, F.: "Heterogeneous Chemistry in the Troposphere" Dissertation, Utrecht University, Utrecht (1993).

Dentener, F. and P. J. Crutzen: "Reaction of N_2O_5 on Tropospheric Aerosols: Impact on the Global Distributions of NO_x, O_3 and OH" *J. Geophys. Res.* **98**, 7149-7163 (1993).

Dianov-Klokov, V.I. and L.N. Yurganov: "A Spectroscopic Study of the Global Space-Time Distribution of Atmospheric CO" *Tellus* **33**, 262-273 (1981).

Ehhalt, D.H. and J.W. Drummond: "NO_x Sources and the Tropospheric Distribution of NO_x during STRATOZ III" in *Tropospheric Ozone* I.S.A. Isaksen (Ed.), D. Reidel, Dordrecht, p.217-237 (1988).

Ehhalt, D.H., F. Rohrer and A. Wahner: "Sources and Distribution of NO_x in the Upper Troposphere at Northern Mid-Latitudes" *J. Geophys. Res.* **97**, 3725-3738 (1992).

Fortuin, J.P.F. and U. Langematz: "An Update on the Global Ozone Climatology and on Concurrent Ozone and Temperature Trends" in *Atmospheric Sensing and Modeling* R.P. Santer (Ed.) Proc. SPIE 2311 Washington, DC, p.207-216 (1995).

Fortuin, J.P.F., R. van Dorland, W.M.F. Wauben and H. Kelder: "Greenhouse Effects of Aircraft Emissions as Calculated by a Radiative Transfer Model" *Ann. Geophysicae*, in press (1995).

Fung, I., J. John, J. Lerner, E. Matthews, M. Prather, L.P. Steele and P.J. Fraser: "Three-Dimensional Model Synthesis of the Global Methane Cycle" *J. Geophys. Res.* **96**, 13003-13065 (1991).

Heimann, M.: "The Global Atmospheric Tracer Model TM2: Model Description and User Manual" to appear as DKRZ Report, Hamburg (1995).

Hein, R.: "Inverse Modellierung des Atmosphärischen Methan-Kreislaufs unter Verwendung eines Drei-Dimensionalen Modells des Transport und der Chemie der Troposphäre" Examensarbeit Nr. 25, Max-Planck-Institut für Meteorologie, Hamburg (1994).

Hidalgo, H. and P.J. Crutzen: "The Tropospheric and Stratospheric Composition Perturbed by NO_x Emissions of High Altitude Aircraft" *J. Geophys. Res.* **82**, 5833-5866 (1977).

Holton, J.R: "On the Global Exchange of Mass between the Stratosphere and Troposphere" *J. Atmos. Sci.* **47**, 392-395 (1990).

Intergovernmental Panel on Climate Change (IPCC): "The Supplementary Report to the IPCC Scientific Assessment" Cambridge University Press, Cambridge (1992).

Kasibhatla, P.S., H. Levy II, W.J. Moxim and W.L. Chameides: "The Relative Impact of Stratospheric Photochemical Production on Tropospheric NO_y Levels: A Model Study" *J. Geophys. Res.* **96**, 18631-18646 (1991).

Kouwenhoven, J.P.M.: Private communication (1995).

Kowalczyk, M. and E. Bauer: "Lightning as a Source of NO in the Troposphere" Rep. FAA-EE-82-4, U.S. Dep. of Transp., Washington, DC (1982).

Louis, J.F.: "A Parametric Model of Vertical Eddy Fluxes in the Atmosphere" *Boundary-Layer Meteorol.* **17**, 187-202 (1979).

McInnes, G. and C.T. Walker: "The Global Distribution of Aircraft Air Pollutant Emissions" Report No. LR 872, Warren Spring Lab., Stevenage (1992).

Muller, J.F.: "Geographical Distribution and Seasonal Variation of Surface Emissions and Deposition Velocities of Atmospheric Trace Gases" *J. Geophys. Res.* **97**, 3787-3804 (1992).

Newell, R.W., J.W. Kidson, D.G. Vincent and G.J. Boer: "The General Circulation of the Tropical Atmosphere and Interactions with Extratropical Latitudes" Vol. 2, MIT press, Cambridge, MA (1974).

Olivier, J.G.J.: "Scenarios for Global Emissions from Air Traffic. The development of regional and gridded ($5° \times 5°$) emissions scenarios for aircraft and for surface sources, based on CPB scenarios and existing emission inventories for aircraft and surface sources" Report no. 773002 003, RIVM, Bilthoven (1995).

POLINAT: "Pollution from Aircraft Emissions in the North Atlantic Flight Corridor", Progress Report, EU Project (1994).

Price, C. and D. Rind: "A Simple Lightning Parameterization for Calculating Global Lightning Distributions" *J. Geophys. Res.* **97**, 9919-9933 (1990).

Russell, G. L. and J. A. Lerner: "A New Finite-Differencing Scheme for the Tracer Transport Equation" *J. Appl. Meteorol.* **20**, 1483-1498 (1981).

Schumann, U.: "On the Effect of Emissions from Aircraft Engines on the State of the Atmosphere" *Ann. Geophysicae* **12**, 365-384 (1994).

Tiedtke, M.: "A Comprehensive Mass Flux Scheme for Cumulus Parameterization in Large-Scale Models" *Mon. Wea. Rev.* **117**, 1779-1800 (1989).

NASA: "U.S. Standard Atmosphere" U.S. Government Printing Office, Washington, DC (1976).

Velders, G.J.M., L.C.J. Heijboer and H. Kelder: "The Simulation of the Transport of Aircraft Emissions by a Three-Dimensional Global Model" *Ann. Geophysicae* **12**, 385-393 (1994).

Wauben, W.M.F., P.F.J. van Velthoven and H. Kelder: "Chemistry and Transport of NO_x Aircraft Emissions in a Global 3-D Chemical Transport Model" in *International Scientific Colloquium on the Impact of Emissions from Aircraft and Spacecraft upon the Atmosphere*, DLR Mitteilungen 94-06, Cologne, p.241-246 (1994).

Wuebbles, D.J., D. Maidon, R.K. Seals Jr., S.L. Baughcum, M. Metwally and A. Mortlock: "Emission Scenarios Development: Report of the Emission Scenarios Committee" in *The Atmospheric Effects of Stratospheric Aircraft: A Third Program Report*, R.S. Stolarski and H.L. Wesoky (Eds.), NASA Reference Publication 1313, Hampton, VA, p.63-208 (1993).

Bijgaand treft U een overzicht aan van recentelijk in deze serie gepubliceerde titels. Een komplete lijst wordt U op verzoek toegezonden. U kunt Uw aanvraag richten aan de KNMI Bibliotheek, Postbus 201, 3730 AE De Bilt (030-206855). Hier kan men U tevens informeren over de verkrijgbaarheid en prijzen van deze publicaties.

89-05 Statistical forecasts of sunshine duration / Li Zhihong and S. Kruizinga.

90-01 The effect of a doubling atmospheric CO2 on the stormtracks in the climate of a general circulation model / P.C. Siegmund.

90-02 Analysis of regional differences of forecasts with the multilayer AMT-model in the Netherlands / E.I.F. de Bruin, Li Tao Guang and Gao Kang.

90-03 Description of the CRAU data-set : Meteosat data, radiosonde data, sea surface temperatures : comparison of Meteosat and Heimann data / S.H. Muller, H. The, W. Kohsiek and W.A.A. Monna.

90-04 A guide to the NEDWAM wave model / G. Burgers.

91-01 A parametrization of the convective atmospheric boundary layer and its application into a global climate model / A.A.M. Holtslag, B.A. Boville and C.-H. Moeng.

91-02 Turbulent exchange coefficients over a Douglas fir forest / F.C. Bosveld.

92-01 Experimental evaluation of an arrival time difference lightning positioning system / H.R.A.Wessels.

92-02 GCM control run of UK Meteorological Office compared with the real climate in the NW European winter / J.J. Beersma.

92-03 The parameterization of vertical turbulent mixing processes in a General Circulation Model of the Tropical Pacific / G. Janssen.

92-04 A scintillation experiment over a forest / W.Kohsiek.

92-05 Grondtemperaturen / P.C.T.van der Hoeven en W.N.Lablans

92-06 Automatic supression of anomalous propagation clutter for noncoherent weather radars / H.R.A. Wessels and J.H. Beekhuis.

93-01 Searching for stationary stable solutions of Euler's equation / R. Salden.

93-02 Modelling daily precipitation as a function of temperature for climatic change impact studies / A.M.G. Klein Tank and T.A. Buishand.

93-03 An analytic conceptual model of extratropical cyclones / L.C. Heijboer.

93-04 A synoptic climatology of convective weather in the Netherlands / Dong Hongnian.

93-05 Conceptual models of severe convective weather in the Netherlands / Dong Hongnian.

94-01 Seismische analyse van aardbevingen in Noord-Nederland : bijdrage aan het multidisciplinaire onderzoek naar de relatie tussen gaswinning en aardbevingen / H.W.Haak en T. de Crook.

94-02 Storm activity over the North Sea and the Netherlands in two climate models compared with observations / J.J. Beersema.

94-03 Atmospheric effects of high-flying subsonic aircraft / W. Fransen.

94-04 Cloud-radiation-hydrological interactions : measuring and modeling / A.J. Feijt, R. van Dorland, A.C.A.P. van Lammeren, E. van Meijgaard en P. Stammes.

94-05 Spectral ultraviolet radiation measurements and correlation with atmospheric parameters / F. Kuik and H. Kelder

95-01 Transformation of precipitation time series for climate change impact studies / A.M.G. Klein Tank and T.A. Buishand

95-02 Internal variability of the ocean generated by a stochastic forcing / M.B.H. van Noordenburg

95-03 Applicability of weakly nonlinear theory for the planetary-scale flow / E.A. Kartashova

95-04 Changes in tropospheric NOx and O3 due to subsonic aircraft emissions / W.M.F. Wauben, P.F.J. van Velthoven and H. Kelder